

EUROPEAN ORGANISATION FOR NUCLEAR RESEARCH (CERN)



Submitted to: Phys. Rev. D.



CERN-EP-2024-285
November 4, 2024

A search for triple Higgs boson production in the $6b$ final state using pp collisions at $\sqrt{s} = 13$ TeV with the ATLAS detector

The ATLAS Collaboration

A search for the production of three Higgs bosons (HHH) in the $b\bar{b}b\bar{b}b\bar{b}$ final state is presented. The search uses 126 fb^{-1} of proton–proton collision data at $\sqrt{s} = 13$ TeV collected with the ATLAS detector at the Large Hadron Collider. The analysis targets both non-resonant and resonant production of HHH . The resonant interpretations primarily consider a cascade decay topology of $X \rightarrow SH \rightarrow HHH$ with masses of the new scalars X and S up to 1.5 TeV and 1 TeV, respectively. In addition to scenarios where S is off-shell, the non-resonant interpretation includes a search for standard model (SM) HHH production, with limits on the tri-linear and quartic Higgs self-coupling set. No evidence for HHH production is observed. An upper limit of 59 fb is set, at 95% confidence level, on the cross-section for Standard-Model HHH production.

1 Introduction

Since the discovery of the 125 GeV Higgs boson (H) [1, 2] at the Large Hadron Collider’s (LHC) ATLAS and CMS experiments, a core part of the LHC research program has been to investigate the properties of the Higgs boson and establish if they are in agreement with the predictions of the Standard Model (SM) [3, 4]. Two key parts of the SM Higgs mechanism are the tri-linear (λ_3) and quartic (λ_4) self-coupling constants, which are a crucial part of the electroweak symmetry breaking mechanism and determine the shape of the Higgs field potential. Higgs self-coupling modifiers κ_3 and κ_4 are introduced using the κ framework, in which they are defined as $\kappa_i = \lambda_i/\lambda_i^{\text{SM}}$ for $i = 3, 4$, such that $\kappa_i = 1$ corresponds to the couplings predicted by the SM [5]. Combinations of searches for di-Higgs production constrain κ_3 (also often referred to as κ_λ) to be between -1.2 and 7.2 at 95% confidence level (CL) [3, 4, 6]. The most recent combination of results for single- and di-Higgs production further constrains κ_3 to be between -0.4 and 6.3 (when other Higgs boson couplings are assumed to have their SM values) [7]. However, there have been no experimental constraints on λ_4 or its relation to λ_3 prior to the results presented in this paper.

This paper presents searches for the simultaneous production of three Higgs bosons — tri-Higgs (HHH) — in the six b -jet final state. Data collected during Run 2 of the LHC by the ATLAS experiment [8] between 2016 and 2018 are used. As well as a unique dependence on λ_4 and a dependence on λ_3 , HHH provides new sensitivity to Beyond SM (BSM) physics with extended scalar sectors. The results are interpreted in terms of three benchmark models.

First, SM-like scenarios are considered to place constraints on the Higgs self-coupling modifiers κ_3 and κ_4 . All leading-order gluon–gluon fusion (ggF) production modes represented in Figure 1 are included.

Second, scenarios extending the SM by adding two real SM-Higgs-like spin-0 bosons X and S are probed, which are hypothesised in several BSM models. The mass ranges $325 < m_X < 575$ GeV and $200 < m_S < 350$ GeV are considered and by convention $m_X > m_S$. The scenarios include cases in which either resonant or non-resonant production is dominant. All leading-order ggF production modes (illustrated in Figure 1) are considered, including interference between all diagrams, both BSM and SM. Models including the Two Real Scalar Model (TRSM) [9] and a “simple model for dark matter and CP violation” (DM-CPV) [10] feature this extension to the SM. For suitable parameter choices the HHH production cross-section is preferentially enhanced without increasing single- or di-Higgs production beyond experimental constraints. Negligible differences are found in the HHH event kinematics between the TRSM and DM-CPV models, so Monte Carlo (MC) simulated events are generated only in the TRSM as described in Section 3, and results are interpretable in both models. Furthermore, the mass ranges are chosen to fulfill perturbative unitarity bounds in the TRSM [9].

Finally, scenarios with resonant production of generic heavy spin-0 bosons X and S are also considered, with masses $m_X > m_S$, covering $550 < m_X < 1500$ GeV, and $275 < m_S < 1000$ GeV. The search covers benchmark scenarios in which both particles have either narrow or wide decay width, with resonances that have a width below or just above the detector resolution, respectively. Only resonant ggF production (Figure 1(a)) is chosen for consideration to give a simplified treatment. This interpretation allows the search to probe generically for resonances that lie beyond the masses permitted by the TRSM benchmark.

To enable these interpretations, the analysis is divided into three searches based on the kinematics of the signal models considered: “Non-resonant”, “Resonant” and “Heavy-resonant”. The Non-resonant search is used for the TRSM parameter space dominated by non-resonant production and the SM-like interpretation, the Resonant search is used for the TRSM parameter space dominated by resonant production, and the Heavy-resonant search is used for the generic heavy resonance signal models. Each search follows the

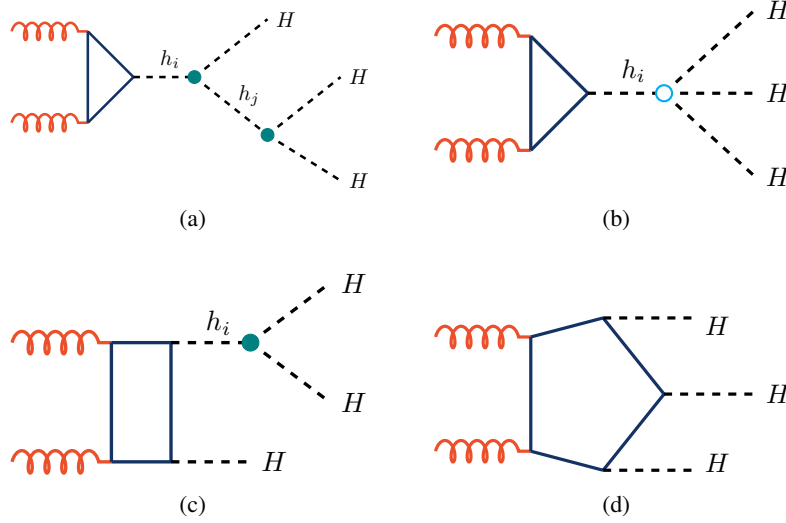


Figure 1: Leading-order Feynman diagrams for gluon–gluon fusion triple Higgs-boson production. The symbols h_i and h_j represent any of the SM Higgs H or heavy scalars, X and S . In particular, the resonant cascade decay is shown in (a). For the case where $h_i = h_j = H$ the solid circle indicates the tri-linear self-coupling λ_3 , and the open circle indicates the quartic-linear self-coupling λ_4 .

same general analysis strategy. Deep neural network (DNN) classifiers are trained to discriminate between the relevant signals and the SM background. The dominant SM background process in all searches is Quantum Chromodynamics (QCD) multijet production, which is estimated by using an entirely data-driven approach based on an extrapolation between different b -jet multiplicities. To obtain the final results in each search, a profile likelihood fit is performed over the binned DNN score distribution.

The structure of this paper is as follows. In Section 2 the ATLAS detector is described, followed by a summary of the data and MC simulated events used in Section 3. Section 4 explains how events are reconstructed, and Section 5 explains the analysis strategy and how signal events are selected. In Section 6, the estimate of the SM background is described, followed by an explanation of the statistical interpretation in Section 7. A summary of the uncertainties considered is presented in Section 8 and finally the results and conclusions are provided in Sections 9 and 10, respectively.

2 ATLAS detector

The ATLAS experiment [8] at the LHC is a multipurpose particle detector with a forward–backward symmetric cylindrical geometry and a near 4π coverage in solid angle.¹ It consists of an inner tracking detector (ID) surrounded by a thin superconducting solenoid providing a 2 T axial magnetic field, electromagnetic and hadronic calorimeters, and a muon spectrometer. The inner tracking detector

¹ ATLAS uses a right-handed coordinate system with its origin at the nominal interaction point (IP) in the centre of the detector and the z -axis along the beam pipe. The x -axis points from the IP to the centre of the LHC ring, and the y -axis points upwards. Polar coordinates (r, ϕ) are used in the transverse plane, ϕ being the azimuthal angle around the z -axis. The pseudorapidity is defined in terms of the polar angle θ as $\eta = -\ln \tan(\theta/2)$ and is equal to the rapidity $y = \frac{1}{2} \ln \left(\frac{E+p_z}{E-p_z} \right)$ in the relativistic limit. Angular distance is measured in units of $\Delta R \equiv \sqrt{(\Delta y)^2 + (\Delta \phi)^2}$.

covers the pseudorapidity range $|\eta| < 2.5$. It consists of silicon pixel, silicon microstrip, and transition radiation tracking detectors. Lead/liquid-argon (LAr) sampling calorimeters provide electromagnetic (EM) energy measurements with high granularity within the region $|\eta| < 3.2$. A steel/scintillator-tile hadronic calorimeter covers the central pseudorapidity range ($|\eta| < 1.7$). The endcap and forward regions are instrumented with LAr calorimeters for EM and hadronic energy measurements up to $|\eta| = 4.9$. The muon spectrometer (MS) surrounds the calorimeters and is based on three large superconducting air-core toroidal magnets with eight coils each. The field integral of the toroids ranges between 2.0 and 6.0 T m across most of the detector. The muon spectrometer includes a system of precision tracking chambers up to $|\eta| = 2.7$ and fast detectors for triggering up to $|\eta| = 2.4$. The luminosity is measured mainly by the LUCID-2 [11] detector, which is located close to the beampipe. A two-level trigger system is used to select events [12]. The first-level (L1) trigger is implemented in hardware and uses a subset of the detector information to accept events at a rate below 100 kHz. This is followed by a software-based trigger (HLT) that reduces the accepted event rate to 1 kHz on average depending on the data-taking conditions. A software suite [13] is used in data simulation, in the reconstruction and analysis of real and simulated data, in detector operations, and in the trigger and data acquisition systems of the experiment.

3 Data and Monte Carlo simulations

3.1 Data and triggers

The proton–proton (pp) collisions used in this paper were collected between 2016 and 2018, at a center-of-mass energy of $\sqrt{s} = 13$ TeV. They correspond to an integrated luminosity of 126 fb^{-1} , with an uncertainty of 0.84% [14] obtained using the LUCID-2 detector for the primary luminosity measurements, complemented by measurements using the inner detector and calorimeters. Only events that satisfy data quality requirements that ensure the stable operation of the ATLAS detector [15] are considered.

Events from each year satisfy triggers requiring multiple jets and b -tagged jets [16], which were implemented in 2016. These jets are reconstructed using the anti- k_t algorithm with radius parameter $R = 0.4$ [17, 18]. Jets originating from b -quarks are tagged using the MV2c20 (MV2c10) algorithm in 2016 (2017–2018) [16] operating at 60 – 70% identification efficiency as measured using simulated $t\bar{t}$ events. For all years, the triggers used require four jets with transverse momentum $p_T > 15$ GeV and $|\eta| < 2.5$ at L1 level. In 2016 and 2018, the trigger used requires two b -tagged jets and two additional jets at HLT level, all with $p_T > 35$ GeV (2b+2j). In 2017, a trigger requiring three b -tagged jets and one additional jet at HLT level, all with $p_T > 35$ GeV (3b+1j) is used instead. The triggers selected maximize the efficiency for the resonant (m_X, m_S) phase space within the TRSM perturbative unitarity bounds. Depending on the mass point and data-taking year, the triggers used are 90–98% efficient. During 2016, a fraction of the data taking (8.3 fb^{-1}) was affected by an inefficiency in the trigger-level vertex reconstruction, which reduced the efficiency of the algorithms used to identify b -tagged jets; those events are not retained for further analysis.

3.2 Signal models and event simulation

For all signal samples described in this section, MC simulated signal events are generated using MADGRAPH [19] 2.9.5 at leading-order in the strong coupling constant, using the NNPDF3.0NLO parton distribution function (PDF) set [20] with the A14 set of tuned parameters (tune) [21]. The $H \rightarrow b\bar{b}$

branching fraction is taken to be 0.582, and its total width 4.088 MeV corresponding to the SM values for a Higgs boson mass of 125 GeV [22]. All events are showered with PYTHIA 8.245 [23], and a generation-level filter requiring at least four b -tagged² jets with $p_T > 25$ GeV is applied.

For the SM-like interpretation in the Non-resonant search a single sample is generated at $(\kappa_3, \kappa_4) = (1, 1)$. All diagrams in Figure 1 are included, fully accounting for interference between them. The Higgs bosons are decayed exclusively to $b\bar{b}$. A reweighting [24] allows the sample kinematics to be altered to reflect different values of κ_3 and κ_4 , which follows a similar procedure to that outlined in Ref. [25]. The SM HHH ggF production cross-section at a center-of-mass energy of $\sqrt{s} = 13$ TeV is taken as $\sigma_{HHH}^{SM} = 0.079^{+0.012}_{-0.013}$ fb at next-to-next-to-leading-order (NNLO), calculated by extrapolating cross-sections at higher \sqrt{s} values presented in Ref. [26] and including uncertainties from missing higher-order corrections (+5%, -8%) and the finite top quark mass approximation ($\pm 15\%$).

For the Resonant and Non-resonant searches, Benchmark 3 of the TRSM, defined in Ref. [9], is used for signal generation³. Here, the SM is extended by two neutral CP-even scalars, X and S . Interactions between X/S and non-Higgs SM particles come via the mixing between the X/S fields and the SM Higgs field, making the couplings proportional to the SM-Higgs couplings. Here, by choice, $m_X \geq m_S \geq m_H$. The benchmark chosen sets the TRSM parameters to maximize HHH production through a resonant cascade decay $gg \rightarrow X \rightarrow HS \rightarrow HHH$, though all possible leading-order $gg \rightarrow HHH$ diagrams are generated together with interference.

For the TRSM signals, the Higgs bosons are decayed inclusively using PYTHIA 8.245 [23]. A set of 27 (m_X, m_S) points are chosen within the perturbative unitarity bounds of the TRSM, with $325 \leq m_X \leq 575$ GeV and $200 \leq m_S \leq 350$ GeV. This includes two categories: 19 “resonant” points where $m_X > m_S + m_H$ and $m_S > 2m_H$ such that the resonant cascade decay is on-shell and dominant, and eight “non-resonant” points where $m_S \leq 2m_H$ such that the resonant cascade is off-shell and non-resonant diagrams become dominant.

The results of the Resonant and Non-resonant searches can also be interpreted in the DM-CPV model, presented in Ref. [10], using benchmarks 1 and 3 defined therein. These benchmarks are defined to maximize HHH production, and can be extended across the same (m_X, m_S) plane as the TRSM. In the nomenclature of Ref. [10], $X = h_3$ and $S = h_2$.

For the Heavy-resonant search, more generic benchmark models are considered, to represent a broader class of possible BSM models to which this analysis is sensitive. The TRSM Benchmark 3 is used as a starting point, but only the cascade resonance decay (Figure 1(a)) is generated. The widths of the X and S particles are set to 1% (20%) of their masses, to define narrow (wide) width signal models. These modifications lead to generic signal samples that no longer represent the TRSM.

The generic heavy-resonant signals are generated similarly to the other models, but using MADSPIN [28] for the $S \rightarrow HH$ decay. The Higgs bosons are decayed exclusively to $b\bar{b}$. At each width, 45 samples are produced, with $550 \leq m_X \leq 1500$ GeV and $275 \leq m_S \leq 1000$ GeV.

For all generated signal events, the detector response is simulated [29] using a fast parameterized simulation of the calorimeters [30], and the full GEANT4 [31] simulation for the other sub-detectors. Events are processed using the same reconstruction software used for the data. The effect of multiple interactions in

² At truth-level, b -tagged jets are defined as jets which have a b -hadron of $p_T > 5$ GeV lying within a cone of size $\Delta R = 0.3$ from their axis.

³ A more recent benchmark satisfying additional constraints from the electroweak phase transition is presented in Ref. [27], but the kinematic differences between the new benchmark and the one used here are minimal.

the same and neighboring bunch crossings (pileup) is modeled by overlaying the simulated hard-scattering event with inelastic pp events generated with PYTHIA 8.186 [32] using the NNPDF2.3LO PDF set [33] and the A3 set of tuned parameters [34].

4 Event reconstruction

For proton–proton collision events, primary vertices are reconstructed using at least two charged-particle tracks with $p_T > 500$ MeV, measured in the ID [35]. The primary vertex with the largest sum of squared track momenta is assigned as the hard-scatter vertex.

Hadronic jets are reconstructed from particle flow objects [36], using the anti- k_t algorithm with a radius parameter of $R = 0.4$. These are calibrated using a multi-step procedure as outlined in Ref. [37]. Jets are required to have $p_T > 20$ GeV and $|\eta| < 2.5$. To suppress jets originating from pileup, a neural-network based jet vertex tagger (NNJVT) is used, which is an updated version relative to the likelihood based algorithm described in Ref. [38]. Jets with $20 < p_T < 60$ GeV are required to satisfy a selection on the NNJVT with a 0.88 – 0.99 probability of correctly identifying hard-scatter jets depending on the p_T , as evaluated in $Z(\rightarrow \mu\mu) + \text{jets}$ events with a mean of 33.7 interactions per bunch crossing. Outside of this p_T range, no NNJVT requirement is applied.

Jets originating from b -quarks are identified using a DNN-based algorithm (DL1d) [39–41]. The identification requirement used selects jets with $p_T > 20$ GeV containing b -hadrons, with an efficiency of 77%, and has a probability of 0.38% (15.5%) of misidentifying light-flavor (charm) jets as determined in a sample of simulated $t\bar{t}$ events. The b -tagging efficiencies in simulated events are corrected to match those measured in data [42–44]. Uncertainties related to the trigger-level and offline flavor-tagging selections are described in Section 8.

To account for energy lost to muons in semileptonic b -hadron decays, a momentum correction [45] is applied. For this purpose, muons are reconstructed. Muon candidates are found by matching ID tracks with either MS tracks or aligned individual hits in the MS and performing a combined track fit [46]. They are required to have $p_T > 4$ GeV, $|\eta| < 2.5$, and to satisfy the Medium identification criteria defined in Ref. [46]. If any muons are within a cone of $\Delta R = \min(0.4, 0.04 + 10/p_T^\mu [\text{GeV}])$ around the jet axis, their four-momentum is added to that of the jet. Additionally, the energy in the calorimeter deposited by the muons (computed according to Ref. [47]) is subtracted from the jet to avoid double-counting.

Corrections are applied to all signal MC simulated events to account for differences observed between the jet trigger efficiencies in data and simulation. These corrections (scale factors, SFs) are calculated from the ratios of event-level jet trigger efficiencies in data and MC, which are in turn constructed from per-jet trigger efficiencies. The efficiencies are estimated in $t\bar{t}$ MC simulated events and data satisfying a $t\bar{t}$ -like event selection with at least one top quark decaying leptonically and collected using triggers requiring one muon and one jet to obtain an unbiased sample enriched in b -jets. The $t\bar{t}$ events were simulated using POWHEG Box v2 [48–51] at NLO with the NNPDF3.0NLO [20] PDF set and A14 tune [21]. PYTHIA 8.230 [23] was used to model the parton shower, hadronization, and underlying event. Separate SFs are estimated for the L1 and HLT, and for each jet as a function of p_T .

For each of the jets in the event selection, and for each data-taking year, the L1 trigger per-jet efficiencies are calculated. The efficiency is defined as the fraction of the n^{th} p_T -ordered jets geometrically matched⁴ to an

⁴ The geometric matching requires $\Delta R < 0.4$ between the reconstructed and trigger-level jets.

L1 jet and passing the L1 trigger threshold in that year. Similarly, the HLT per-jet efficiencies are calculated as the fraction of these L1-trigger-passing n^{th} jets that are geometrically matched to an HLT jet and pass the HLT trigger threshold in that year. The L1 and HLT per-jet efficiencies are both calculated in bins of jet p_{T} . These are combined to give overall event-level L1 and HLT jet trigger efficiencies, accounting for the combinatorial possibilities of selecting four jets that fired the trigger in events with more than four jets. The L1 and HLT SFs are then calculated and multiplied to provide an overall SF for each event.

5 Analysis strategy

5.1 Event selection and strategy overview

To be considered in the analysis, all data and MC simulated events must satisfy the trigger requirements defined in Section 3.1 and a set of preselection requirements, now described. At least six jets are required, with at least four having $p_{\text{T}} > 40 \text{ GeV}$ in line with the trigger requirements. At least four jets must be b -tagged.

The analysis further categorizes events into three orthogonal regions, based on the multiplicity of b -tagged jets. Denoted $4b$, $5b$ and $6b$ respectively, these regions are defined to satisfy the preselection and required to have exactly four, exactly five, or at least six b -tagged jets. The $6b$ region is enriched in the signal processes and is also referred to as the signal region (SR). The $5b$ and $4b$ regions are control regions (CRs) enriched in background processes and are used to derive the $6b$ background estimate. The overall acceptance times efficiency for the SM signal (for which only the $H \rightarrow bb$ decay is considered) to fall into the $6b$ region is 5.5%. For the $4b$ and $5b$ regions the acceptance times efficiency is 27% and 17% respectively.

The general analysis strategy is the same for each of the three searches: Non-resonant, Resonant and Heavy-resonant. In each case a DNN classifier is trained to discriminate between the signal models and the SM background, which is dominated by multijet production. A profile likelihood fit is performed over the binned DNN score distribution to obtain the final results.

The kinematic properties of the reconstructed Higgs boson candidates provide important input features for the DNNs. A mass-based pairing algorithm is used to assign jets to each of three Higgs boson candidates, as described in Section 5.2.

A fully data-driven background estimate is used for the analysis. The approach assumes that the kinematic properties of the background processes are similar between events with four, five, or six identified b -jets in the final state. Systematic uncertainties arising from this approach and its core assumption are discussed in Section 8. The background estimate in the $6b$ search region is obtained by extrapolating each DNN score distribution in data from the $4b$ and $5b$ regions. Both the $5b$ and $6b$ regions are included in the fit.

Figure 2 shows a diagram of the different regions in the analysis and how they are used in the final fit. Each DNN score distribution is divided into three regions. The ‘‘High-Score’’ region contains 90% of the combined yields of the relevant signal samples, and provides the bulk of the analysis sensitivity in the fit. The ‘‘Low-Score’’ region is enriched in background, and is used to constrain the background estimate in the fit as well as to derive systematic uncertainties on it. The Low-Score $4b$ data are used in the systematic uncertainty estimate but are not included in the final fits, preventing any double counting of degrees of freedom. The ‘‘Excluded’’ region lies below the Low-Score region and is defined as the region in which the DNN score distribution extrapolation fails to model the observed $6b$ data within one standard deviation of

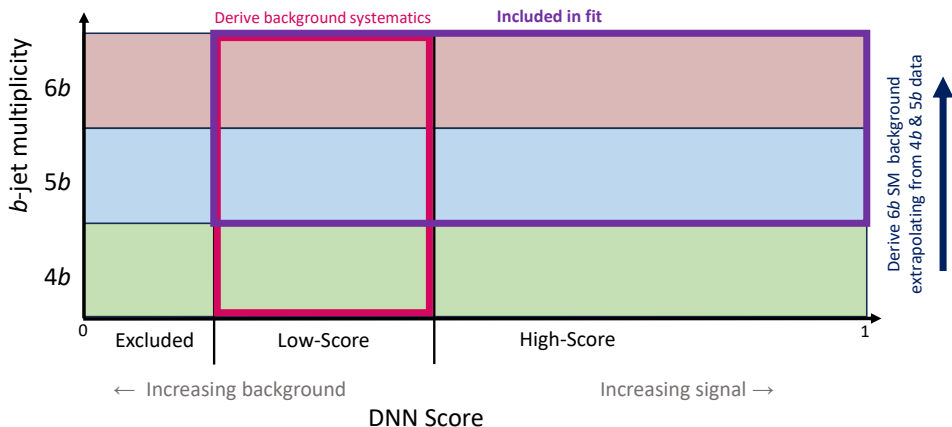


Figure 2: A schematic diagram of the analysis strategy and regions. The strategy is the same for each DNN, although the precise selections defining the Excluded, Low-Score, and High-Score regions differ. The procedure to form the $6b$ background estimate by extrapolating from data in the $4b$ and $5b$ regions is described in Section 6.

the statistical uncertainty. Discarding the Excluded region reduces the size of the systematic uncertainties arising from the small differences in kinematics between the remaining Low- and High-Score regions.

5.2 Higgs boson reconstruction

To reconstruct the three Higgs boson candidates in signal events, which is useful to help discriminate between the signals and background, the six jets from the Higgs decays (labeled jets $a - f$) must be selected and paired. Pairing is performed on all events satisfying the preselection requirements. In the case of $6b$ events, the six jets to pair are the six highest p_T b -tagged jets. For $4b$ ($5b$) events, the six jets to pair are all of the b -tagged jets, plus the two (one) highest- p_T non- b -tagged jets.

The pairing algorithm used is defined by minimizing

$$|m_{H1} - 120 \text{ GeV}| + |m_{H2} - 115 \text{ GeV}| + |m_{H3} - 110 \text{ GeV}|, \quad (1)$$

over all possible permutations of jet pairs (for jets $a - f$) that satisfy these transverse-momentum constraints:

$$p_T^{ab} > p_T^{cd} > p_T^{ef}, \text{ where } p_T^{H1} = p_T^{ab}, p_T^{H2} = p_T^{cd} \text{ and } p_T^{H3} = p_T^{ef}.$$

The numeric constants in Eq. 1 are chosen based on the peaks of the m_{Hi} distributions in simulated signal events. These differ from the observed Higgs boson mass of 125 GeV due to detector effects, energy lost to neutrinos from the b -hadron decays, and out-of-cone radiation.

The performance of the pairing algorithm is assessed using the pairing efficiency, which is defined as the fraction of signal events that were correctly paired out of all events where a correct pairing is possible. Correct pairing may not be possible if the jets cannot all be geometrically matched to truth-level b -quarks from each Higgs boson decay. This can occur if any of the six jets falls out of the tracker acceptance ($|\eta| > 2.5$), or if two b -quarks are close enough together than they are matched to the same jet. The correct pairing is defined using a geometric matching between MC truth jets (reconstructed using the anti- k_r algorithm with $R = 0.4$ on stable, final-state particles from MC generators) and reconstructed jets. Correct pairing is possible in 74–84% of BSM signals, depending on m_X and m_S . The pairing efficiencies for

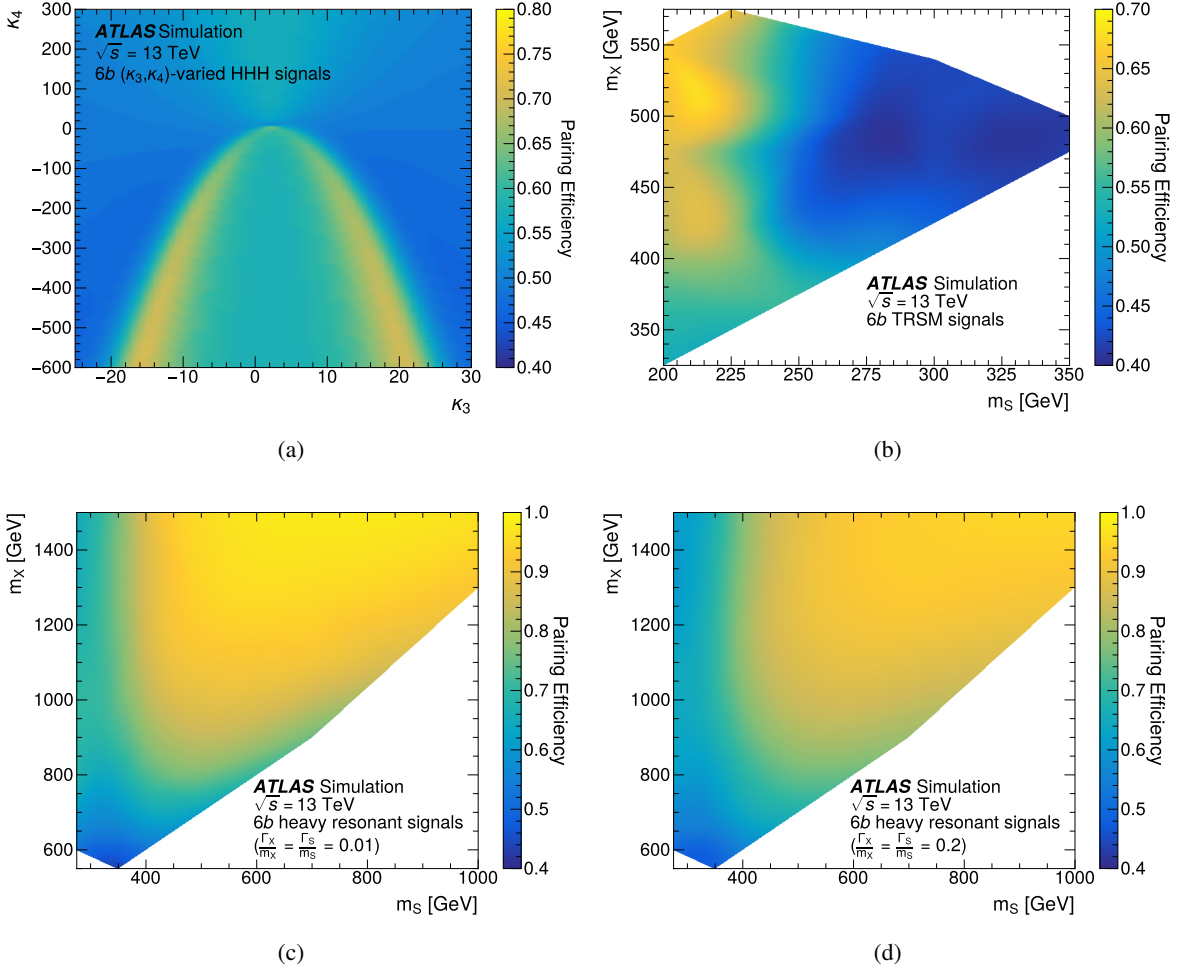


Figure 3: Jet pairing efficiencies over the parameter space for the (a) SM-like (κ_3, κ_4) scan, (b) TRSM, and (c) narrow-width or (d) wide-width heavy resonance signals. The pairing efficiency is evaluated in the $6b$ region when a correct pairing is possible — that is, the six leading jets are geometrically matched to truth-level b -quarks. A cubic Bézier polynomial is used to interpolate across the plane. Areas of the (m_X, m_S) phase space not covered by this search are shown in white.

each signal model parameter plane are shown in Figure 3. In scans over the (m_X, m_S) space the pairing efficiency is calculated at each simulated mass point and a cubic interpolation using the nearest four points is used. For the scan of the (κ_3, κ_4) space a parametric reweighting is used and therefore an arbitrarily smooth evaluation of pairing efficiency is achieved. A correct pairing is possible in 81% of SM signal events, and the pairing efficiency is 61%. The change in pairing efficiencies over the signal planes is a result of changing kinematics — the higher the p_T of the Higgses, the easier the pairing. For the SM-like and TRSM planes, the kinematic changes are due to the changes in interference between diagrams across the parameter space.

5.3 Machine learning classifiers

A DNN is trained to classify events as signal- or background-like for each search: Non-resonant (nonresDNN), Resonant (resDNN) and Heavy-resonant (heavyresDNN). The resulting classifier score distribution for each search is used as the final analysis discriminant.

For all DNNs, data events in the $5b$ region (which form the basis of the background estimation, as is discussed in Section 6) are used as the background training sample. Potential signal contamination in $5b$ data is considered to have a negligible impact for this purpose, as it has yields of $O(1\%)$ of the $5b$ data yield, depending on the signal model. All resonant TRSM signals are combined to form the resDNN signal training sample, and all heavy resonance signals (both narrow and wide width) are combined to form the heavyresDNN signal training sample. Each simulated (m_X, m_S) point is equally weighted in the training samples. For nonresDNN, the SM HHH signal, which has similar kinematics to the non-resonant TRSM signals, is used as the signal training sample.

These signals were chosen to maximize training sample size and to group samples with similar enough kinematics for the DNN to perform well. The performance is enhanced by assigning “class weights” to the background such that the effective yield matches the signal yields during training. To avoid overtraining and benefit from the full set of available events, orthogonal training and testing/validation datasets are used, through a k -fold splitting procedure with $k = 2$ [52], split by odd vs even event numbers. Two DNNs are trained such that the network trained on one half of the events is applied to the other half of the events in the analysis.

For each DNN ten discriminating kinematic variables are chosen as input features. The ten variables were chosen from a larger set of kinematic variables that have good shape separation between signals and backgrounds. The ten chosen features have the highest Shapley values [53] (a common measure to quantify how impactful an input feature is on the classifier output), and minimize absolute correlations between variables to reduce redundancy. Variables that are correlated differently in signal and background samples are *not* excluded as they provide discriminating power. In addition variables are chosen to have minimal correlation with the b -jet multiplicity to reduce the size of the systematic uncertainties in the b -jet multiplicity extrapolation.

The input features for each DNN are listed and defined in Table 1, and the distributions of the most powerful kinematic variable for each DNN are shown in Figure 4. Distributions for $4b$, $5b$ and $6b$ data and example signal samples are shown. Ratios of data with different b -jet multiplicities, including the double ratio (ratio $6b/5b$ over ratio $5b/4b$) are additionally shown. The double ratio is used to estimate the background modeling systematic uncertainties as described in Section 8.

The DNNs are implemented using Keras [54] with a Tensorflow [55] backend. A standard binary cross-entropy loss function is used, with rectified linear unit (ReLU) activation [56, 57], an Adam [58] optimizer, and dropout regularization [59] between layers. The hyperparameters were optimized to maximize the sensitivity of the analysis. These include three hidden layers with 24 hidden nodes per layer, a learning rate of 0.01 (0.005), a batch size of 128 (256), and a dropout rate of 0.1, for resDNN (nonresDNN). For heavyresDNN, this includes four hidden layers with 24 hidden nodes per layer, a learning rate of 0.005, a batch size of 256, and a dropout rate of 0.1.

All DNN score distributions span from zero to one. For nonresDNN, the Low-Score region starts above 0.100 (defined such that below this value the background DNN score distribution extrapolation fails to model the observed $6b$ data within one standard deviation), and the High-Score region (containing 90% of

Table 1: Summary of the input variables used in each DNN. Check marks denote which input is used for each DNN.

Variable	Definition	nonres	res	heavyres
m_H -radius	Euclidean distance between the event and the pairing center (120, 115, 110) GeV in the (m_{H1}, m_{H2}, m_{H3}) volume.	✓		✓
m_{H1}	Reconstructed mass of the highest p_T Higgs boson candidate.	✓		✓
$\text{RMS}(m_{ij})$	Root-mean-squared (RMS) of the invariant mass of all possible jet pairs that can form a Higgs boson candidate.	✓		✓
$\text{RMS}(\Delta R_{ij})$	RMS of the angular separation between all possible jet pairs that can form a Higgs boson candidate.	✓	✓	✓
$\text{RMS}(\eta)$	RMS of the pseudo-rapidity of the Higgs boson candidates.	✓		✓
Skewness ΔA_{ij}	Skewness of $\cosh(\Delta\eta_{ik}) - \cos(\Delta\phi_{ik})$, where i, k are all possible jet pairs that can form a Higgs boson candidate.		✓	
H_T^{6j}	Scalar sum of the p_T of the 6 jets selected to reconstruct the 3 Higgs boson candidates.		✓	
$\cos\theta$	In the (m_{H1}, m_{H2}, m_{H3}) coordinate system, θ is the angle between the vector from the origin to the event's reconstructed mass of the Higgs boson candidates, and the vector from the origin to (120, 115, 110) GeV.		✓	
Aplanarity $_{6j}$	The fraction of p_T from the 6 jets selected to reconstruct the 3 Higgs boson candidates lying outside the plane formed by the 2 highest p_T jets.	✓	✓	✓
Sphericity $_{6j}$	Isotropy of the momenta of the 6 jets selected to reconstruct the 3 Higgs boson candidates.		✓	
Transverse Sphericity $_{6j}$	Isotropy of the p_T of the 6 jets used for Higgs reconstruction, within the $x - y$ plane.	✓		
Sphericity	Isotropy of the momenta of all jets in the event.			✓
$\eta - m_{HHH}$ fraction	$\frac{\sum_{i,k} 2p_T^i p_T^k (\cosh(\Delta\eta(ik)) - 1)}{m_{HHH}^2}$ where i, k are all possible jet pairs that can form a Higgs boson candidate, and m_{HHH} is the reconstructed tri-Higgs invariant mass.		✓	
ΔR_{H1}	Angular separation between the jets paired to form the highest p_T Higgs boson candidate.	✓	✓	✓
ΔR_{H2}	Angular separation between the jets paired to form the second-highest p_T Higgs boson candidate.	✓	✓	✓
ΔR_{H3}	Angular separation between the jets paired to form the lowest p_T Higgs boson candidate.	✓	✓	✓

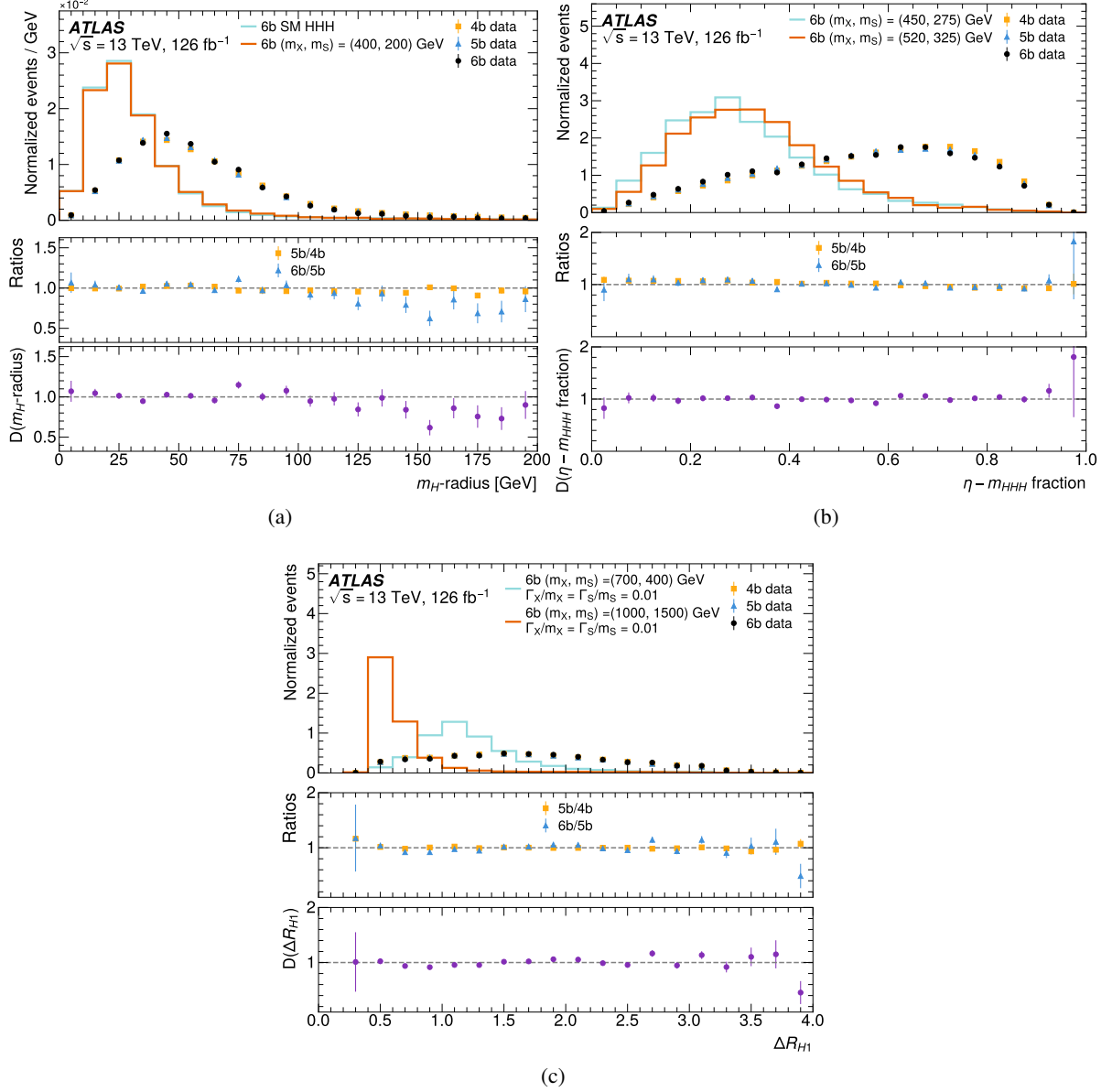


Figure 4: In the top panel of each plot, the distribution of the most discriminating variable used in each DNN training is shown: (a) m_H -radius for nonresDNN, (b) $\eta - m_{HHH}$ fraction for resDNN, and (c) ΔR_{H1} for heavyresDNN. The distributions for the $4b$, $5b$ and $6b$ data and example signal samples are shown, with all histograms normalized to unit area. In the middle panel of each plot, the ratios of data with different b -jet multiplicities are shown. Finally in the bottom panel, the ratio $6b/5b$ divided by the ratio $5b/4b$ — D — is shown for data; D is used to estimate the size of the systematic uncertainty in the b -jet extrapolation method as described in Section 8.

the combined signal yield) above 0.552. For resDNN, the Low-Score region starts above 0.05, and the High-Score region above 0.367. For heavyresDNN, the Low-Score region starts above 0.100, and the High-Score region above 0.790.

6 Background estimation

As introduced in Section 5, the dominant background process for a final state of ≥ 6 b -quarks is QCD multijet production. The background is modeled via a data-driven approach using the data with four and five b -jets to predict the background yields with at least six b -jets. The assumption of this method is that the kinematic properties of the background do not significantly change relative to b -jet multiplicity, as is observed in Figure 4 for the most important kinematic features used in the DNNs. The assumption is further validated by comparing the ratio of $4b$ and $5b$ data evaluated exclusively in the Low- and High-Score regions. Therefore, background-enriched regions in DNN score and b -jet multiplicity are used to construct the $6b$ background model and its associated systematic uncertainties in the search region. The feature selection strategy (described in Section 5.3) minimizes the difference between the shape of the DNN score distribution in $4b$ and $5b$ data and therefore reduces the size of the associated uncertainties, which are discussed in Section 8.

Both the Low- and High-Score regions for $5b$ and $6b$ data are included in the fit, as discussed in Section 5. The Low-Score region is used to estimate the background shape uncertainties, as discussed in Section 8. The Excluded region tends to have large shape differences between $4b$, $5b$ and $6b$ data and is not used for the remainder of the analysis. The removal of the Excluded region is crucial to ensure that the analysis operates in a region where the kinematic properties are not highly dependent on b -jet multiplicity, reducing the size of the systematic uncertainties and ensuring that by construction the assumptions of the method remain valid in the Low- and High-Score regions.

Data in the $4b$ and $5b$ Low- and High-Score regions are used to model the expected background contribution in the $6b$ Low- and High-Score regions, respectively. For each DNN an extrapolation across b -jet multiplicities is performed in the DNN score to model the expected background contribution in the $6b$ region:

$$N_i^{6b, \text{predicted}} = \mu_{\text{NF}} \cdot B_i \cdot \left(\frac{(N^{5b}/N^{4b})_i}{N^{5b}/N^{4b}} \right), \quad (2)$$

where N is the observed number of events (except when explicitly noted as in $N_i^{6b, \text{predicted}}$), B are a set of unconstrained bin-by-bin parameters fit from the $5b$ region, the superscript denotes the region ($4b$, $5b$, or $6b$), and the subscript i denotes the i^{th} bin in the DNN score distribution. The normalization on the background model is μ_{NF} , which is fit in situ to the data as described in the next section. In the case where there is no signal contribution, $\mu_{\text{NF}} = N^{6b}/N^{5b}$ and $B_i = N_i^{5b}$. However, when the signal strength is non-zero $\mu_{\text{NF}} < N^{6b}/N^{5b}$ and $B_i < N_i^{5b}$.

The inclusion of the term $(N^{5b}/N^{4b})_i/(N^{5b}/N^{4b})$ in Eq. 2 extrapolates the shape of the DNN score distribution as a function of b -jet multiplicity. Such a shape extrapolation is observed to produce better modeling in the Low-Score region.

7 Statistical interpretation

Test statistics are built from the profile likelihood ratio (PLR) following the prescription for discovery of a positive signal and one-sided upper limits detailed in Ref. [60]. The likelihood model assumes independent Poisson-distributed event counts in each bin of the $5b$ and $6b$ DNN score distributions in the Low-Score and High-Score regions, which are included in the fit. Nuisance parameters (NPs) describing the effect of systematic uncertainties in the signal ($\vec{\phi}$) are fully correlated between the $5b$ and $6b$ regions. An orthogonal set of NPs $\vec{\theta}$ describes the background extrapolation from the $5b$ to $6b$ region. The full expression of the parameterized likelihood model of the observed yields is:

$$\begin{aligned}
\mathcal{L}(\vec{N}^{5b,6b}, \vec{S}^{5b,6b} | \vec{\theta}, \vec{\phi}, \vec{\gamma}^{5b,6b}, \mu_s, \mu_{\text{NF}}) = & \prod_{i \in \text{bins}} \left[\text{Pois} \left(N_i^{6b} \middle| \mu_{\text{NF}} f_i(\vec{\theta}) B_i + \mu_s w_i^{6b}(\vec{\phi}) \gamma_i^{6b} S_i^{6b} \right) \right. \\
& \times \text{Pois} \left(N_i^{5b} \middle| B_i + \mu_s w_i^{5b}(\vec{\phi}) \gamma_i^{5b} S_i^{5b} \right) \left. \right] \\
& \times \prod_{m \in \text{bkg. systs}} \frac{1}{\sqrt{2\pi}} e^{-\theta_m^2/2} \\
& \times \prod_{k \in \text{sig. systs}} \frac{1}{\sqrt{2\pi}} e^{-\phi_k^2/2} \\
& \times \prod_{i \in \text{bins}} \left[P_\Gamma \left(v_i^{5b} \middle| \gamma_i^{5b} v_i^{5b} \right) P_\Gamma \left(v_i^{6b} \middle| \gamma_i^{6b} v_i^{6b} \right) \right].
\end{aligned} \tag{3}$$

The first two Poissonian terms describe the constraints from the observed data \vec{N} . Superscripts $5b$ and $6b$ are used throughout to distinguish the $5b$ CR from the $6b$ SR. Signal leakage into the $5b$ region is considered via S_i^{5b} . B_i are an unconstrained set of bin-by-bin yields fit from the CR and μ_s is the signal strength and the parameter of interest. The precise manner in which $\vec{\phi}$ and $\vec{\theta}$ change each bin of the yields is encapsulated in $w_i(\vec{\phi})$ and $f_i(\vec{\theta})$, respectively. The nominal value of $f_i(\vec{\theta})$ is the ratio of the DNN score shapes for the $5b$ and $4b$ data, $((N^{5b}/N^{4b})_i)/(N^{5b}/N^{4b})$, as appears in Eq. 2. Therefore, $f_i(\vec{\theta})$ performs the DNN score shape extrapolation to the $6b$ region. The uncertainties in the extrapolation are assessed using alternative shapes as discussed in Section 8. The nominal value of $w_i(\vec{\phi})$ is unity, and it describes the way theoretical and experimental uncertainties both change the shape and normalization of the signal.

The third and fourth terms (products over m and k) describe the Gaussian constraints for the NPs. The observed MC signal yields \vec{S} are multiplied by nuisance parameters $\vec{\gamma}$ in the final term to account for the limited MC sample size. The generalization of the Poisson distribution to continuous variables P_Γ is used to represent the MC statistical uncertainty by constraining $\vec{\gamma}$. The \vec{v} are constants constructed to provide the correct uncertainty sizes in the constraint term; they can be viewed as “effective” numbers of MC events, accounting for event weighting.

The choice of binning is different for each of the three DNNs. The resDNN score distribution is fit from 0.05–1.0 in 19 bins of equal width 0.05. The heavyresDNN score distribution is fit from 0.1–1.0 with equally spaced bins of 0.05. Likewise, the nonresDNN score is fit in the region 0.1–1.0 with equal bins of width 0.05, except for the final bin which is subdivided into two equally sized bins of width 0.025. Dividing the final bin in this search increases sensitivity. The choice of binning is a trade-off between sensitivity and

the ability to model systematic uncertainties in the data-driven background shape, as discussed in the next section.

8 Systematic uncertainties

The systematic uncertainties considered include experimental uncertainties, uncertainties in the shape of the data-driven background modeling of the DNN score distribution, and theoretical modeling uncertainties in the simulated signal samples.

The dominant systematic uncertainty in this search is the uncertainty in the shape of the background DNN score distribution. As described in Section 6, the background model extrapolates the shape of the DNN score distribution as a function of the b -jet multiplicity, with the normalization of the background model μ_{NF} determined in situ by the fit to the observed data. Due to the data-driven nature of the background estimate, the shape extrapolation uncertainty is the only systematic uncertainty that affects the background prediction. The shape extrapolation will agree with the $6b$ data perfectly when the DNN score shape differences between the $6b$ and $5b$ regions agree with the shape differences between $5b$ and $4b$. However, this cannot be assumed, and the size of the non-closure in the extrapolation method in the signal-depleted Low-Score region is used to estimate the systematic uncertainty in the extrapolation method. The double ratio $D(v)$ is introduced, which compares the shape differences between the $6b$ and $5b$ regions and the $5b$ and $4b$ regions (each themselves ratios) as a function of the DNN input variable v :

$$D(v) = \left(\frac{(N^{6b}/N^{5b})(v)}{N^{6b}/N^{5b}} \right)_{\text{Low-Score}} \div \left(\frac{(N^{5b}/N^{4b})(v)}{N^{5b}/N^{4b}} \right)_{\text{Low-Score}} \quad (4)$$

where the ratios in the numerators are functions of the DNN input variable v in the Low-Score region. The double ratio $D(v)$ is thus the non-closure in the multiplicative extrapolation method in the Low-Score region as a function of v . The binned quantity $D_i(v)$ is $D(v)$ averaged over the events in bin i of the DNN score distribution. In this context i runs over both Low- and High-Score regions, thereby applying the observed non-closure in the Low-Score region as a systematic uncertainty in the High-Score region.

Non-closure in the extrapolation method is quantified by deviations from $D_i(v) = 1$. The nominal background model (Eq. 2) is re-weighted by the value of $D_i(v)$ to produce a set of systematically varied models, with each of the 10 DNN inputs producing a different template. The variations are considered fully correlated between each bin i of the DNN. This method does not rely on any assumption that $D_i(v) = 1$. Rather, it assumes that deviations from $D_i(v) = 1$ due to background processes are similar in the Low-Score and High-Score regions. This assumption is validated in the background-enriched $4b$ and $5b$ regions. It is observed that the ratios $(N^{5b}/N^{4b})(v)$ evaluated in the Low- and High-Score regions are compatible within statistical fluctuations, an agreement which has been reinforced by removing the very low score events (Excluded region) from the analysis. The multiplicative variations to the nominal background template from $D_i(v)$ are symmetrized about $D_i(v) = 1$ for up and down variations.

Only a subset of 10 possible shape variations (one for each of the 10 DNN input variables) are applied as systematic uncertainties. A pruning procedure is used that removes shape variations that are expressible as linear combinations of other shape variations to avoid double counting. The pruning procedure is to iteratively add new systematic variations (ordered by largest single bin deviation) until the set of excluded variations are well modeled by the set of included variations. Specifically, a profile likelihood fit to each of

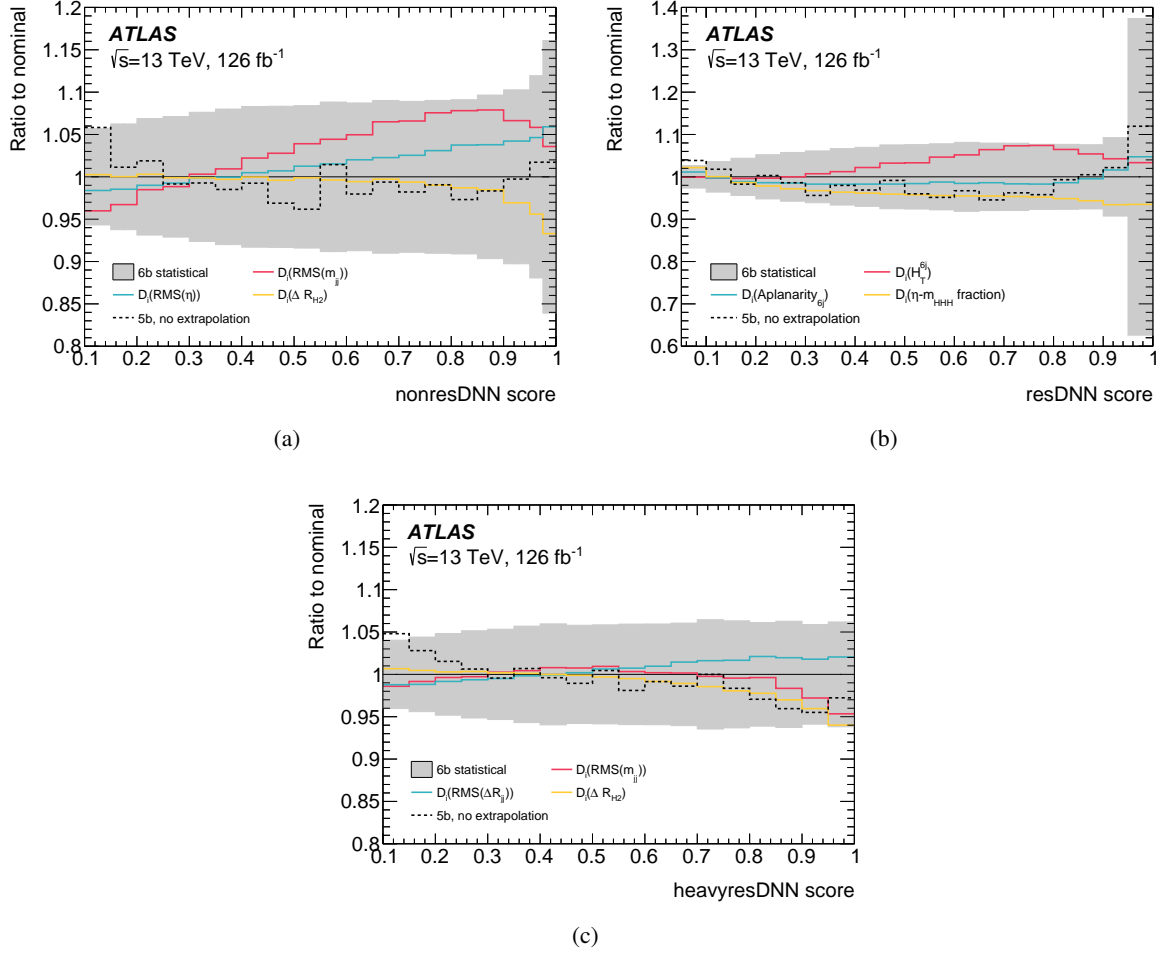


Figure 5: Ratios of the shape-varied models relative to the nominal background models ($D_i(v)$) for the selected input kinematics that survived pruning of the (a) nonresDNN (b) resDNN and (c) heavyresDNN. The gray band is the size of the statistical uncertainty in the expected $6b$ background for reference. The dashed line is the shape of the $5b$ data with no extrapolation applied. The shape systematic uncertainties are all smaller than the expected $6b$ background statistical uncertainty for each bin and are on the same order as the size of the extrapolation from $5b$ data. The binning matches exactly the scheme used for the PLR fit as described in Section 7.

the excluded variations is performed, with the only degrees of freedom being the included shape variations. The procedure terminates once the maximum χ^2 of all of the fits to the excluded shapes is less than 1. It is found that for each DNN, a subset of three shape variations is enough to model all 10 shapes sufficiently well.

Figure 5 shows the pruned subset of shape variations for each of the DNNs. The shape variations are always smaller than the statistical uncertainty in the expected $6b$ data. For reference the $5b$ data without extrapolation is shown. The difference between the observed $5b$ data and the extrapolated nominal $6b$ template is on the same order as the derived shape systematic variations.

Experimental uncertainties in luminosity, pileup reweighting, jet energy scale and resolution, NNJVT efficiency, trigger efficiency, and b -tagging efficiency are considered. As the background model is entirely data-driven, these uncertainties only affect the simulated signal MC events. The pileup uncertainty is

estimated according to the methods described in Ref. [61]. Uncertainties in the jet energy scale and resolution, NNJVT efficiency, and b -tagging efficiency are applied on a per-jet level and are estimated from calibrations and comparisons between different event simulation models [36, 37, 62]. The uncertainty in the NNJVT efficiency is estimated following the technique in Ref. [38].

The uncertainty in the trigger efficiency is estimated in data and MC using triggers requiring one muon and one jet so as not to bias the fully hadronic trigger efficiency measurement. The uncertainty in the jet-level trigger SF is estimated as the difference between the nominal SF and a SF derived using $t\bar{t}$ MC samples with different matrix elements and parton shower models. One alternative sample uses an alternative matrix element next-to-leading-order (NLO) matching scale (pThard), and another uses Herwig7 [63] in place of Pythia8 for the parton showering. The event-level SF applied is built from the jet-level SFs considering all possible combinations of which jets may have fired the trigger.

A 5% uncertainty is applied to the signal MC samples to cover the differences between the b -tagging applied at trigger level (MV2c10 for 2016 and MV2c20 for 2017–2018) [16] and at reconstruction level (DL1d) [39–41]. Given that an event has satisfied the offline selection of six b -jets, it has a larger than 99% chance of satisfying the trigger’s online b -tagging. Therefore the 5% uncertainty is much larger than the trigger inefficiency in the region most sensitive to the presence of a signal.

Modeling uncertainties in the signal MC event simulations are also considered and are calculated using an identical procedure for all signal models considered. To estimate the uncertainty due to higher-order terms in the perturbative expansion of the cross-section a 7-point variation in renormalization and factorization scales is used. Both scales are either kept at their nominal values or varied independently up and down by a factor of 2 and 0.5, while the schemes in which one scale is varied up and the other is varied down are excluded for a total of seven possible choices of renormalization and factorization scales. The uncertainty applied to the signal MC is an envelope around the seven variations. An alternative value of the strong coupling constant α_S is also used and the difference is taken as an uncertainty. A systematic uncertainty in the choice of PDF is applied as the standard deviation of 100 variations in the NNPDF3.0NLO PDF set.

Table 2 summarizes the impact of each set of systematic uncertainties in the expected upper limit. Each row shows the difference between the upper limit with all sources of uncertainty considered and the upper limit with a subset of the systematic uncertainties excluded. Each cell shows the range of impacts for the various mass hypotheses m_X and m_S considered for each of the three DNNs. The systematic uncertainties in the background shape are the dominant sources of systematic uncertainty, changing the expected limit by 15 to 43% depending on the model and BSM masses m_X and m_S . Flavor tagging, jet reconstruction and trigger efficiency uncertainties are the sub-leading sources of systematic uncertainty, with an impact of up to 10% on the expected upper limit.

Table 2: Summary of the impact on the analysis of different sources of systematic uncertainty. The impact is estimated as the absolute value of the difference between the expected upper limit with all sources of uncertainty included and the upper limit with a subset of systematic uncertainties excluded. In the left-hand column, more heavily indented rows are a sub-category of the less indented row above.

Uncertainty source	Relative impact of systematic uncertainties [%]			
	SM-like	TRSM non-resonant	TRSM resonant	Heavy resonance
All uncertainties	24	20–46	33–42	24–53
Experimental	22	20–45	33–41	24–53
Detector response	7.4	6.6–14	16–24	4.1–15
Luminosity and pileup	<1	<1	<1	<1
Flavor tagging	3.2	2.8–5	6.9–8.8	1.5–5.6
Jet reconstruction	2.7	2.3–6.5	3.6–7.1	1.0–6.3
Trigger efficiency	2.0	1.8–3.5	6–10	1.4–4.2
Background modeling	16	14–36	18–30	20–45
Theoretical	1.5	<1	<1	<1
MC statistical	<1	<1	<1	<1

9 Results

The distributions of the nonResDNN, resDNN, and heavyResDNN scores in the $6b$ region after the profile likelihood fit described in Section 7 can be found in Figure 6. One representative signal point is overlaid on each score distribution, scaled to the same area as the background distribution. For nonresDNN, the SM HHH signal and a non-resonant TRSM signal with $(m_X, m_S) = (400, 200)$ GeV are both shown in Figure 6(a) and Figure 6(b), respectively. In all cases, the observed data agree well with the background, and no significant excess is seen. For the Resonant search no upward deviation from the SM prediction is observed. A one-sided test statistic is used, and the best fit signal is precisely zero for all mass points considered. For the Non-resonant search, the largest deviation is at $(m_X, m_S) = (550, 200)$ GeV with a local significance of 0.19σ . For the Heavy-resonant search, the largest deviation is at $(m_X, m_S) = (1500, 275)$ GeV with a local significance of 0.51σ .

Upper limits for each signal model considered are placed on the allowed HHH production cross-section, at 95% CL. They are calculated using the CL_s method [64] with the asymptotic approximation [60].

For the TRSM and DM-CPV models, expected and observed cross-section upper limits are shown over the (m_X, m_S) plane in Figures 7(a) and 7(b), respectively. The $m_S > 250$ GeV region forms the Resonant search, where resDNN is used in the fit, whereas the $m_S < 250$ GeV region is part of the Non-resonant search, where nonresDNN is used in the fit. The expected (observed) cross-section upper limit varies with m_X and m_S , within the range of 46 – 350 fb (48 – 310 fb). The limits are evaluated at the simulated (m_X, m_S) points as described in Section 3. For all results in the analysis, a cubic Bézier polynomial is used to interpolate across the plane.

The cross-section upper limits for the Heavy Resonance search are shown in Figure 8 in the (m_X, m_S) plane. Expected (observed) limits for the narrow heavy resonance signals are presented in Figure 8(a)

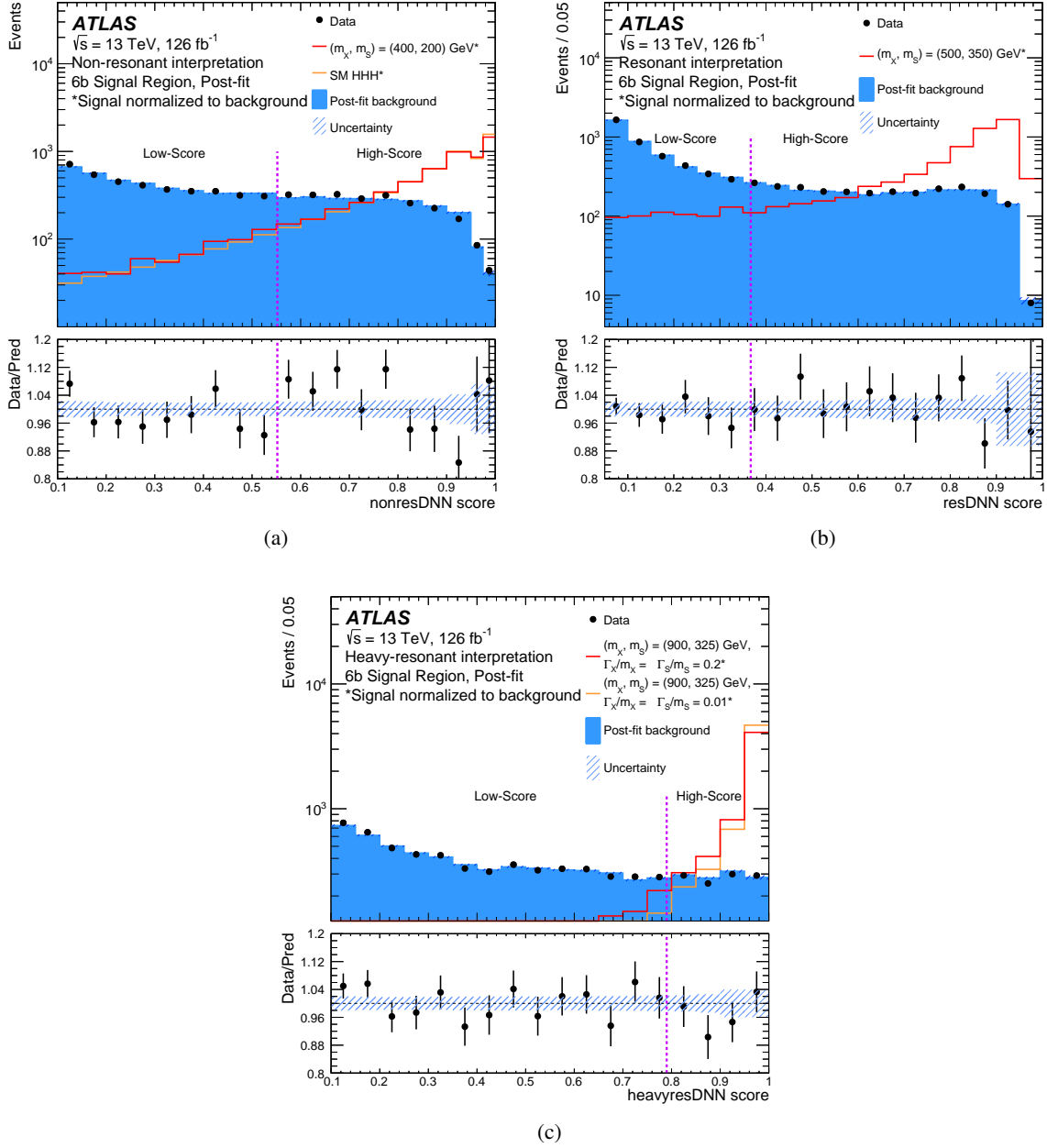


Figure 6: Distributions of scores for (a) nonresDNN, (b) resDNN and (c) heavyresDNN in $6b$ data and the background prediction after background-only fits to the observed data. The boundary between the Low- and High-Score regions is shown by a dashed vertical line. Benchmark signal models (normalized to the background) are overlaid in each case: (a) SM HHH signal and non-resonant TRSM signal with $(m_X, m_S) = (400, 200) \text{ GeV}$, (b) resonant TRSM signal with $(m_X, m_S) = (500, 350) \text{ GeV}$ overlaid, and (c) narrow- large-width heavy resonances with $(m_X, m_S) = (900, 325) \text{ GeV}$ overlaid. The lower panel in each plot shows the ratio of the data and the post-fit background (Pred) in markers, with the uncertainty on the prediction shown as a hatched band centered on unity.

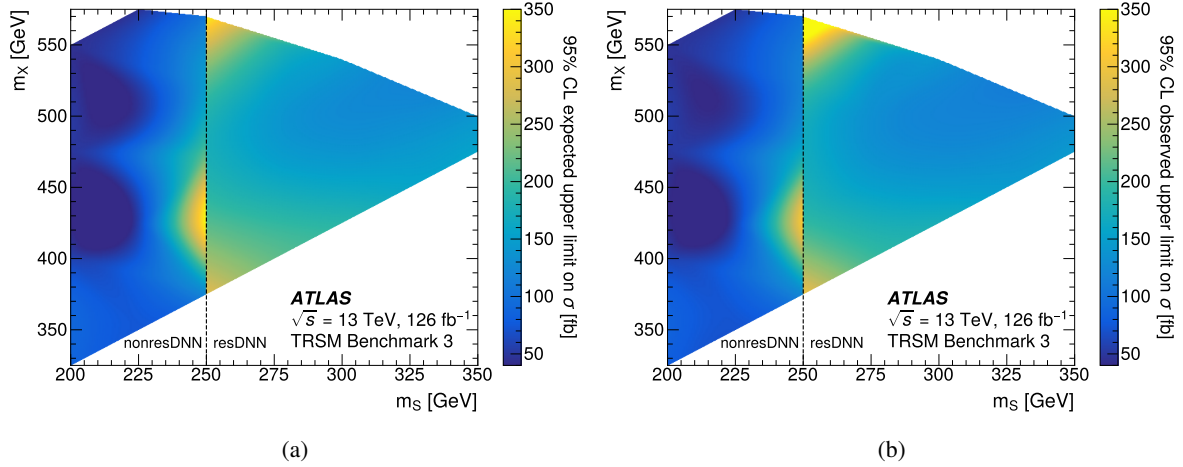


Figure 7: (a) Expected and (b) observed 95% CL HHH cross section upper limits for the phase space within the perturbative unitarity bounds of the TRSM. While the points were generated under Benchmark point 3 of the TRSM, they can also be interpreted in the DM-CPV model. The white areas correspond to regions of the (m_X, m_S) phase space not considered here. A cubic Bézier polynomial is used to interpolate across the plane.

(Figure 8(c)), and range between 4.7 – 69 fb (5.7 – 38 fb). Expected (observed) limits for the wide heavy resonance signals are presented in Figure 8(b) (Figure 8(d)), and range between 5.2 – 53 fb (6.3 – 39 fb).

Limits on the coupling modifiers κ_3 and κ_4 are shown in Figure 9. The gray dashed line shows the region where perturbative unitarity holds (provided that κ_3 and κ_4 are the only modifications to the SM), as calculated in Ref. [65]. At the 95% CL none of the phase space inside the unitarity bounds is excluded. Outside the unitarity bounds the kappa framework requires additional modification to preserve unitarity, and as such it is not recommended to interpret this result as excluding any relevant phase space in the kappa framework. Rather, the scan of κ_3 and κ_4 serves as a benchmark of performance for future searches and projections, as well as other new-physics models which may produce similar phenomenology.

The 95% CL upper limit on the signal strength for SM HHH production $\mu = \sigma_{HHH}/\sigma_{HHH}^{SM}$ is 750, corresponding to a cross-section upper limit of 59 fb. Assuming $\kappa_4 = 1$ then κ_3 is restricted to be between -11 and 17 at 95% CL. For comparison, a combination of previous di-Higgs searches and single Higgs production constraints limited κ_3 to be between -0.4 and 6.3 at 95% CL [7]. Assuming $\kappa_3 = 1$ then κ_4 is restricted to be between -230 and 240 at 95% CL.

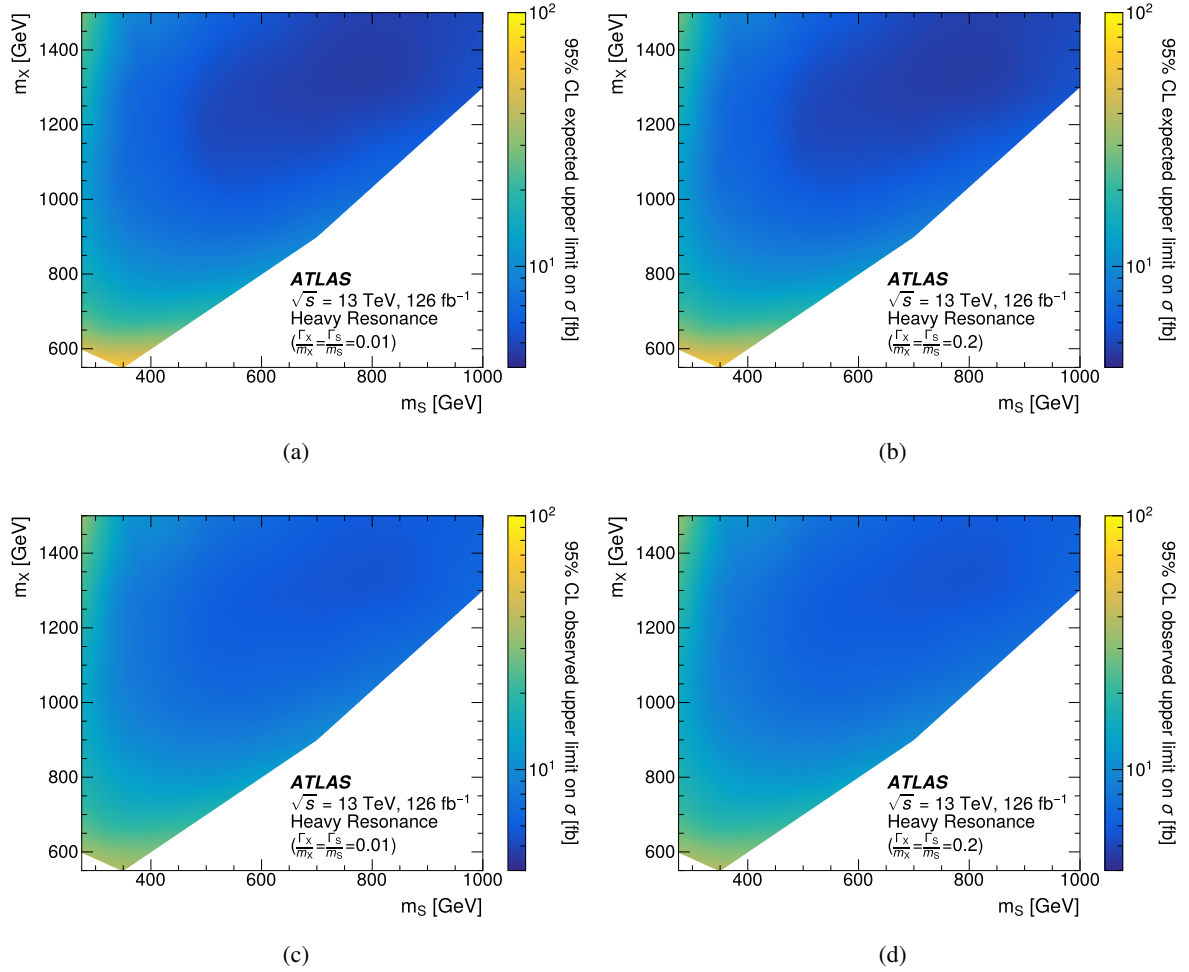


Figure 8: (a,b) Expected and (c,d) observed 95% CL HHH cross section upper limits for the (a,c) narrow-width or (b,d) wide-width heavy resonance signals. The white areas correspond to regions of the (m_X, m_S) phase space not considered here. A cubic Bézier polynomial is used to interpolate across the plane.

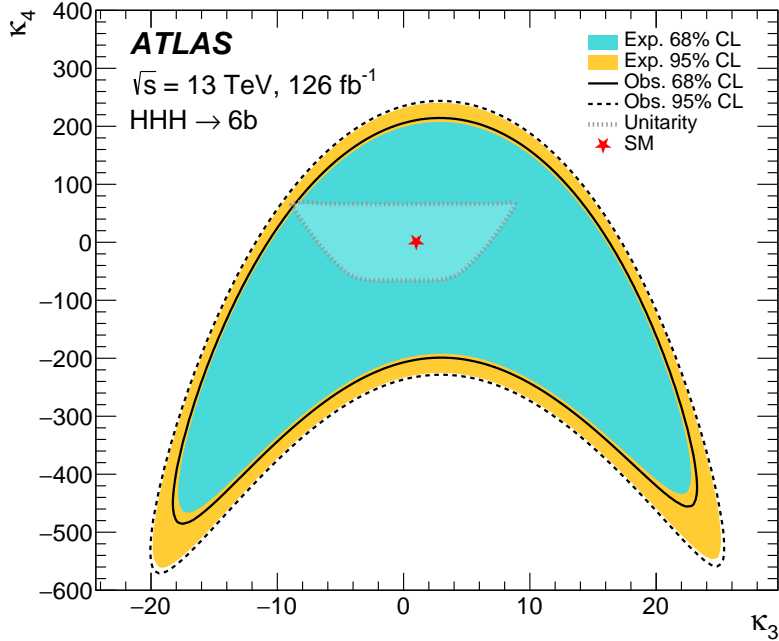


Figure 9: Expected (filled regions) and observed (black solid and dashed lines) 95% and 68% CL constraints on κ_3 and κ_4 , the ratios of the Higgs tri-linear and quartic self-couplings to their predicted SM values. Unitarity limits, calculated in Ref. [65], are overlaid in the region bounded by the gray dashed line. The red star is the SM: $\kappa_3 = \kappa_4 = 1$.

10 Conclusion

This paper presents a search for triple-Higgs production in the $b\bar{b}b\bar{b}b\bar{b}$ final state. The search uses 126 fb^{-1} of pp collision data at $\sqrt{s} = 13 \text{ TeV}$ collected with the ATLAS detector at the LHC. The data are interpreted using three different DNNs, which are each optimized to search for non-resonant, resonant, and heavy resonant (outside the perturbative unitarity bounds of the TRSM) signals with additional scalars. The non-resonant interpretation includes a search for SM-like signals with coupling modifiers on the tri-linear and quartic Higgs self couplings κ_3 and κ_4 . The SM background is modeled using a data-driven extrapolation method, derived from the observed DNN score spectra in events with four or five b -jets to estimate the background shape in events with at least six b -jets. The sensitivity of the search is impacted mainly by the statistical precision and the uncertainty in the data-driven extrapolation method.

No significant excess above the SM expectation is observed in the search for SM-like HHH production, nor is any significant excess observed in the search for various BSM signals with two additional heavy scalars X and S . A 95% CL upper limit of 59 fb is set on the cross-section for SM-like HHH production. The BSM searches include non-resonant production where $m_S < 250 \text{ GeV}$, and resonant production up to $(m_X, m_S) = (1500, 1000) \text{ GeV}$.

Acknowledgments

We thank CERN for the very successful operation of the LHC and its injectors, as well as the support staff at CERN and at our institutions worldwide without whom ATLAS could not be operated efficiently.

The crucial computing support from all WLCG partners is acknowledged gratefully, in particular from CERN, the ATLAS Tier-1 facilities at TRIUMF/SFU (Canada), NDGF (Denmark, Norway, Sweden), CC-IN2P3 (France), KIT/GridKA (Germany), INFN-CNAF (Italy), NL-T1 (Netherlands), PIC (Spain), RAL (UK) and BNL (USA), the Tier-2 facilities worldwide and large non-WLCG resource providers. Major contributors of computing resources are listed in Ref. [66].

We gratefully acknowledge the support of ANPCyT, Argentina; YerPhI, Armenia; ARC, Australia; BMWFW and FWF, Austria; ANAS, Azerbaijan; CNPq and FAPESP, Brazil; NSERC, NRC and CFI, Canada; CERN; ANID, Chile; CAS, MOST and NSFC, China; Minciencias, Colombia; MEYS CR, Czech Republic; DNRF and DNSRC, Denmark; IN2P3-CNRS and CEA-DRF/IRFU, France; SRNSFG, Georgia; BMBF, HGF and MPG, Germany; GSRI, Greece; RGC and Hong Kong SAR, China; ICHEP and Academy of Sciences and Humanities, Israel; INFN, Italy; MEXT and JSPS, Japan; CNRST, Morocco; NWO, Netherlands; RCN, Norway; MNiSW, Poland; FCT, Portugal; MNE/IFA, Romania; MSTDI, Serbia; MSSR, Slovakia; ARIS and MVZI, Slovenia; DSI/NRF, South Africa; MICIU/AEI, Spain; SRC and Wallenberg Foundation, Sweden; SERI, SNSF and Cantons of Bern and Geneva, Switzerland; NSTC, Taipei; TENMAK, Türkiye; STFC/UKRI, United Kingdom; DOE and NSF, United States of America.

Individual groups and members have received support from BCKDF, CANARIE, CRC and DRAC, Canada; CERN-CZ, FORTE and PRIMUS, Czech Republic; COST, ERC, ERDF, Horizon 2020, ICSC-NextGenerationEU and Marie Skłodowska-Curie Actions, European Union; Investissements d’Avenir Labex, Investissements d’Avenir Idex and ANR, France; DFG and AvH Foundation, Germany; Herakleitos, Thales and Aristeia programmes co-financed by EU-ESF and the Greek NSRF, Greece; BSF-NSF and MINERVA, Israel; NCN and NAWA, Poland; La Caixa Banking Foundation, CERCA Programme Generalitat de Catalunya and PROMETEO and GenT Programmes Generalitat Valenciana, Spain; Göran Gustafssons Stiftelse, Sweden; The Royal Society and Leverhulme Trust, United Kingdom.

In addition, individual members wish to acknowledge support from Armenia: Yerevan Physics Institute (FAPERJ); CERN: European Organization for Nuclear Research (CERN DOCT); Chile: Agencia Nacional de Investigación y Desarrollo (FONDECYT 1230812, FONDECYT 1230987, FONDECYT 1240864); China: Chinese Ministry of Science and Technology (MOST-2023YFA1605700), National Natural Science Foundation of China (NSFC - 12175119, NSFC 12275265, NSFC-12075060); Czech Republic: Czech Science Foundation (GACR - 24-11373S), Ministry of Education Youth and Sports (FORTE CZ.02.01.01/00/22_008/0004632), PRIMUS Research Programme (PRIMUS/21/SCI/017); EU: H2020 European Research Council (ERC - 101002463); European Union: European Research Council (ERC - 948254, ERC 101089007), European Union, Future Artificial Intelligence Research (FAIR-NextGenerationEU PE00000013), Italian Center for High Performance Computing, Big Data and Quantum Computing (ICSC, NextGenerationEU); France: Agence Nationale de la Recherche (ANR-20-CE31-0013, ANR-21-CE31-0013, ANR-21-CE31-0022, ANR-22-EDIR-0002); Germany: Baden-Württemberg Stiftung (BW Stiftung-Postdoc Eliteprogramme), Deutsche Forschungsgemeinschaft (DFG - 469666862, DFG - CR 312/5-2); Italy: Istituto Nazionale di Fisica Nucleare (ICSC, NextGenerationEU), Ministero dell’Università e della Ricerca (PRIN - 20223N7F8K - PNRR M4.C2.1.1); Japan: Japan Society for the Promotion of Science (JSPS KAKENHI JP22H01227, JSPS KAKENHI JP22H04944, JSPS KAKENHI JP22KK0227, JSPS KAKENHI JP23KK0245); Norway: Research Council of Norway (RCN-314472);

Poland: Ministry of Science and Higher Education (IDUB AGH, POB8, D4 no 9722), Polish National Agency for Academic Exchange (PPN/PPO/2020/1/00002/U/00001), Polish National Science Centre (NCN 2021/42/E/ST2/00350, NCN OPUS nr 2022/47/B/ST2/03059, NCN UMO-2019/34/E/ST2/00393, NCN & H2020 MSCA 945339, UMO-2020/37/B/ST2/01043, UMO-2021/40/C/ST2/00187, UMO-2022/47/O/ST2/00148, UMO-2023/49/B/ST2/04085, UMO-2023/51/B/ST2/00920); Spain: Generalitat Valenciana (Artemisa, FEDER, IDIFEDER/2018/048), Ministry of Science and Innovation (MCIN & NextGenEU PCI2022-135018-2, MICIN & FEDER PID2021-125273NB, RYC2019-028510-I, RYC2020-030254-I, RYC2021-031273-I, RYC2022-038164-I); Sweden: Carl Trygger Foundation (Carl Trygger Foundation CTS 22:2312), Swedish Research Council (Swedish Research Council 2023-04654, VR 2018-00482, VR 2022-03845, VR 2022-04683, VR 2023-03403, VR grant 2021-03651), Knut and Alice Wallenberg Foundation (KAW 2018.0458, KAW 2019.0447, KAW 2022.0358); Switzerland: Swiss National Science Foundation (SNSF - PCEFP2_194658); United Kingdom: Leverhulme Trust (Leverhulme Trust RPG-2020-004), Royal Society (NIF-R1-231091); United States of America: U.S. Department of Energy (ECA DE-AC02-76SF00515), Neubauer Family Foundation.

References

- [1] ATLAS Collaboration, *Observation of a new particle in the search for the Standard Model Higgs boson with the ATLAS detector at the LHC*, *Phys. Lett. B* **716** (2012) 1, arXiv: [1207.7214 \[hep-ex\]](#).
- [2] CMS Collaboration, *Observation of a new boson at a mass of 125 GeV with the CMS experiment at the LHC*, *Phys. Lett. B* **716** (2012) 30, arXiv: [1207.7235 \[hep-ex\]](#).
- [3] ATLAS Collaboration, *A detailed map of Higgs boson interactions by the ATLAS experiment ten years after the discovery*, *Nature* **607** (2022) 52, arXiv: [2207.00092 \[hep-ex\]](#), Erratum: *Nature* **612** (2022) E24.
- [4] CMS Collaboration, *A portrait of the Higgs boson by the CMS experiment ten years after the discovery*, *Nature* **607** (2022) 60, arXiv: [2207.00043 \[hep-ex\]](#), Erratum: *Nature* **623** (2023) E4.
- [5] LHC Higgs Cross Section Working Group, *LHC HXSWG interim recommendations to explore the coupling structure of a Higgs-like particle*, (2012), arXiv: [1209.0040 \[hep-ph\]](#), URL: <https://arxiv.org/abs/1209.0040>.
- [6] ATLAS Collaboration, *Combination of Searches for Higgs Boson Pair Production in pp Collisions at $\sqrt{s} = 13$ TeV with the ATLAS detector*, *Phys. Rev. Lett.* **133** (2024) 101801, arXiv: [2406.09971 \[hep-ex\]](#).
- [7] ATLAS Collaboration, *Constraints on the Higgs boson self-coupling from single- and double-Higgs production with the ATLAS detector using pp collisions at $\sqrt{s} = 13$ TeV*, *Phys. Lett. B* **843** (2023) 137745, arXiv: [2211.01216 \[hep-ex\]](#).
- [8] ATLAS Collaboration, *The ATLAS Experiment at the CERN Large Hadron Collider*, *JINST* **3** (2008) S08003.
- [9] A. Papaefstathiou, T. Robens, and G. Tetlalmatzi-Xolocotzi, *Triple Higgs Boson Production at the Large Hadron Collider with Two Real Singlet Scalars*, *JHEP* **05** (2021) 193, arXiv: [2101.00037 \[hep-ph\]](#).
- [10] T.-K. Chen, C.-W. Chiang, and I. Low, *A Simple Model of Dark Matter and CP Violation*, *Phys. Rev. D* **05** (2022) 105, arXiv: [2202.02954 \[hep-ph\]](#).
- [11] G. Avoni et al., *The new LUCID-2 detector for luminosity measurement and monitoring in ATLAS*, *JINST* **13** (2018) P07017.
- [12] ATLAS Collaboration, *Performance of the ATLAS trigger system in 2015*, *Eur. Phys. J. C* **77** (2017) 317, arXiv: [1611.09661 \[hep-ex\]](#).
- [13] ATLAS Collaboration, *Software and computing for Run 3 of the ATLAS experiment at the LHC*, (2024), arXiv: [2404.06335 \[hep-ex\]](#).
- [14] ATLAS Collaboration, *Luminosity determination in pp collisions at $\sqrt{s} = 13$ TeV using the ATLAS detector at the LHC*, *Eur. Phys. J. C* **83** (2023) 982, arXiv: [2212.09379 \[hep-ex\]](#).
- [15] ATLAS Collaboration, *ATLAS data quality operations and performance for 2015–2018 data-taking*, *JINST* **15** (2020) P04003, arXiv: [1911.04632 \[physics.ins-det\]](#).
- [16] ATLAS Collaboration, *Configuration and performance of the ATLAS b-jet triggers in Run 2*, *Eur. Phys. J. C* **81** (2021) 1087, arXiv: [2106.03584 \[hep-ex\]](#).

- [17] M. Cacciari, G. P. Salam, and G. Soyez, *The anti- k_t jet clustering algorithm*, *JHEP* **04** (2008) 063, arXiv: [0802.1189 \[hep-ph\]](#).
- [18] M. Cacciari, G. P. Salam, and G. Soyez, *FastJet user manual*, *Eur. Phys. J. C* **72** (2012) 1896, arXiv: [1111.6097 \[hep-ph\]](#).
- [19] J. Alwall, M. Herquet, F. Maltoni, O. Mattelaer, and T. Stelzer, *MadGraph 5: going beyond*, *JHEP* **06** (2011) 128, arXiv: [1106.0522 \[hep-ph\]](#).
- [20] NNPDF Collaboration, R. D. Ball, et al., *Parton distributions for the LHC run II*, *JHEP* **04** (2015) 040, arXiv: [1410.8849 \[hep-ph\]](#).
- [21] ATLAS Collaboration, *ATLAS Pythia 8 tunes to 7 TeV data*, ATL-PHYS-PUB-2014-021, 2014, URL: <https://cds.cern.ch/record/1966419>.
- [22] D. de Florian et al., *Handbook of LHC Higgs Cross Sections: 4. Deciphering the Nature of the Higgs Sector*, (2017), arXiv: [1610.07922 \[hep-ph\]](#).
- [23] T. Sjöstrand et al., *An introduction to PYTHIA 8.2*, *Comput. Phys. Commun.* **191** (2015) 159, arXiv: [1410.3012 \[hep-ph\]](#).
- [24] O. Mattelaer, *On the maximal use of Monte Carlo samples: re-weighting events at NLO accuracy*, *Eur. Phys. J. C* **76** (2016) 674, arXiv: [1607.00763 \[hep-ph\]](#).
- [25] A. Papaefstathiou and K. Sakurai, *Triple Higgs boson production at a 100 TeV proton-proton collider*, *JHEP* **02** (2016) 006, arXiv: [1508.06524 \[hep-ph\]](#).
- [26] D. de Florian, I. Fabre, and J. Mazzitelli, *Triple Higgs production at hadron colliders at NNLO in QCD*, *JHEP* **2020** (2020) 155, arXiv: [1912.02760 \[hep-ph\]](#).
- [27] O. Karkout et al., *Triple Higgs boson production and electroweak phase transition in the two-real-singlet model*, (2024), arXiv: [2404.12425 \[hep-ph\]](#).
- [28] P. Artoisenet, R. Frederix, O. Mattelaer, and R. Rietkerk, *Automatic spin-entangled decays of heavy resonances in Monte Carlo simulations*, *JHEP* **03** (2013) 015, arXiv: [1212.3460 \[hep-ph\]](#).
- [29] ATLAS Collaboration, *The ATLAS Simulation Infrastructure*, *Eur. Phys. J. C* **70** (2010) 823, arXiv: [1005.4568 \[physics.ins-det\]](#).
- [30] ATLAS Collaboration, *AtlFast3: The Next Generation of Fast Simulation in ATLAS*, *Comput. Softw. Big Sci.* **6** (2022) 7, arXiv: [2109.02551 \[hep-ex\]](#).
- [31] S. Agostinelli et al., *GEANT4 – a simulation toolkit*, *Nucl. Instrum. Meth. A* **506** (2003) 250.
- [32] T. Sjöstrand, S. Mrenna, and P. Skands, *A brief introduction to PYTHIA 8.1*, *Comput. Phys. Commun.* **178** (2008) 852, arXiv: [0710.3820 \[hep-ph\]](#).
- [33] NNPDF Collaboration, R. D. Ball, et al., *Parton distributions with LHC data*, *Nucl. Phys. B* **867** (2013) 244, arXiv: [1207.1303 \[hep-ph\]](#).
- [34] ATLAS Collaboration, *The Pythia 8 A3 tune description of ATLAS minimum bias and inelastic measurements incorporating the Donnachie–Landshoff diffractive model*, ATL-PHYS-PUB-2016-017, 2016, URL: <https://cds.cern.ch/record/2206965>.

- [35] ATLAS Collaboration, *Reconstruction of primary vertices at the ATLAS experiment in Run 1 proton–proton collisions at the LHC*, *Eur. Phys. J. C* **77** (2017) 332, arXiv: [1611.10235 \[hep-ex\]](#).
- [36] ATLAS Collaboration, *Jet reconstruction and performance using particle flow with the ATLAS Detector*, *Eur. Phys. J. C* **77** (2017) 466, arXiv: [1703.10485 \[hep-ex\]](#).
- [37] ATLAS Collaboration, *Jet energy scale and resolution measured in proton–proton collisions at $\sqrt{s} = 13$ TeV with the ATLAS detector*, *Eur. Phys. J. C* **81** (2021) 689, arXiv: [2007.02645 \[hep-ex\]](#).
- [38] ATLAS Collaboration, *Performance of pile-up mitigation techniques for jets in pp collisions at $\sqrt{s} = 8$ TeV using the ATLAS detector*, *Eur. Phys. J. C* **76** (2016) 581, arXiv: [1510.03823 \[hep-ex\]](#).
- [39] ATLAS Collaboration, *Neural Network Jet Flavour Tagging with the Upgraded ATLAS Inner Tracker Detector at the High-Luminosity LHC*, ATL-PHYS-PUB-2022-047, 2022, URL: <https://cds.cern.ch/record/2839913>.
- [40] ATLAS Collaboration, *Deep Sets based Neural Networks for Impact Parameter Flavour Tagging in ATLAS*, ATL-PHYS-PUB-2020-014, 2020, URL: <https://cds.cern.ch/record/2718948>.
- [41] ATLAS Collaboration, *ATLAS flavour-tagging algorithms for the LHC Run 2 pp collision dataset*, *Eur. Phys. J. C* **83** (2023) 681, arXiv: [2211.16345 \[physics.data-an\]](#).
- [42] ATLAS Collaboration, *ATLAS b-jet identification performance and efficiency measurement with $t\bar{t}$ events in pp collisions at $\sqrt{s} = 13$ TeV*, *Eur. Phys. J. C* **79** (2019) 970, arXiv: [1907.05120 \[hep-ex\]](#).
- [43] ATLAS Collaboration, *Measurement of b-tagging efficiency of c-jets in $t\bar{t}$ events using a likelihood approach with the ATLAS detector*, ATLAS-CONF-2018-001, 2018, URL: <https://cds.cern.ch/record/2306649>.
- [44] ATLAS Collaboration, *Calibration of light-flavour b-jet mistagging rates using ATLAS proton–proton collision data at $\sqrt{s} = 13$ TeV*, ATLAS-CONF-2018-006, 2018, URL: <https://cds.cern.ch/record/2314418>.
- [45] ATLAS Collaboration, *Evidence for the $H \rightarrow b\bar{b}$ decay with the ATLAS detector*, *JHEP* **12** (2017) 024, arXiv: [1708.03299 \[hep-ex\]](#).
- [46] ATLAS Collaboration, *Muon reconstruction and identification efficiency in ATLAS using the full Run 2 pp collision data set at $\sqrt{s} = 13$ TeV*, *Eur. Phys. J. C* **81** (2021) 578, arXiv: [2012.00578 \[hep-ex\]](#).
- [47] ATLAS Collaboration, *Muon reconstruction performance of the ATLAS detector in proton–proton collision data at $\sqrt{s} = 13$ TeV*, *Eur. Phys. J. C* **76** (2016) 292, arXiv: [1603.05598 \[hep-ex\]](#).
- [48] S. Frixione, G. Ridolfi, and P. Nason, *A positive-weight next-to-leading-order Monte Carlo for heavy flavour hadroproduction*, *JHEP* **09** (2007) 126, arXiv: [0707.3088 \[hep-ph\]](#).
- [49] P. Nason, *A new method for combining NLO QCD with shower Monte Carlo algorithms*, *JHEP* **11** (2004) 040, arXiv: [hep-ph/0409146](#).

- [50] S. Frixione, P. Nason, and C. Oleari, *Matching NLO QCD computations with parton shower simulations: the POWHEG method*, *JHEP* **11** (2007) 070, arXiv: [0709.2092 \[hep-ph\]](#).
- [51] S. Alioli, P. Nason, C. Oleari, and E. Re, *A general framework for implementing NLO calculations in shower Monte Carlo programs: the POWHEG BOX*, *JHEP* **06** (2010) 043, arXiv: [1002.2581 \[hep-ph\]](#).
- [52] M. Stone, *Cross-Validatory Choice and Assessment of Statistical Predictions*, *J. R. Stat. Soc. Ser. B Stat. Method.* **36** (1974) 111.
- [53] B. Rozemberczki et al., *The Shapley Value in Machine Learning*, 2022, arXiv: [2202.05594 \[cs.LG\]](#).
- [54] F. Chollet et al., *Keras*, 2015, URL: <https://keras.io>.
- [55] Martín Abadi et al., *TensorFlow: Large-Scale Machine Learning on Heterogeneous Systems*, Software available from tensorflow.org, 2015, URL: <https://www.tensorflow.org/>.
- [56] K. Fukushima, *Visual Feature Extraction by a Multilayered Network of Analog Threshold Elements*, *IEEE Transactions on Systems Science and Cybernetics* **5** (1969) 322.
- [57] V. Nair and G. E. Hinton, “Rectified linear units improve restricted boltzmann machines,” *Proceedings of the 27th International Conference on International Conference on Machine Learning*, ICML’10, Haifa, Israel: Omnipress, 2010 807, ISBN: 9781605589077.
- [58] D. P. Kingma and J. Ba, *Adam: A Method for Stochastic Optimization*, 2017, arXiv: [1412.6980 \[cs.LG\]](#).
- [59] N. Srivastava, G. Hinton, A. Krizhevsky, I. Sutskever, and R. Salakhutdinov, *Dropout: A Simple Way to Prevent Neural Networks from Overfitting*, *JMLR* **15** (2014) 1929.
- [60] G. Cowan, K. Cranmer, E. Gross, and O. Vitells, *Asymptotic formulae for likelihood-based tests of new physics*, *Eur. Phys. J. C* **71** (2011) 1554, arXiv: [1007.1727 \[physics.data-an\]](#), Erratum: *Eur. Phys. J. C* **73** (2013) 2501.
- [61] ATLAS Collaboration, *Measurement of the Inelastic Proton–Proton Cross Section at $\sqrt{s} = 13$ TeV with the ATLAS Detector at the LHC*, *Phys. Rev. Lett.* **117** (2016) 182002, arXiv: [1606.02625 \[hep-ex\]](#).
- [62] ATLAS Collaboration, *Topological cell clustering in the ATLAS calorimeters and its performance in LHC Run 1*, *Eur. Phys. J. C* **77** (2017) 490, arXiv: [1603.02934 \[hep-ex\]](#).
- [63] J. Bellm et al., *Herwig 7.0/Herwig++ 3.0 release note*, *Eur. Phys. J. C* **76** (2016) 196, arXiv: [1512.01178 \[hep-ph\]](#).
- [64] A. L. Read, *Presentation of search results: the CL_s technique*, *J. Phys. G* **28** (2002) 2693.
- [65] P. Stylianou and G. Weiglein, *Constraints on the trilinear and quartic Higgs couplings from triple Higgs production at the LHC and beyond*, *Eur. Phys. J. C* **84** (2024) 366, arXiv: [2312.04646 \[hep-ph\]](#).
- [66] ATLAS Collaboration, *ATLAS Computing Acknowledgements*, ATL-SOFT-PUB-2023-001, 2023, URL: <https://cds.cern.ch/record/2869272>.

The ATLAS Collaboration

G. Aad ¹⁰⁴, E. Aakvaag ¹⁷, B. Abbott ¹²³, S. Abdelhameed ^{119a}, K. Abeling ⁵⁶, N.J. Abicht ⁵⁰, S.H. Abidi ³⁰, M. Aboeela ⁴⁶, A. Aboulhorma ^{36e}, H. Abramowicz ¹⁵⁵, Y. Abulaiti ¹²⁰, B.S. Acharya ^{70a,70b,m}, A. Ackermann ^{64a}, C. Adam Bourdarios ⁴, L. Adamczyk ^{87a}, S.V. Addepalli ¹⁴⁷, M.J. Addison ¹⁰³, J. Adelman ¹¹⁸, A. Adiguzel ^{22c}, T. Adye ¹³⁷, A.A. Affolder ¹³⁹, Y. Afik ⁴¹, M.N. Agaras ¹³, A. Aggarwal ¹⁰², C. Agheorghiesei ^{28c}, F. Ahmadov ^{40,ab}, S. Ahuja ⁹⁷, X. Ai ^{63e}, G. Aielli ^{77a,77b}, A. Aikot ¹⁶⁸, M. Ait Tamliah ^{36e}, B. Aitbenkikh ^{36a}, M. Akbiyik ¹⁰², T.P.A. Åkesson ¹⁰⁰, A.V. Akimov ¹⁴⁹, D. Akiyama ¹⁷³, N.N. Akolkar ²⁵, S. Aktas ^{22a}, G.L. Alberghi ^{24b}, J. Albert ¹⁷⁰, P. Albicocco ⁵⁴, G.L. Albouy ⁶¹, S. Alderweireldt ⁵³, Z.L. Alegria ¹²⁴, M. Aleksa ³⁷, I.N. Aleksandrov ⁴⁰, C. Alexa ^{28b}, T. Alexopoulos ¹⁰, F. Alfonsi ^{24b}, M. Algren ⁵⁷, M. Alhroob ¹⁷², B. Ali ¹³⁵, H.M.J. Ali ^{93,v}, S. Ali ³², S.W. Alibocus ⁹⁴, M. Aliev ^{34c}, G. Alimonti ^{72a}, W. Alkahi ⁵⁶, C. Allaire ⁶⁷, B.M.M. Allbrooke ¹⁵⁰, J.S. Allen ¹⁰³, J.F. Allen ⁵³, P.P. Allport ²¹, A. Aloisio ^{73a,73b}, F. Alonso ⁹², C. Alpigiani ¹⁴², Z.M.K. Alsolami ⁹³, A. Alvarez Fernandez ¹⁰², M. Alves Cardoso ⁵⁷, M.G. Alviggi ^{73a,73b}, M. Aly ¹⁰³, Y. Amaral Coutinho ^{84b}, A. Ambler ¹⁰⁶, C. Amelung ³⁷, M. Amerl ¹⁰³, C.G. Ames ¹¹¹, D. Amidei ¹⁰⁸, B. Amini ⁵⁵, K.J. Amirie ¹⁵⁹, A. Amirkhanov ⁴⁰, S.P. Amor Dos Santos ^{133a}, K.R. Amos ¹⁶⁸, D. Amperiadou ¹⁵⁶, S. An ⁸⁵, V. Ananiev ¹²⁸, C. Anastopoulos ¹⁴³, T. Andeen ¹¹, J.K. Anders ⁹⁴, A.C. Anderson ⁶⁰, A. Andreazza ^{72a,72b}, S. Angelidakis ⁹, A. Angerami ⁴³, A.V. Anisenkov ³⁹, A. Annovi ^{75a}, C. Antel ⁵⁷, E. Antipov ¹⁴⁹, M. Antonelli ⁵⁴, F. Anulli ^{76a}, M. Aoki ⁸⁵, T. Aoki ¹⁵⁷, M.A. Aparo ¹⁵⁰, L. Aperio Bella ⁴⁹, C. Appelt ¹⁵⁵, A. Apyan ²⁷, S.J. Arbiol Val ⁸⁸, C. Arcangeletti ⁵⁴, A.T.H. Arce ⁵², J-F. Arguin ¹¹⁰, S. Argyropoulos ¹⁵⁶, J.-H. Arling ⁴⁹, O. Arnaez ⁴, H. Arnold ¹⁴⁹, G. Artoni ^{76a,76b}, H. Asada ¹¹³, K. Asai ¹²¹, S. Asai ¹⁵⁷, N.A. Asbah ³⁷, R.A. Ashby Pickering ¹⁷², A.M. Aslam ⁹⁷, K. Assamagan ³⁰, R. Astalos ^{29a}, K.S.V. Astrand ¹⁰⁰, S. Atashi ¹⁶³, R.J. Atkin ^{34a}, H. Atmani ^{36f}, P.A. Atmasiddha ¹³¹, K. Augsten ¹³⁵, A.D. Auriol ⁴², V.A. Austrup ¹⁰³, G. Avolio ³⁷, K. Axiotis ⁵⁷, G. Azuelos ^{110,af}, D. Babal ^{29b}, H. Bachacou ¹³⁸, K. Bachas ^{156,q}, A. Bachi ³⁵, E. Bachmann ⁵¹, M.J. Backes ^{64a}, A. Badea ⁴¹, T.M. Baer ¹⁰⁸, P. Bagnaia ^{76a,76b}, M. Bahmani ¹⁹, D. Bahner ⁵⁵, K. Bai ¹²⁶, J.T. Baines ¹³⁷, L. Baines ⁹⁶, O.K. Baker ¹⁷⁷, E. Bakos ¹⁶, D. Bakshi Gupta ⁸, L.E. Balabram Filho ^{84b}, V. Balakrishnan ¹²³, R. Balasubramanian ⁴, E.M. Baldin ³⁹, P. Balek ^{87a}, E. Ballabene ^{24b,24a}, F. Balli ¹³⁸, L.M. Baltes ^{64a}, W.K. Balunas ³³, J. Balz ¹⁰², I. Bamwidhi ^{119b}, E. Banas ⁸⁸, M. Bandieramonte ¹³², A. Bandyopadhyay ²⁵, S. Bansal ²⁵, L. Barak ¹⁵⁵, M. Barakat ⁴⁹, E.L. Barberio ¹⁰⁷, D. Barberis ^{58b,58a}, M. Barbero ¹⁰⁴, M.Z. Barel ¹¹⁷, T. Barillari ¹¹², M-S. Barisits ³⁷, T. Barklow ¹⁴⁷, P. Baron ¹²⁵, D.A. Baron Moreno ¹⁰³, A. Baroncelli ^{63a}, A.J. Barr ¹²⁹, J.D. Barr ⁹⁸, F. Barreiro ¹⁰¹, J. Barreiro Guimarães da Costa ¹⁴, M.G. Barros Teixeira ^{133a}, S. Barsov ³⁹, F. Bartels ^{64a}, R. Bartoldus ¹⁴⁷, A.E. Barton ⁹³, P. Bartos ^{29a}, A. Basan ¹⁰², M. Baselga ⁵⁰, S. Bashiri ⁸⁸, A. Bassalat ^{67,b}, M.J. Basso ^{160a}, S. Bataju ⁴⁶, R. Bate ¹⁶⁹, R.L. Bates ⁶⁰, S. Batlamous ¹⁰¹, M. Battaglia ¹³⁹, D. Battulga ¹⁹, M. Baucé ^{76a,76b}, M. Bauer ⁸⁰, P. Bauer ²⁵, L.T. Bayer ⁴⁹, L.T. Bazzano Hurrell ³¹, J.B. Beacham ¹¹², T. Beau ¹³⁰, J.Y. Beaucamp ⁹², P.H. Beauchemin ¹⁶², P. Bechtel ²⁵, H.P. Beck ^{20,p}, K. Becker ¹⁷², A.J. Beddall ⁸³, V.A. Bednyakov ⁴⁰, C.P. Bee ¹⁴⁹, L.J. Beemster ¹⁶, M. Begalli ^{84d}, M. Begel ³⁰, J.K. Behr ⁴⁹, J.F. Beirer ³⁷, F. Beisiegel ²⁵, M. Belfkir ^{119b}, G. Bella ¹⁵⁵, L. Bellagamba ^{24b}, A. Bellerive ³⁵, P. Bellos ²¹, K. Beloborodov ³⁹, D. Benchebroun ^{36a}, F. Bendebba ^{36a}, Y. Benhammou ¹⁵⁵, K.C. Benkendorfer ⁶², L. Beresford ⁴⁹, M. Beretta ⁵⁴, E. Bergeas Kuutmann ¹⁶⁶, N. Berger ⁴,

B. Bergmann ¹³⁵, J. Beringer ^{18a}, G. Bernardi ⁵, C. Bernius ¹⁴⁷, F.U. Bernlochner ²⁵,
 F. Bernon ³⁷, A. Berrocal Guardia ¹³, T. Berry ⁹⁷, P. Berta ¹³⁶, A. Berthold ⁵¹, S. Bethke ¹¹²,
 A. Betti ^{76a,76b}, A.J. Bevan ⁹⁶, N.K. Bhalla ⁵⁵, S. Bharthuar ¹¹², S. Bhatta ¹⁴⁹,
 D.S. Bhattacharya ¹⁷¹, P. Bhattarai ¹⁴⁷, Z.M. Bhatti ¹²⁰, K.D. Bhide ⁵⁵, V.S. Bhopatkar ¹²⁴,
 R.M. Bianchi ¹³², G. Bianco ^{24b,24a}, O. Biebel ¹¹¹, M. Biglietti ^{78a}, C.S. Billingsley ⁴⁶,
 Y. Bimgdi ^{36f}, M. Bindi ⁵⁶, A. Bingham ¹⁷⁶, A. Bingul ^{22b}, C. Bini ^{76a,76b}, G.A. Bird ³³,
 M. Birman ¹⁷⁴, M. Biros ¹³⁶, S. Biryukov ¹⁵⁰, T. Bisanz ⁵⁰, E. Bisceglie ^{45b,45a}, J.P. Biswal ¹³⁷,
 D. Biswas ¹⁴⁵, I. Bloch ⁴⁹, A. Blue ⁶⁰, U. Blumenschein ⁹⁶, J. Blumenthal ¹⁰²,
 V.S. Bobrovnikov ⁴⁰, M. Boehler ⁵⁵, B. Boehm ¹⁷¹, D. Bogavac ³⁷, A.G. Bogdanchikov ³⁹,
 L.S. Boggia ¹³⁰, V. Boisvert ⁹⁷, P. Bokan ³⁷, T. Bold ^{87a}, M. Bomben ⁵, M. Bona ⁹⁶,
 M. Boonekamp ¹³⁸, A.G. Borbély ⁶⁰, I.S. Bordulev ³⁹, G. Borissov ⁹³, D. Bortoletto ¹²⁹,
 D. Boscherini ^{24b}, M. Bosman ¹³, K. Bouaouda ^{36a}, N. Bouchhar ¹⁶⁸, L. Boudet ⁴,
 J. Boudreau ¹³², E.V. Bouhova-Thacker ⁹³, D. Boumediene ⁴², R. Bouquet ^{58b,58a}, A. Boveia ¹²²,
 J. Boyd ³⁷, D. Boye ³⁰, I.R. Boyko ⁴⁰, L. Bozianu ⁵⁷, J. Bracinek ²¹, N. Brahimi ⁴,
 G. Brandt ¹⁷⁶, O. Brandt ³³, B. Brau ¹⁰⁵, J.E. Brau ¹²⁶, R. Brenner ¹⁷⁴, L. Brenner ¹¹⁷,
 R. Brenner ¹⁶⁶, S. Bressler ¹⁷⁴, G. Brianti ^{79a,79b}, D. Britton ⁶⁰, D. Britzger ¹¹², I. Brock ²⁵,
 R. Brock ¹⁰⁹, G. Brooijmans ⁴³, A.J. Brooks ⁶⁹, E.M. Brooks ^{160b}, E. Brost ³⁰, L.M. Brown ¹⁷⁰,
 L.E. Bruce ⁶², T.L. Bruckler ¹²⁹, P.A. Bruckman de Renstrom ⁸⁸, B. Brüers ⁴⁹, A. Bruni ^{24b},
 G. Bruni ^{24b}, D. Brunner ^{48a,48b}, M. Bruschi ^{24b}, N. Bruscolo ^{76a,76b}, T. Buanes ¹⁷, Q. Buat ¹⁴²,
 D. Buchin ¹¹², A.G. Buckley ⁶⁰, O. Bulekov ³⁹, B.A. Bullard ¹⁴⁷, S. Burdin ⁹⁴, C.D. Burgard ⁵⁰,
 A.M. Burger ³⁷, B. Burghgrave ⁸, O. Burlayenko ⁵⁵, J. Burleson ¹⁶⁷, J.T.P. Burr ³³,
 J.C. Burzynski ¹⁴⁶, E.L. Busch ⁴³, V. Büscher ¹⁰², P.J. Bussey ⁶⁰, J.M. Butler ²⁶, C.M. Buttar ⁶⁰,
 J.M. Butterworth ⁹⁸, W. Buttinger ¹³⁷, C.J. Buxo Vazquez ¹⁰⁹, A.R. Buzykaev ⁴⁰,
 S. Cabrera Urbán ¹⁶⁸, L. Cadamuro ⁶⁷, D. Caforio ⁵⁹, H. Cai ¹³², Y. Cai ^{24b,114c,24a}, Y. Cai ^{114a},
 V.M.M. Cairo ³⁷, O. Cakir ^{3a}, N. Calace ³⁷, P. Calafiura ^{18a}, G. Calderini ¹³⁰, P. Calfayan ³⁵,
 G. Callea ⁶⁰, L.P. Caloba ^{84b}, D. Calvet ⁴², S. Calvet ⁴², R. Camacho Toro ¹³⁰, S. Camarda ³⁷,
 D. Camarero Munoz ²⁷, P. Camarri ^{77a,77b}, M.T. Camerlingo ^{73a,73b}, D. Cameron ³⁷,
 C. Camincher ¹⁷⁰, M. Campanelli ⁹⁸, A. Camplani ⁴⁴, V. Canale ^{73a,73b}, A.C. Canbay ^{3a},
 E. Canonero ⁹⁷, J. Cantero ¹⁶⁸, Y. Cao ¹⁶⁷, F. Capocasa ²⁷, M. Capua ^{45b,45a}, A. Carbone ^{72a,72b},
 R. Cardarelli ^{77a}, J.C.J. Cardenas ⁸, M.P. Cardiff ²⁷, G. Carducci ^{45b,45a}, T. Carli ³⁷,
 G. Carlino ^{73a}, J.I. Carlotto ¹³, B.T. Carlson ^{132,r}, E.M. Carlson ¹⁷⁰, J. Carmignani ⁹⁴,
 L. Carminati ^{72a,72b}, A. Carnelli ¹³⁸, M. Carnesale ³⁷, S. Caron ¹¹⁶, E. Carquin ^{140f},
 I.B. Carr ¹⁰⁷, S. Carrá ^{72a}, G. Carratta ^{24b,24a}, A.M. Carroll ¹²⁶, M.P. Casado ^{13,h}, M. Caspar ⁴⁹,
 F.L. Castillo ⁴, L. Castillo Garcia ¹³, V. Castillo Gimenez ¹⁶⁸, N.F. Castro ^{133a,133e},
 A. Catinaccio ³⁷, J.R. Catmore ¹²⁸, T. Cavaliere ⁴, V. Cavaliere ³⁰, L.J. Caviedes Betancourt ^{23b},
 Y.C. Cekmecelioglu ⁴⁹, E. Celebi ⁸³, S. Cella ³⁷, V. Cepaitis ⁵⁷, K. Cerny ¹²⁵,
 A.S. Cerqueira ^{84a}, A. Cerri ^{75a,75b}, L. Cerrito ^{77a,77b}, F. Cerutti ^{18a}, B. Cervato ¹⁴⁵,
 A. Cervelli ^{24b}, G. Cesarini ⁵⁴, S.A. Cetin ⁸³, P.M. Chabrilat ¹³⁰, J. Chan ^{18a}, W.Y. Chan ¹⁵⁷,
 J.D. Chapman ³³, E. Chapon ¹³⁸, B. Chargeishvili ^{153b}, D.G. Charlton ²¹, C. Chauhan ¹³⁶,
 Y. Che ^{114a}, S. Chekanov ⁶, S.V. Chekulaev ^{160a}, G.A. Chelkov ^{40,a}, B. Chen ¹⁵⁵, B. Chen ¹⁷⁰,
 H. Chen ^{114a}, H. Chen ³⁰, J. Chen ^{63c}, J. Chen ¹⁴⁶, M. Chen ¹²⁹, S. Chen ⁸⁹, S.J. Chen ^{114a},
 X. Chen ^{63c}, X. Chen ^{15,ae}, C.L. Cheng ¹⁷⁵, H.C. Cheng ^{65a}, S. Cheong ¹⁴⁷, A. Cheplakov ⁴⁰,
 E. Cheremushkina ⁴⁹, E. Cherepanova ¹¹⁷, R. Cherkaoui El Moursli ^{36e}, E. Cheu ⁷, K. Cheung ⁶⁶,
 L. Chevalier ¹³⁸, V. Chiarella ⁵⁴, G. Chiarelli ^{75a}, N. Chiedde ¹⁰⁴, G. Chiodini ^{71a},
 A.S. Chisholm ²¹, A. Chitan ^{28b}, M. Chitishvili ¹⁶⁸, M.V. Chizhov ^{40,s}, K. Choi ¹¹, Y. Chou ¹⁴²,
 E.Y.S. Chow ¹¹⁶, K.L. Chu ¹⁷⁴, M.C. Chu ^{65a}, X. Chu ^{14,114c}, Z. Chubinidze ⁵⁴, J. Chudoba ¹³⁴,
 J.J. Chwastowski ⁸⁸, D. Cieri ¹¹², K.M. Ciesla ^{87a}, V. Cindro ⁹⁵, A. Ciocio ^{18a}, F. Ciroto ^{73a,73b},

Z.H. Citron ¹⁷⁴, M. Citterio ^{72a}, D.A. Ciubotaru ^{28b}, A. Clark ⁵⁷, P.J. Clark ⁵³, N. Clarke Hall ⁹⁸, C. Clarry ¹⁵⁹, S.E. Clawson ⁴⁹, C. Clement ^{48a,48b}, Y. Coadou ¹⁰⁴, M. Cobal ^{70a,70c}, A. Coccaro ^{58b}, R.F. Coelho Barrue ^{133a}, R. Coelho Lopes De Sa ¹⁰⁵, S. Coelli ^{72a}, L.S. Colangeli ¹⁵⁹, B. Cole ⁴³, P. Collado Soto ¹⁰¹, J. Collot ⁶¹, P. Conde Muiño ^{133a,133g}, M.P. Connell ^{34c}, S.H. Connell ^{34c}, E.I. Conroy ¹²⁹, F. Conventi ^{73a,ag}, H.G. Cooke ²¹, A.M. Cooper-Sarkar ¹²⁹, F.A. Corchia ^{24b,24a}, A. Cordeiro Oudot Choi ¹³⁰, L.D. Corpe ⁴², M. Corradi ^{76a,76b}, F. Corriveau ^{106,aa}, A. Cortes-Gonzalez ¹⁹, M.J. Costa ¹⁶⁸, F. Costanza ⁴, D. Costanzo ¹⁴³, B.M. Cote ¹²², J. Couthures ⁴, G. Cowan ⁹⁷, K. Cranmer ¹⁷⁵, L. Cremer ⁵⁰, D. Cremonini ^{24b,24a}, S. Crépe-Renaudin ⁶¹, F. Crescioli ¹³⁰, M. Cristinziani ¹⁴⁵, M. Cristoforetti ^{79a,79b}, V. Croft ¹¹⁷, J.E. Crosby ¹²⁴, G. Crosetti ^{45b,45a}, A. Cueto ¹⁰¹, H. Cui ⁹⁸, Z. Cui ⁷, W.R. Cunningham ⁶⁰, F. Curcio ¹⁶⁸, J.R. Curran ⁵³, P. Czodrowski ³⁷, M.J. Da Cunha Sargedas De Sousa ^{58b,58a}, J.V. Da Fonseca Pinto ^{84b}, C. Da Via ¹⁰³, W. Dabrowski ^{87a}, T. Dado ³⁷, S. Dahbi ¹⁵², T. Dai ¹⁰⁸, D. Dal Santo ²⁰, C. Dallapiccola ¹⁰⁵, M. Dam ⁴⁴, G. D'amen ³⁰, V. D'Amico ¹¹¹, J. Damp ¹⁰², J.R. Dandoy ³⁵, D. Dannheim ³⁷, M. Danninger ¹⁴⁶, V. Dao ¹⁴⁹, G. Darbo ^{58b}, S.J. Das ³⁰, F. Dattola ⁴⁹, S. D'Auria ^{72a,72b}, A. D'Avanzo ^{73a,73b}, T. Davidek ¹³⁶, I. Dawson ⁹⁶, H.A. Day-hall ¹³⁵, K. De ⁸, C. De Almeida Rossi ¹⁵⁹, R. De Asmundis ^{73a}, N. De Biase ⁴⁹, S. De Castro ^{24b,24a}, N. De Groot ¹¹⁶, P. de Jong ¹¹⁷, H. De la Torre ¹¹⁸, A. De Maria ^{114a}, A. De Salvo ^{76a}, U. De Sanctis ^{77a,77b}, F. De Santis ^{71a,71b}, A. De Santo ¹⁵⁰, J.B. De Vivie De Regie ⁶¹, J. Debevc ⁹⁵, D.V. Dedovich ⁴⁰, J. Degens ⁹⁴, A.M. Deiana ⁴⁶, J. Del Peso ¹⁰¹, L. Delagrangé ¹³⁰, F. Deliot ¹³⁸, C.M. Delitzsch ⁵⁰, M. Della Pietra ^{73a,73b}, D. Della Volpe ⁵⁷, A. Dell'Acqua ³⁷, L. Dell'Asta ^{72a,72b}, M. Delmastro ⁴, C.C. Delogu ¹⁰², P.A. Delsart ⁶¹, S. Demers ¹⁷⁷, M. Demichev ⁴⁰, S.P. Denisov ³⁹, H. Denizli ^{22a,k}, L. D'Eramo ⁴², D. Derendarz ⁸⁸, F. Derue ¹³⁰, P. Dervan ⁹⁴, K. Desch ²⁵, C. Deutsch ²⁵, F.A. Di Bello ^{58b,58a}, A. Di Ciaccio ^{77a,77b}, L. Di Ciaccio ⁴, A. Di Domenico ^{76a,76b}, C. Di Donato ^{73a,73b}, A. Di Girolamo ³⁷, G. Di Gregorio ³⁷, A. Di Luca ^{79a,79b}, B. Di Micco ^{78a,78b}, R. Di Nardo ^{78a,78b}, K.F. Di Petrillo ⁴¹, M. Diamantopoulou ³⁵, F.A. Dias ¹¹⁷, T. Dias Do Vale ¹⁴⁶, M.A. Diaz ^{140a,140b}, A.R. Didenko ⁴⁰, M. Didenko ¹⁶⁸, E.B. Diehl ¹⁰⁸, S. Díez Cornell ⁴⁹, C. Diez Pardos ¹⁴⁵, C. Dimitriadi ¹⁴⁸, A. Dimitrievska ²¹, A. Dimri ¹⁴⁹, J. Dingfelder ²⁵, T. Dingley ¹²⁹, I-M. Dinu ^{28b}, S.J. Dittmeier ^{64b}, F. Dittus ³⁷, M. Divisek ¹³⁶, B. Dixit ⁹⁴, F. Djama ¹⁰⁴, T. Djobava ^{153b}, C. Doglioni ^{103,100}, A. Dohnalova ^{29a}, Z. Dolezal ¹³⁶, K. Domijan ^{87a}, K.M. Dona ⁴¹, M. Donadelli ^{84d}, B. Dong ¹⁰⁹, J. Donini ⁴², A. D'Onofrio ^{73a,73b}, M. D'Onofrio ⁹⁴, J. Dopke ¹³⁷, A. Doria ^{73a}, N. Dos Santos Fernandes ^{133a}, P. Dougan ¹⁰³, M.T. Dova ⁹², A.T. Doyle ⁶⁰, M.A. Draguet ¹²⁹, M.P. Drescher ⁵⁶, E. Dreyer ¹⁷⁴, I. Drivas-koulouris ¹⁰, M. Drnevich ¹²⁰, M. Drozdova ⁵⁷, D. Du ^{63a}, T.A. du Pree ¹¹⁷, F. Dubinin ³⁹, M. Dubovsky ^{29a}, E. Duchovni ¹⁷⁴, G. Duckeck ¹¹¹, O.A. Ducu ^{28b}, D. Duda ⁵³, A. Dudarev ³⁷, E.R. Duden ²⁷, M. D'uffizi ¹⁰³, L. Duflot ⁶⁷, M. Dührssen ³⁷, I. Duminica ^{28g}, A.E. Dumitriu ^{28b}, M. Dunford ^{64a}, S. Dungs ⁵⁰, K. Dunne ^{48a,48b}, A. Duperrin ¹⁰⁴, H. Duran Yildiz ^{3a}, M. Düren ⁵⁹, A. Durglishvili ^{153b}, B.L. Dwyer ¹¹⁸, G.I. Dyckes ^{18a}, M. Dyndal ^{87a}, B.S. Dziedzic ³⁷, Z.O. Earnshaw ¹⁵⁰, G.H. Eberwein ¹²⁹, B. Eckerova ^{29a}, S. Eggebrecht ⁵⁶, E. Egidio Purcino De Souza ^{84e}, G. Eigen ¹⁷, K. Einsweiler ^{18a}, T. Ekelof ¹⁶⁶, P.A. Ekman ¹⁰⁰, S. El Farkh ^{36b}, Y. El Ghazali ^{63a}, H. El Jarrari ³⁷, A. El Moussaouy ^{36a}, V. Ellajosyula ¹⁶⁶, M. Ellert ¹⁶⁶, F. Ellinghaus ¹⁷⁶, N. Ellis ³⁷, J. Elmsheuser ³⁰, M. Elsayy ^{119a}, M. Elsing ³⁷, D. Emeliyanov ¹³⁷, Y. Enari ⁸⁵, I. Ene ^{18a}, S. Epari ¹³, D. Ernani Martins Neto ⁸⁸, M. Errenst ¹⁷⁶, M. Escalier ⁶⁷, C. Escobar ¹⁶⁸, E. Etzion ¹⁵⁵, G. Evans ^{133a}, H. Evans ⁶⁹, L.S. Evans ⁹⁷, A. Ezhilov ³⁹, S. Ezzarqtouni ^{36a}, F. Fabbri ^{24b,24a}, L. Fabbri ^{24b,24a}, G. Facini ⁹⁸, V. Fadeyev ¹³⁹, R.M. Fakhrutdinov ³⁹, D. Fakoudis ¹⁰², S. Falciano ^{76a},

L.F. Falda Ulhoa Coelho ^{133a}, F. Fallavollita ¹¹², G. Falsetti ^{45b,45a}, J. Faltova ¹³⁶, C. Fan ¹⁶⁷,
 K.Y. Fan ^{65b}, Y. Fan ¹⁴, Y. Fang ^{14,114c}, M. Fanti ^{72a,72b}, M. Faraj ^{70a,70b}, Z. Farazpay ⁹⁹,
 A. Farbin ⁸, A. Farilla ^{78a}, T. Farooque ¹⁰⁹, J.N. Farr ¹⁷⁷, S.M. Farrington ^{137,53}, F. Fassi ^{36e},
 D. Fassouliotis ⁹, L. Fayard ⁶⁷, P. Federic ¹³⁶, P. Federicova ¹³⁴, O.L. Fedin ^{39,a}, M. Feickert ¹⁷⁵,
 L. Feligioni ¹⁰⁴, D.E. Fellers ¹²⁶, C. Feng ^{63b}, Z. Feng ¹¹⁷, M.J. Fenton ¹⁶³, L. Ferencz ⁴⁹,
 P. Fernandez Martinez ⁶⁸, M.J.V. Fernoux ¹⁰⁴, J. Ferrando ⁹³, A. Ferrari ¹⁶⁶, P. Ferrari ^{117,116},
 R. Ferrari ^{74a}, D. Ferrere ⁵⁷, C. Ferretti ¹⁰⁸, M.P. Fewell ¹, D. Fiacco ^{76a,76b}, F. Fiedler ¹⁰²,
 P. Fiedler ¹³⁵, S. Filimonov ³⁹, A. Filipčič ⁹⁵, E.K. Filmer ^{160a}, F. Filthaut ¹¹⁶,
 M.C.N. Fiolhais ^{133a,133c,c}, L. Fiorini ¹⁶⁸, W.C. Fisher ¹⁰⁹, T. Fitschen ¹⁰³, P.M. Fitzhugh ¹³⁸,
 I. Fleck ¹⁴⁵, P. Fleischmann ¹⁰⁸, T. Flick ¹⁷⁶, M. Flores ^{34d,ac}, L.R. Flores Castillo ^{65a},
 L. Flores Sanz De Acedo ³⁷, F.M. Follega ^{79a,79b}, N. Fomin ³³, J.H. Foo ¹⁵⁹, A. Formica ¹³⁸,
 A.C. Forti ¹⁰³, E. Fortin ³⁷, A.W. Fortman ^{18a}, L. Fountas ^{9,i}, D. Fournier ⁶⁷, H. Fox ⁹³,
 P. Francavilla ^{75a,75b}, S. Francescato ⁶², S. Franchellucci ⁵⁷, M. Franchini ^{24b,24a},
 S. Franchino ^{64a}, D. Francis ³⁷, L. Franco ¹¹⁶, V. Franco Lima ³⁷, L. Franconi ⁴⁹, M. Franklin ⁶²,
 G. Frattari ²⁷, Y.Y. Frid ¹⁵⁵, J. Friend ⁶⁰, N. Fritzsche ³⁷, A. Froch ⁵⁷, D. Froidevaux ³⁷,
 J.A. Frost ¹²⁹, Y. Fu ¹⁰⁹, S. Fuenzalida Garrido ^{140f}, M. Fujimoto ¹⁰⁴, K.Y. Fung ^{65a},
 E. Furtado De Simas Filho ^{84e}, M. Furukawa ¹⁵⁷, J. Fuster ¹⁶⁸, A. Gaa ⁵⁶, A. Gabrielli ^{24b,24a},
 A. Gabrielli ¹⁵⁹, P. Gadow ³⁷, G. Gagliardi ^{58b,58a}, L.G. Gagnon ^{18a}, S. Gaid ¹⁶⁵,
 S. Galantzan ¹⁵⁵, J. Gallagher ¹, E.J. Gallas ¹²⁹, A.L. Gallen ¹⁶⁶, B.J. Gallop ¹³⁷, K.K. Gan ¹²²,
 S. Ganguly ¹⁵⁷, Y. Gao ⁵³, A. Garabaglu ¹⁴², F.M. Garay Walls ^{140a,140b}, B. Garcia ³⁰,
 C. García ¹⁶⁸, A. Garcia Alonso ¹¹⁷, A.G. Garcia Caffaro ¹⁷⁷, J.E. García Navarro ¹⁶⁸,
 M. Garcia-Sciveres ^{18a}, G.L. Gardner ¹³¹, R.W. Gardner ⁴¹, N. Garelli ¹⁶², R.B. Garg ¹⁴⁷,
 J.M. Gargan ⁵³, C.A. Garner ¹⁵⁹, C.M. Garvey ^{34a}, V.K. Gassmann ¹⁶², G. Gaudio ^{74a}, V. Gautam ¹³,
 P. Gauzzi ^{76a,76b}, J. Gavranovic ⁹⁵, I.L. Gavrilenko ³⁹, A. Gavrilyuk ³⁹, C. Gay ¹⁶⁹,
 G. Gaycken ¹²⁶, E.N. Gazis ¹⁰, A. Gekow ¹²², C. Gemme ^{58b}, M.H. Genest ⁶¹, A.D. Gentry ¹¹⁵,
 S. George ⁹⁷, W.F. George ²¹, T. Geralis ⁴⁷, A.A. Gerwin ¹²³, P. Gessinger-Befurt ³⁷,
 M.E. Geyik ¹⁷⁶, M. Ghani ¹⁷², K. Ghorbanian ⁹⁶, A. Ghosal ¹⁴⁵, A. Ghosh ¹⁶³, A. Ghosh ⁷,
 B. Giacobbe ^{24b}, S. Giagu ^{76a,76b}, T. Giani ¹¹⁷, A. Giannini ^{63a}, S.M. Gibson ⁹⁷, M. Gignac ¹³⁹,
 D.T. Gil ^{87b}, A.K. Gilbert ^{87a}, B.J. Gilbert ⁴³, D. Gillberg ³⁵, G. Gilles ¹¹⁷, L. Ginabat ¹³⁰,
 D.M. Gingrich ^{2,af}, M.P. Giordani ^{70a,70c}, P.F. Giraud ¹³⁸, G. Giugliarelli ^{70a,70c}, D. Giugni ^{72a},
 F. Giuli ^{77a,77b}, I. Gkialas ^{9,i}, L.K. Gladilin ³⁹, C. Glasman ¹⁰¹, G. Glemža ⁴⁹, M. Glisic ¹²⁶,
 I. Gnesi ^{45b}, Y. Go ³⁰, M. Goblirsch-Kolb ³⁷, B. Gocke ⁵⁰, D. Godin ¹¹⁰, B. Gokturk ^{22a},
 S. Goldfarb ¹⁰⁷, T. Golling ⁵⁷, M.G.D. Gololo ^{34c}, D. Golubkov ³⁹, J.P. Gombas ¹⁰⁹,
 A. Gomes ^{133a,133b}, G. Gomes Da Silva ¹⁴⁵, A.J. Gomez Delegido ¹⁶⁸, R. Gonçalves ^{133a},
 L. Gonella ²¹, A. Gongadze ^{153c}, F. Gonnella ²¹, J.L. Gonski ¹⁴⁷, R.Y. González Andana ⁵³,
 S. González de la Hoz ¹⁶⁸, R. Gonzalez Lopez ⁹⁴, C. Gonzalez Renteria ^{18a},
 M.V. Gonzalez Rodrigues ⁴⁹, R. Gonzalez Suarez ¹⁶⁶, S. Gonzalez-Sevilla ⁵⁷, L. Goossens ³⁷,
 B. Gorini ³⁷, E. Gorini ^{71a,71b}, A. Gorišek ⁹⁵, T.C. Gosart ¹³¹, A.T. Goshaw ⁵², M.I. Gostkin ⁴⁰,
 S. Goswami ¹²⁴, C.A. Gottardo ³⁷, S.A. Gotz ¹¹¹, M. Gouighri ^{36b}, A.G. Goussiou ¹⁴²,
 N. Govender ^{34c}, R.P. Grabarczyk ¹²⁹, I. Grabowska-Bold ^{87a}, K. Graham ³⁵, E. Gramstad ¹²⁸,
 S. Grancagnolo ^{71a,71b}, C.M. Grant ^{1,138}, P.M. Gravila ^{28f}, F.G. Gravili ^{71a,71b}, H.M. Gray ^{18a},
 M. Greco ¹¹², M.J. Green ¹, C. Grefe ²⁵, A.S. Grefsrud ¹⁷, I.M. Gregor ⁴⁹, K.T. Greif ¹⁶³,
 P. Grenier ¹⁴⁷, S.G. Grewe ¹¹², A.A. Grillo ¹³⁹, K. Grimm ³², S. Grinstein ^{13,w}, J.-F. Grivaz ⁶⁷,
 E. Gross ¹⁷⁴, J. Grosse-Knetter ⁵⁶, L. Guan ¹⁰⁸, G. Guerrieri ³⁷, R. Gugel ¹⁰², J.A.M. Guhit ¹⁰⁸,
 A. Guida ¹⁹, E. Guilloton ¹⁷², S. Guindon ³⁷, F. Guo ^{14,114c}, J. Guo ^{63c}, L. Guo ⁴⁹,
 L. Guo ^{114b,u}, Y. Guo ¹⁰⁸, A. Gupta ⁵⁰, R. Gupta ¹³², S. Gurbuz ²⁵, S.S. Gurdasani ⁴⁹,
 G. Gustavino ^{76a,76b}, P. Gutierrez ¹²³, L.F. Gutierrez Zagazeta ¹³¹, M. Gutsche ⁵¹,

C. Gutschow ⁹⁸, C. Gwenlan ¹²⁹, C.B. Gwilliam ⁹⁴, E.S. Haaland ¹²⁸, A. Haas ¹²⁰,
 M. Habedank ⁶⁰, C. Haber ^{18a}, H.K. Hadavand ⁸, A. Haddad ⁴², A. Hadeif ⁵¹, A.I. Hagan ⁹³,
 J.J. Hahn ¹⁴⁵, E.H. Haines ⁹⁸, M. Haleem ¹⁷¹, J. Haley ¹²⁴, G.D. Hallewell ¹⁰⁴, L. Halser ²⁰,
 K. Hamano ¹⁷⁰, M. Hamer ²⁵, E.J. Hampshire ⁹⁷, J. Han ^{63b}, L. Han ^{114a}, L. Han ^{63a},
 S. Han ^{18a}, K. Hanagaki ⁸⁵, M. Hance ¹³⁹, D.A. Hangal ⁴³, H. Hanif ¹⁴⁶, M.D. Hank ¹³¹,
 J.B. Hansen ⁴⁴, P.H. Hansen ⁴⁴, D. Harada ⁵⁷, T. Harenberg ¹⁷⁶, S. Harkusha ¹⁷⁸,
 M.L. Harris ¹⁰⁵, Y.T. Harris ²⁵, J. Harrison ¹³, N.M. Harrison ¹²², P.F. Harrison ¹⁷²,
 N.M. Hartman ¹¹², N.M. Hartmann ¹¹¹, R.Z. Hasan ^{97,137}, Y. Hasegawa ¹⁴⁴, F. Haslbeck ¹²⁹,
 S. Hassan ¹⁷, R. Hauser ¹⁰⁹, C.M. Hawkes ²¹, R.J. Hawkings ³⁷, Y. Hayashi ¹⁵⁷, D. Hayden ¹⁰⁹,
 C. Hayes ¹⁰⁸, R.L. Hayes ¹¹⁷, C.P. Hays ¹²⁹, J.M. Hays ⁹⁶, H.S. Hayward ⁹⁴, F. He ^{63a},
 M. He ^{14,114c}, Y. He ⁴⁹, Y. He ⁹⁸, N.B. Heatley ⁹⁶, V. Hedberg ¹⁰⁰, A.L. Heggelund ¹²⁸,
 C. Heidegger ⁵⁵, K.K. Heidegger ⁵⁵, J. Heilman ³⁵, S. Heim ⁴⁹, T. Heim ^{18a}, J.G. Heinlein ¹³¹,
 J.J. Heinrich ¹²⁶, L. Heinrich ^{112,ad}, J. Hejbal ¹³⁴, A. Held ¹⁷⁵, S. Hellesund ¹⁷,
 C.M. Helling ¹⁶⁹, S. Hellman ^{48a,48b}, L. Henkelmann ³³, A.M. Henriques Correia ³⁷, H. Herde ¹⁰⁰,
 Y. Hernández Jiménez ¹⁴⁹, L.M. Herrmann ²⁵, T. Herrmann ⁵¹, G. Herten ⁵⁵, R. Hertenberger ¹¹¹,
 L. Hervas ³⁷, M.E. Hesping ¹⁰², N.P. Hessey ^{160a}, J. Hessler ¹¹², M. Hidaoui ^{36b}, N. Hidic ¹³⁶,
 E. Hill ¹⁵⁹, S.J. Hillier ²¹, J.R. Hinds ¹⁰⁹, F. Hinterkeuser ²⁵, M. Hirose ¹²⁷, S. Hirose ¹⁶¹,
 D. Hirschbuehl ¹⁷⁶, T.G. Hitchings ¹⁰³, B. Hiti ⁹⁵, J. Hobbs ¹⁴⁹, R. Hobincu ^{28e}, N. Hod ¹⁷⁴,
 M.C. Hodgkinson ¹⁴³, B.H. Hodgkinson ¹²⁹, A. Hoecker ³⁷, D.D. Hofer ¹⁰⁸, J. Hofer ¹⁶⁸,
 M. Holzbock ³⁷, L.B.A.H. Hommels ³³, B.P. Honan ¹⁰³, J.J. Hong ⁶⁹, J. Hong ^{63c},
 T.M. Hong ¹³², B.H. Hooberman ¹⁶⁷, W.H. Hopkins ⁶, M.C. Hoppesch ¹⁶⁷, Y. Horii ¹¹³,
 M.E. Horstmann ¹¹², S. Hou ¹⁵², M.R. Housenga ¹⁶⁷, A.S. Howard ⁹⁵, J. Howarth ⁶⁰, J. Hoya ⁶,
 M. Hrabovsky ¹²⁵, T. Hryn'ova ⁴, P.J. Hsu ⁶⁶, S.-C. Hsu ¹⁴², T. Hsu ⁶⁷, M. Hu ^{18a}, Q. Hu ^{63a},
 S. Huang ³³, X. Huang ^{14,114c}, Y. Huang ¹³⁶, Y. Huang ^{114b}, Y. Huang ¹⁰², Y. Huang ¹⁴,
 Z. Huang ¹⁰³, Z. Hubacek ¹³⁵, M. Huebner ²⁵, F. Huegging ²⁵, T.B. Huffman ¹²⁹,
 M. Hufnagel Maranha De Faria ^{84a}, C.A. Hugli ⁴⁹, M. Huhtinen ³⁷, S.K. Huiberts ¹⁷,
 R. Hulsken ¹⁰⁶, C.E. Hultquist ^{18a}, N. Huseynov ^{12,f}, J. Huston ¹⁰⁹, J. Huth ⁶², R. Hyneman ⁷,
 G. Iacobucci ⁵⁷, G. Iakovidis ³⁰, L. Iconomidou-Fayard ⁶⁷, J.P. Iddon ³⁷, P. Iengo ^{73a,73b},
 R. Iguchi ¹⁵⁷, Y. Iiyama ¹⁵⁷, T. Iizawa ¹²⁹, Y. Ikegami ⁸⁵, D. Iliadis ¹⁵⁶, N. Ilic ¹⁵⁹,
 H. Imam ^{84c}, G. Inacio Goncalves ^{84d}, S.A. Infante Cabanas ^{140c}, T. Ingebretsen Carlson ^{48a,48b},
 J.M. Inglis ⁹⁶, G. Introzzi ^{74a,74b}, M. Iodice ^{78a}, V. Ippolito ^{76a,76b}, R.K. Irwin ⁹⁴, M. Ishino ¹⁵⁷,
 W. Islam ¹⁷⁵, C. Issever ¹⁹, S. Istin ^{22a,ak}, H. Ito ¹⁷³, R. Iuppa ^{79a,79b}, A. Ivina ¹⁷⁴, V. Izzo ^{73a},
 P. Jacka ¹³⁴, P. Jackson ¹, P. Jain ⁴⁹, K. Jakobs ⁵⁵, T. Jakoubek ¹⁷⁴, J. Jamieson ⁶⁰,
 W. Jang ¹⁵⁷, M. Javurkova ¹⁰⁵, P. Jawahar ¹⁰³, L. Jeanty ¹²⁶, J. Jejelava ^{153a}, P. Jenni ^{55,e},
 C.E. Jessiman ³⁵, C. Jia ^{63b}, H. Jia ¹⁶⁹, J. Jia ¹⁴⁹, X. Jia ^{14,114c}, Z. Jia ^{114a}, C. Jiang ⁵³,
 Q. Jiang ^{65b}, S. Jiggins ⁴⁹, J. Jimenez Pena ¹³, S. Jin ^{114a}, A. Jinaru ^{28b}, O. Jinnouchi ¹⁴¹,
 P. Johansson ¹⁴³, K.A. Johns ⁷, J.W. Johnson ¹³⁹, F.A. Jolly ⁴⁹, D.M. Jones ¹⁵⁰, E. Jones ⁴⁹,
 K.S. Jones ⁸, P. Jones ³³, R.W.L. Jones ⁹³, T.J. Jones ⁹⁴, H.L. Joos ^{56,37}, R. Joshi ¹²²,
 J. Jovicevic ¹⁶, X. Ju ^{18a}, J.J. Junggeburth ³⁷, T. Junkermann ^{64a}, A. Juste Rozas ^{13,w},
 M.K. Juzek ⁸⁸, S. Kabana ^{140e}, A. Kaczmarzka ⁸⁸, M. Kado ¹¹², H. Kagan ¹²², M. Kagan ¹⁴⁷,
 A. Kahn ¹³¹, C. Kahra ¹⁰², T. Kaji ¹⁵⁷, E. Kajomovitz ¹⁵⁴, N. Kakati ¹⁷⁴, I. Kalaitzidou ⁵⁵,
 N.J. Kang ¹³⁹, D. Kar ^{34g}, K. Karava ¹²⁹, E. Karentzos ²⁵, O. Karkout ¹¹⁷, S.N. Karpov ⁴⁰,
 Z.M. Karpova ⁴⁰, V. Kartvelishvili ⁹³, A.N. Karyukhin ³⁹, E. Kasimi ¹⁵⁶, J. Katzy ⁴⁹,
 S. Kaur ³⁵, K. Kawade ¹⁴⁴, M.P. Kawale ¹²³, C. Kawamoto ⁸⁹, T. Kawamoto ^{63a}, E.F. Kay ³⁷,
 F.I. Kaya ¹⁶², S. Kazakos ¹⁰⁹, V.F. Kazanin ³⁹, Y. Ke ¹⁴⁹, J.M. Keaveney ^{34a}, R. Keeler ¹⁷⁰,
 G.V. Kehris ⁶², J.S. Keller ³⁵, J.J. Kempster ¹⁵⁰, O. Kepka ¹³⁴, J. Kerr ^{160b}, B.P. Kerridge ¹³⁷,
 B.P. Kerševan ⁹⁵, L. Keszeghova ^{29a}, R.A. Khan ¹³², A. Khanov ¹²⁴, A.G. Kharlamov ³⁹,

T. Kharlamova [ID³⁹](#), E.E. Khoda [ID¹⁴²](#), M. Kholodenko [ID^{133a}](#), T.J. Khoo [ID¹⁹](#), G. Khoraiuli [ID¹⁷¹](#), J. Khubua [ID^{153b,*}](#), Y.A.R. Khwaira [ID¹³⁰](#), B. Kibirige^{34g}, D. Kim [ID⁶](#), D.W. Kim [ID^{48a,48b}](#), Y.K. Kim [ID⁴¹](#), N. Kimura [ID⁹⁸](#), M.K. Kingston [ID⁵⁶](#), A. Kirchhoff [ID⁵⁶](#), C. Kirfel [ID²⁵](#), F. Kirfel [ID²⁵](#), J. Kirk [ID¹³⁷](#), A.E. Kiryunin [ID¹¹²](#), S. Kita [ID¹⁶¹](#), C. Kitsaki [ID¹⁰](#), O. Kivernyk [ID²⁵](#), M. Klassen [ID¹⁶²](#), C. Klein [ID³⁵](#), L. Klein [ID¹⁷¹](#), M.H. Klein [ID⁴⁶](#), S.B. Klein [ID⁵⁷](#), U. Klein [ID⁹⁴](#), A. Klimentov [ID³⁰](#), T. Klioutchnikova [ID³⁷](#), P. Kluit [ID¹¹⁷](#), S. Kluth [ID¹¹²](#), E. Kneringer [ID⁸⁰](#), T.M. Knight [ID¹⁵⁹](#), A. Knue [ID⁵⁰](#), D. Kobylanskii [ID¹⁷⁴](#), S.F. Koch [ID¹²⁹](#), M. Kocian [ID¹⁴⁷](#), P. Kodyš [ID¹³⁶](#), D.M. Koeck [ID¹²⁶](#), P.T. Koenig [ID²⁵](#), T. Koffas [ID³⁵](#), O. Kolay [ID⁵¹](#), I. Koletsou [ID⁴](#), T. Komarek [ID⁸⁸](#), K. Köneke [ID⁵⁶](#), A.X.Y. Kong [ID¹](#), T. Kono [ID¹²¹](#), N. Konstantinidis [ID⁹⁸](#), P. Kontaxakis [ID⁵⁷](#), B. Konya [ID¹⁰⁰](#), R. Kopeliansky [ID⁴³](#), S. Koperny [ID^{87a}](#), K. Korcyl [ID⁸⁸](#), K. Kordas [ID^{156,d}](#), A. Korn [ID⁹⁸](#), S. Korn [ID⁵⁶](#), I. Korolkov [ID¹³](#), N. Korotkova [ID³⁹](#), B. Kortman [ID¹¹⁷](#), O. Kortner [ID¹¹²](#), S. Kortner [ID¹¹²](#), W.H. Kostecka [ID¹¹⁸](#), V.V. Kostyukhin [ID¹⁴⁵](#), A. Kotsokechagia [ID³⁷](#), A. Kotwal [ID⁵²](#), A. Koulouris [ID³⁷](#), A. Kourkoumeli-Charalampidi [ID^{74a,74b}](#), C. Kourkoumelis [ID⁹](#), E. Kourlitis [ID^{112,ad}](#), O. Kovanda [ID¹²⁶](#), R. Kowalewski [ID¹⁷⁰](#), W. Kozanecki [ID¹²⁶](#), A.S. Kozhin [ID³⁹](#), V.A. Kramarenko [ID³⁹](#), G. Kramberger [ID⁹⁵](#), P. Kramer [ID²⁵](#), M.W. Krasny [ID¹³⁰](#), A. Krasznahorkay [ID¹⁰⁵](#), A.C. Kraus [ID¹¹⁸](#), J.W. Kraus [ID¹⁷⁶](#), J.A. Kremer [ID⁴⁹](#), T. Kresse [ID⁵¹](#), L. Kretschmann [ID¹⁷⁶](#), J. Kretschmar [ID⁹⁴](#), K. Kreul [ID¹⁹](#), P. Krieger [ID¹⁵⁹](#), K. Krizka [ID²¹](#), K. Kroeninger [ID⁵⁰](#), H. Kroha [ID¹¹²](#), J. Kroll [ID¹³⁴](#), J. Kroll [ID¹³¹](#), K.S. Krowpman [ID¹⁰⁹](#), U. Kruchonak [ID⁴⁰](#), H. Krüger [ID²⁵](#), N. Krumnack⁸², M.C. Kruse [ID⁵²](#), O. Kuchinskaia [ID³⁹](#), S. Kuday [ID^{3a}](#), S. Kuehn [ID³⁷](#), R. Kuesters [ID⁵⁵](#), T. Kuhl [ID⁴⁹](#), V. Kukhtin [ID⁴⁰](#), Y. Kulchitsky [ID⁴⁰](#), S. Kuleshov [ID^{140d,140b}](#), M. Kumar [ID^{34g}](#), N. Kumari [ID⁴⁹](#), P. Kumari [ID^{160b}](#), A. Kupco [ID¹³⁴](#), T. Kupfer⁵⁰, A. Kupich [ID³⁹](#), O. Kuprash [ID⁵⁵](#), H. Kurashige [ID⁸⁶](#), L.L. Kurchaninov [ID^{160a}](#), O. Kurdysh [ID⁴](#), Y.A. Kurochkin [ID³⁸](#), A. Kurova [ID³⁹](#), M. Kuze [ID¹⁴¹](#), A.K. Kvam [ID¹⁰⁵](#), J. Kvita [ID¹²⁵](#), N.G. Kyriacou [ID¹⁰⁸](#), L.A.O. Laatu [ID¹⁰⁴](#), C. Lacasta [ID¹⁶⁸](#), F. Lacava [ID^{76a,76b}](#), H. Lacker [ID¹⁹](#), D. Lacour [ID¹³⁰](#), N.N. Lad [ID⁹⁸](#), E. Ladygin [ID⁴⁰](#), A. Lafarge [ID⁴²](#), B. Laforge [ID¹³⁰](#), T. Lagouri [ID¹⁷⁷](#), F.Z. Lahbabi [ID^{36a}](#), S. Lai [ID⁵⁶](#), J.E. Lambert [ID¹⁷⁰](#), S. Lammers [ID⁶⁹](#), W. Lampl [ID⁷](#), C. Lampoudis [ID^{156,d}](#), G. Lamprinoudis [ID¹⁰²](#), A.N. Lancaster [ID¹¹⁸](#), E. Lançon [ID³⁰](#), U. Landgraf [ID⁵⁵](#), M.P.J. Landon [ID⁹⁶](#), V.S. Lang [ID⁵⁵](#), O.K.B. Langrekken [ID¹²⁸](#), A.J. Lankford [ID¹⁶³](#), F. Lanni [ID³⁷](#), K. Lantzsck [ID²⁵](#), A. Lanza [ID^{74a}](#), M. Lanzac Berrocal [ID¹⁶⁸](#), J.F. Laporte [ID¹³⁸](#), T. Lari [ID^{72a}](#), F. Lasagni Manghi [ID^{24b}](#), M. Lassnig [ID³⁷](#), V. Latonova [ID¹³⁴](#), S.D. Lawlor [ID¹⁴³](#), Z. Lawrence [ID¹⁰³](#), R. Lazaridou¹⁷², M. Lazzaroni [ID^{72a,72b}](#), H.D.M. Le [ID¹⁰⁹](#), E.M. Le Boulicaut [ID¹⁷⁷](#), L.T. Le Pottier [ID^{18a}](#), B. Leban [ID^{24b,24a}](#), M. LeBlanc [ID¹⁰³](#), F. Ledroit-Guillon [ID⁶¹](#), S.C. Lee [ID¹⁵²](#), T.F. Lee [ID⁹⁴](#), L.L. Leeuw [ID^{34c,ai}](#), M. Lefebvre [ID¹⁷⁰](#), C. Leggett [ID^{18a}](#), G. Lehmann Miotto [ID³⁷](#), M. Leigh [ID⁵⁷](#), W.A. Leight [ID¹⁰⁵](#), W. Leinonen [ID¹¹⁶](#), A. Leisos [ID^{156,t}](#), M.A.L. Leite [ID^{84c}](#), C.E. Leitgeb [ID¹⁹](#), R. Leitner [ID¹³⁶](#), K.J.C. Leney [ID⁴⁶](#), T. Lenz [ID²⁵](#), S. Leone [ID^{75a}](#), C. Leonidopoulos [ID⁵³](#), A. Leopold [ID¹⁴⁸](#), J.H. Lepage Bourbonnais [ID³⁵](#), R. Les [ID¹⁰⁹](#), C.G. Lester [ID³³](#), M. Levchenko [ID³⁹](#), J. Levêque [ID⁴](#), L.J. Levinson [ID¹⁷⁴](#), G. Levrini [ID^{24b,24a}](#), M.P. Lewicki [ID⁸⁸](#), C. Lewis [ID¹⁴²](#), D.J. Lewis [ID⁴](#), L. Lewitt [ID¹⁴³](#), A. Li [ID³⁰](#), B. Li [ID^{63b}](#), C. Li¹⁰⁸, C-Q. Li [ID¹¹²](#), H. Li [ID^{63a}](#), H. Li [ID^{63b}](#), H. Li [ID¹⁰³](#), H. Li [ID¹⁵](#), H. Li [ID^{63b}](#), J. Li [ID^{63c}](#), K. Li [ID¹⁴](#), L. Li [ID^{63c}](#), R. Li [ID¹⁷⁷](#), S. Li [ID^{14,114c}](#), S. Li [ID^{63d,63c}](#), T. Li [ID⁵](#), X. Li [ID¹⁰⁶](#), Z. Li [ID¹⁵⁷](#), Z. Li [ID^{14,114c}](#), Z. Li [ID^{63a}](#), S. Liang [ID^{14,114c}](#), Z. Liang [ID¹⁴](#), M. Liberatore [ID¹³⁸](#), B. Liberti [ID^{77a}](#), K. Lie [ID^{65c}](#), J. Lieber Marin [ID^{84e}](#), H. Lien [ID⁶⁹](#), H. Lin [ID¹⁰⁸](#), L. Linden [ID¹¹¹](#), R.E. Lindley [ID⁷](#), J.H. Lindon [ID²](#), J. Ling [ID⁶²](#), E. Lipeles [ID¹³¹](#), A. Lipniacka [ID¹⁷](#), A. Lister [ID¹⁶⁹](#), J.D. Little [ID⁶⁹](#), B. Liu [ID¹⁴](#), B.X. Liu [ID^{114b}](#), D. Liu [ID^{63d,63c}](#), E.H.L. Liu [ID²¹](#), J.K.K. Liu [ID³³](#), K. Liu [ID^{63d}](#), K. Liu [ID^{63d,63c}](#), M. Liu [ID^{63a}](#), M.Y. Liu [ID^{63a}](#), P. Liu [ID¹⁴](#), Q. Liu [ID^{63d,142,63c}](#), X. Liu [ID^{63a}](#), X. Liu [ID^{63b}](#), Y. Liu [ID^{114b,114c}](#), Y.L. Liu [ID^{63b}](#), Y.W. Liu [ID^{63a}](#), S.L. Lloyd [ID⁹⁶](#), E.M. Lobodzinska [ID⁴⁹](#), P. Loch [ID⁷](#), E. Lodhi [ID¹⁵⁹](#), T. Lohse [ID¹⁹](#), K. Lohwasser [ID¹⁴³](#), E. Loiacono [ID⁴⁹](#), J.D. Lomas [ID²¹](#), J.D. Long [ID⁴³](#), I. Longarini [ID¹⁶³](#), R. Longo [ID¹⁶⁷](#), A. Lopez Solis [ID⁴⁹](#), N.A. Lopez-canelas [ID⁷](#), N. Lorenzo Martinez [ID⁴](#), A.M. Lory [ID¹¹¹](#), M. Losada [ID^{119a}](#), G. Lösckke Centeno [ID¹⁵⁰](#), O. Loseva [ID³⁹](#), X. Lou [ID^{48a,48b}](#), X. Lou [ID^{14,114c}](#), A. Lounis [ID⁶⁷](#), P.A. Love [ID⁹³](#), G. Lu [ID^{14,114c}](#), M. Lu [ID⁶⁷](#), S. Lu [ID¹³¹](#), Y.J. Lu [ID¹⁵²](#), H.J. Lubatti [ID¹⁴²](#),

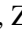












C. Luci ^{76a,76b}, F.L. Lucio Alves ^{114a}, F. Luehring ⁶⁹, B.S. Lunday ¹³¹, O. Lundberg ¹⁴⁸,
 B. Lund-Jensen ^{148,*}, N.A. Luongo ⁶, M.S. Lutz ³⁷, A.B. Lux ²⁶, D. Lynn ³⁰, R. Lysak ¹³⁴,
 E. Lytken ¹⁰⁰, V. Lyubushkin ⁴⁰, T. Lyubushkina ⁴⁰, M.M. Lyukova ¹⁴⁹, M.Firdaus M. Soberi ⁵³,
 H. Ma ³⁰, K. Ma ^{63a}, L.L. Ma ^{63b}, W. Ma ^{63a}, Y. Ma ¹²⁴, J.C. MacDonald ¹⁰²,
 P.C. Machado De Abreu Farias ^{84e}, R. Madar ⁴², T. Madula ⁹⁸, J. Maeda ⁸⁶, T. Maeno ³⁰,
 P.T. Mafa ^{34c,j}, H. Maguire ¹⁴³, V. Maiboroda ¹³⁸, A. Maio ^{133a,133b,133d}, K. Maj ^{87a},
 O. Majersky ⁴⁹, S. Majewski ¹²⁶, R. Makhmanazarov ³⁹, N. Makovec ⁶⁷, V. Maksimovic ¹⁶,
 B. Malaescu ¹³⁰, Pa. Malecki ⁸⁸, V.P. Maleev ³⁹, F. Malek ^{61,o}, M. Mali ⁹⁵, D. Malito ⁹⁷,
 U. Mallik ^{81,*}, S. Maltezos ¹⁰, S. Malyukov ⁴⁰, J. Mamuzic ¹³, G. Mancini ⁵⁴, M.N. Mancini ²⁷,
 G. Manco ^{74a,74b}, J.P. Mandalia ⁹⁶, S.S. Mandarry ¹⁵⁰, I. Mandić ⁹⁵,
 L. Manhaes de Andrade Filho ^{84a}, I.M. Maniatis ¹⁷⁴, J. Manjarres Ramos ⁹¹, D.C. Mankad ¹⁷⁴,
 A. Mann ¹¹¹, S. Manzoni ³⁷, L. Mao ^{63c}, X. Mapekula ^{34c}, A. Marantis ^{156,t}, G. Marchiori ⁵,
 M. Marcisovsky ¹³⁴, C. Marcon ^{72a}, M. Marinescu ²¹, S. Marium ⁴⁹, M. Marjanovic ¹²³,
 A. Markhoos ⁵⁵, M. Markovitch ⁶⁷, M.K. Maroun ¹⁰⁵, E.J. Marshall ⁹³, Z. Marshall ^{18a},
 S. Marti-Garcia ¹⁶⁸, J. Martin ⁹⁸, T.A. Martin ¹³⁷, V.J. Martin ⁵³, B. Martin dit Latour ¹⁷,
 L. Martinelli ^{76a,76b}, M. Martinez ^{13,w}, P. Martinez Agullo ¹⁶⁸, V.I. Martinez Outschoorn ¹⁰⁵,
 P. Martinez Suarez ¹³, S. Martin-Haugh ¹³⁷, G. Martinovicova ¹³⁶, V.S. Martoiu ^{28b},
 A.C. Martyniuk ⁹⁸, A. Marzin ³⁷, D. Mascione ^{79a,79b}, L. Masetti ¹⁰², J. Masik ¹⁰³,
 A.L. Maslennikov ⁴⁰, S.L. Mason ⁴³, P. Massarotti ^{73a,73b}, P. Mastrandrea ^{75a,75b},
 A. Mastroberardino ^{45b,45a}, T. Masubuchi ¹²⁷, T.T. Mathew ¹²⁶, J. Matousek ¹³⁶, D.M. Mattern ⁵⁰,
 J. Maurer ^{28b}, T. Maurin ⁶⁰, A.J. Maury ⁶⁷, B. Maček ⁹⁵, D.A. Maximov ³⁹, A.E. May ¹⁰³,
 R. Mazini ^{34g}, I. Maznas ¹¹⁸, M. Mazza ¹⁰⁹, S.M. Mazza ¹³⁹, E. Mazzeo ^{72a,72b},
 J.P. Mc Gowan ¹⁷⁰, S.P. Mc Kee ¹⁰⁸, C.A. Mc Lean ⁶, C.C. McCracken ¹⁶⁹, E.F. McDonald ¹⁰⁷,
 A.E. McDougall ¹¹⁷, L.F. Mcelhinney ⁹³, J.A. Mcfayden ¹⁵⁰, R.P. McGovern ¹³¹,
 R.P. Mckenzie ^{34g}, T.C. Mclachlan ⁴⁹, D.J. Mclaughlin ⁹⁸, S.J. McMahon ¹³⁷,
 C.M. Mcpartland ⁹⁴, R.A. McPherson ^{170,aa}, S. Mehlhase ¹¹¹, A. Mehta ⁹⁴, D. Melini ¹⁶⁸,
 B.R. Mellado Garcia ^{34g}, A.H. Melo ⁵⁶, F. Meloni ⁴⁹, A.M. Mendes Jacques Da Costa ¹⁰³,
 H.Y. Meng ¹⁵⁹, L. Meng ⁹³, S. Menke ¹¹², M. Mentink ³⁷, E. Meoni ^{45b,45a}, G. Mercado ¹¹⁸,
 S. Merianos ¹⁵⁶, C. Merlassino ^{70a,70c}, C. Meroni ^{72a,72b}, J. Metcalfe ⁶, A.S. Mete ⁶,
 E. Meuser ¹⁰², C. Meyer ⁶⁹, J-P. Meyer ¹³⁸, R.P. Middleton ¹³⁷, L. Mijović ⁵³,
 G. Mikenberg ¹⁷⁴, M. Mikeskikova ¹³⁴, M. Mikuž ⁹⁵, H. Mildner ¹⁰², A. Milic ³⁷,
 D.W. Miller ⁴¹, E.H. Miller ¹⁴⁷, L.S. Miller ³⁵, A. Milov ¹⁷⁴, D.A. Milstead ^{48a,48b}, T. Min ^{114a},
 A.A. Minaenko ³⁹, I.A. Minashvili ^{153b}, A.I. Mincer ¹²⁰, B. Mindur ^{87a}, M. Mineev ⁴⁰,
 Y. Mino ⁸⁹, L.M. Mir ¹³, M. Miralles Lopez ⁶⁰, M. Mironova ^{18a}, M.C. Missio ¹¹⁶, A. Mitra ¹⁷²,
 V.A. Mitsou ¹⁶⁸, Y. Mitsumori ¹¹³, O. Miu ¹⁵⁹, P.S. Miyagawa ⁹⁶, T. Mkrtchyan ^{64a},
 M. Mlinarevic ⁹⁸, T. Mlinarevic ⁹⁸, M. Mlynarikova ³⁷, S. Mobius ²⁰, P. Mogg ¹¹¹,
 M.H. Mohamed Farook ¹¹⁵, A.F. Mohammed ^{14,114c}, S. Mohapatra ⁴³, S. Mohiuddin ¹²⁴,
 G. Mokgatitwane ^{34g}, L. Moleri ¹⁷⁴, B. Mondal ¹⁴⁵, S. Mondal ¹³⁵, K. Mönig ⁴⁹,
 E. Monnier ¹⁰⁴, L. Monsonis Romero ¹⁶⁸, J. Montejo Berlingen ¹³, A. Montella ^{48a,48b},
 M. Montella ¹²², F. Montereali ^{78a,78b}, F. Monticelli ⁹², S. Monzani ^{70a,70c}, A. Morancho Tarda ⁴⁴,
 N. Morange ⁶⁷, A.L. Moreira De Carvalho ⁴⁹, M. Moreno Llácer ¹⁶⁸, C. Moreno Martinez ⁵⁷,
 J.M. Moreno Perez ^{23b}, P. Morettini ^{58b}, S. Morgenstern ³⁷, M. Morii ⁶², M. Morinaga ¹⁵⁷,
 M. Moritsu ⁹⁰, F. Morodei ^{76a,76b}, P. Moschovakos ³⁷, B. Moser ¹²⁹, M. Mosidze ^{153b},
 T. Moskalets ⁴⁶, P. Moskvitina ¹¹⁶, J. Moss ^{32,1}, P. Moszkowicz ^{87a}, A. Moussa ^{36d},
 Y. Moyal ¹⁷⁴, E.J.W. Moyse ¹⁰⁵, O. Mtintsilana ^{34g}, S. Muanza ¹⁰⁴, J. Mueller ¹³², R. Müller ³⁷,
 G.A. Mullier ¹⁶⁶, A.J. Mullin ³³, J.J. Mullin ¹³¹, A.E. Mulski ⁶², D.P. Mungo ¹⁵⁹,
 D. Munoz Perez ¹⁶⁸, F.J. Munoz Sanchez ¹⁰³, M. Murin ¹⁰³, W.J. Murray ^{172,137}, M. Muškinja ⁹⁵,

C. Mwewa ³⁰, A.G. Myagkov ^{39,a}, A.J. Myers ⁸, G. Myers ¹⁰⁸, M. Myska ¹³⁵,
 B.P. Nachman ^{18a}, K. Nagai ¹²⁹, K. Nagano ⁸⁵, R. Nagasaka ¹⁵⁷, J.L. Nagle ^{30,ah}, E. Nagy ¹⁰⁴,
 A.M. Nairz ³⁷, Y. Nakahama ⁸⁵, K. Nakamura ⁸⁵, K. Nakkalil ⁵, H. Nanjo ¹²⁷,
 E.A. Narayanan ⁴⁶, Y. Narukawa ¹⁵⁷, I. Naryshkin ³⁹, L. Nasella ^{72a,72b}, S. Nasri ^{119b},
 C. Nass ²⁵, G. Navarro ^{23a}, J. Navarro-Gonzalez ¹⁶⁸, A. Nayaz ¹⁹, P.Y. Nechaeva ³⁹,
 S. Nechaeva ^{24b,24a}, F. Nechansky ¹³⁴, L. Nedic ¹²⁹, T.J. Neep ²¹, A. Negri ^{74a,74b},
 M. Negrini ^{24b}, C. Nellist ¹¹⁷, C. Nelson ¹⁰⁶, K. Nelson ¹⁰⁸, S. Nemecek ¹³⁴, M. Nessi ^{37,g},
 M.S. Neubauer ¹⁶⁷, F. Neuhaus ¹⁰², J. Newell ⁹⁴, P.R. Newman ²¹, Y.W.Y. Ng ¹⁶⁷, B. Ngair ^{119a},
 H.D.N. Nguyen ¹¹⁰, R.B. Nickerson ¹²⁹, R. Nicolaidou ¹³⁸, J. Nielsen ¹³⁹, M. Niemeyer ⁵⁶,
 J. Niermann ³⁷, N. Nikiforou ³⁷, V. Nikolaenko ^{39,a}, I. Nikolic-Audit ¹³⁰, P. Nilsson ³⁰,
 I. Ninca ⁴⁹, G. Ninio ¹⁵⁵, A. Nisati ^{76a}, N. Nishu ², R. Nisius ¹¹², N. Nitika ^{70a,70c},
 J-E. Nitschke ⁵¹, E.K. Nkadimeng ^{34g}, T. Nobe ¹⁵⁷, T. Nommensen ¹⁵¹, M.B. Norfolk ¹⁴³,
 B.J. Norman ³⁵, M. Noury ^{36a}, J. Novak ⁹⁵, T. Novak ⁹⁵, R. Novotny ¹¹⁵, L. Nozka ¹²⁵,
 K. Ntekas ¹⁶³, N.M.J. Nunes De Moura Junior ^{84b}, J. Ocariz ¹³⁰, A. Ochi ⁸⁶, I. Ochoa ^{133a},
 S. Oerdek ^{49,x}, J.T. Offermann ⁴¹, A. Ogrodnik ¹³⁶, A. Oh ¹⁰³, C.C. Ohm ¹⁴⁸, H. Oide ⁸⁵,
 R. Oishi ¹⁵⁷, M.L. Ojeda ³⁷, Y. Okumura ¹⁵⁷, L.F. Oleiro Seabra ^{133a}, I. Oleksiyuk ⁵⁷,
 S.A. Olivares Pino ^{140d}, G. Oliveira Correa ¹³, D. Oliveira Damazio ³⁰, J.L. Oliver ¹⁶³,
 Ö.O. Öncel ⁵⁵, A.P. O'Neill ²⁰, A. Onofre ^{133a,133e}, P.U.E. Onyisi ¹¹, M.J. Oreglia ⁴¹,
 D. Orestano ^{78a,78b}, R.S. Orr ¹⁵⁹, L.M. Osojnak ¹³¹, Y. Osumi ¹¹³, G. Otero y Garzon ³¹,
 H. Otono ⁹⁰, G.J. Ottino ^{18a}, M. Ouchrif ^{36d}, F. Ould-Saada ¹²⁸, T. Ovsianikova ¹⁴²,
 M. Owen ⁶⁰, R.E. Owen ¹³⁷, V.E. Ozcan ^{22a}, F. Ozturk ⁸⁸, N. Ozturk ⁸, S. Ozturk ⁸³,
 H.A. Pacey ¹²⁹, K. Pachal ^{160a}, A. Pacheco Pages ¹³, C. Padilla Aranda ¹³, G. Padovano ^{76a,76b},
 S. Pagan Griso ^{18a}, G. Palacino ⁶⁹, A. Palazzo ^{71a,71b}, J. Pampel ²⁵, J. Pan ¹⁷⁷, T. Pan ^{65a},
 D.K. Panchal ¹¹, C.E. Pandini ¹¹⁷, J.G. Panduro Vazquez ¹³⁷, H.D. Pandya ¹, H. Pang ¹³⁸,
 P. Pani ⁴⁹, G. Panizzo ^{70a,70c}, L. Panwar ¹³⁰, L. Paolozzi ⁵⁷, S. Parajuli ¹⁶⁷, A. Paramonov ⁶,
 C. Paraskevopoulos ⁵⁴, D. Paredes Hernandez ^{65b}, A. Pareti ^{74a,74b}, K.R. Park ⁴³, T.H. Park ¹¹²,
 F. Parodi ^{58b,58a}, J.A. Parsons ⁴³, U. Parzefall ⁵⁵, B. Pascual Dias ¹¹⁰, L. Pascual Dominguez ¹⁰¹,
 E. Pasqualucci ^{76a}, S. Passaggio ^{58b}, F. Pastore ⁹⁷, P. Patel ⁸⁸, U.M. Patel ⁵², J.R. Pater ¹⁰³,
 T. Pauly ³⁷, F. Pauwels ¹³⁶, C.I. Pazos ¹⁶², M. Pedersen ¹²⁸, R. Pedro ^{133a}, S.V. Peleganchuk ³⁹,
 O. Penc ³⁷, E.A. Pender ⁵³, S. Peng ¹⁵, G.D. Penn ¹⁷⁷, K.E. Pensi ¹¹¹, M. Penzin ³⁹,
 B.S. Peralva ^{84d}, A.P. Pereira Peixoto ¹⁴², L. Pereira Sanchez ¹⁴⁷, D.V. Perepelitsa ^{30,ah},
 G. Perera ¹⁰⁵, E. Perez Codina ^{160a}, M. Perganti ¹⁰, H. Pernegger ³⁷, S. Perrella ^{76a,76b},
 O. Perrin ⁴², K. Peters ⁴⁹, R.F.Y. Peters ¹⁰³, B.A. Petersen ³⁷, T.C. Petersen ⁴⁴, E. Petit ¹⁰⁴,
 V. Petousis ¹³⁵, C. Petridou ^{156,d}, T. Petru ¹³⁶, A. Petrukhin ¹⁴⁵, M. Pettee ^{18a}, A. Petukhov ⁸³,
 K. Petukhova ³⁷, R. Pezoa ^{140f}, L. Pezzotti ^{24b,24a}, G. Pezzullo ¹⁷⁷, L. Pfaffenbichler ³⁷,
 A.J. Pflieger ³⁷, T.M. Pham ¹⁷⁵, T. Pham ¹⁰⁷, P.W. Phillips ¹³⁷, G. Piacquadio ¹⁴⁹, E. Pianori ^{18a},
 F. Piazza ¹²⁶, R. Piegai ³¹, D. Pietreanu ^{28b}, A.D. Pilkington ¹⁰³, M. Pinamonti ^{70a,70c},
 J.L. Pinfeld ², B.C. Pinheiro Pereira ^{133a}, J. Pinol Bel ¹³, A.E. Pinto Pinoargote ¹³⁸,
 L. Pintucci ^{70a,70c}, K.M. Piper ¹⁵⁰, A. Pirttikoski ⁵⁷, D.A. Pizzi ³⁵, L. Pizzimento ^{65b},
 M.-A. Pleier ³⁰, V. Pleskot ¹³⁶, E. Plotnikova ⁴⁰, G. Poddar ⁹⁶, R. Poettgen ¹⁰⁰, L. Poggioli ¹³⁰,
 S. Polacek ¹³⁶, G. Polesello ^{74a}, A. Poley ^{146,160a}, A. Polini ^{24b}, C.S. Pollard ¹⁷²,
 Z.B. Pollock ¹²², E. Pompa Pacchi ¹²³, N.I. Pond ⁹⁸, D. Ponomarenko ⁶⁹, L. Pontecorvo ³⁷,
 S. Popa ^{28a}, G.A. Popeneciu ^{28d}, A. Poreba ³⁷, D.M. Portillo Quintero ^{160a}, S. Pospisil ¹³⁵,
 M.A. Postill ¹⁴³, P. Postolache ^{28c}, K. Potamianos ¹⁷², P.A. Potepa ^{87a}, I.N. Potrap ⁴⁰,
 C.J. Potter ³³, H. Potti ¹⁵¹, J. Poveda ¹⁶⁸, M.E. Pozo Astigarraga ³⁷, A. Prades Ibanez ^{77a,77b},
 J. Pretel ¹⁷⁰, D. Price ¹⁰³, M. Primavera ^{71a}, L. Primomo ^{70a,70c}, M.A. Principe Martin ¹⁰¹,
 R. Privara ¹²⁵, T. Procter ⁶⁰, M.L. Proffitt ¹⁴², N. Proklova ¹³¹, K. Prokofiev ^{65c}, G. Proto ¹¹²,

J. Proudfoot ⁶, M. Przybycien ^{87a}, W.W. Przygoda ^{87b}, A. Psallidas ⁴⁷, J.E. Puddefoot ¹⁴³,
 D. Pudzha ⁵⁵, D. Pyatiizbyantseva ¹¹⁶, J. Qian ¹⁰⁸, R. Qian ¹⁰⁹, D. Qichen ¹⁰³, Y. Qin ¹³,
 T. Qiu ⁵³, A. Quadt ⁵⁶, M. Queitsch-Maitland ¹⁰³, G. Quetant ⁵⁷, R.P. Quinn ¹⁶⁹,
 G. Rabanal Bolanos ⁶², D. Rafanoharana ⁵⁵, F. Raffaelli ^{77a,77b}, F. Ragusa ^{72a,72b}, J.L. Rainbolt ⁴¹,
 J.A. Raine ⁵⁷, S. Rajagopalan ³⁰, E. Ramakoti ³⁹, L. Rambelli ^{58b,58a}, I.A. Ramirez-Berend ³⁵,
 K. Ran ^{49,114c}, D.S. Rankin ¹³¹, N.P. Rapheeha ^{34g}, H. Rasheed ^{28b}, V. Raskina ¹³⁰,
 D.F. Rassloff ^{64a}, A. Rastogi ^{18a}, S. Rave ¹⁰², S. Ravera ^{58b,58a}, B. Ravina ³⁷, I. Ravinovich ¹⁷⁴,
 M. Raymond ³⁷, A.L. Read ¹²⁸, N.P. Readioff ¹⁴³, D.M. Rebuzzi ^{74a,74b}, A.S. Reed ¹¹²,
 K. Reeves ²⁷, J.A. Reidelsturz ¹⁷⁶, D. Reikher ¹²⁶, A. Rej ⁵⁰, C. Rembser ³⁷, H. Ren ^{63a},
 M. Renda ^{28b}, F. Renner ⁴⁹, A.G. Rennie ¹⁶³, A.L. Rescia ⁴⁹, S. Resconi ^{72a},
 M. Ressegotti ^{58b,58a}, S. Rettie ³⁷, W.F. Rettie ³⁵, J.G. Reyes Rivera ¹⁰⁹, E. Reynolds ^{18a},
 O.L. Rezanova ⁴⁰, P. Reznicek ¹³⁶, H. Riani ^{36d}, N. Ribaric ⁵², E. Ricci ^{79a,79b}, R. Richter ¹¹²,
 S. Richter ^{48a,48b}, E. Richter-Was ^{87b}, M. Ridel ¹³⁰, S. Ridouani ^{36d}, P. Rieck ¹²⁰, P. Riedler ³⁷,
 E.M. Riefel ^{48a,48b}, J.O. Rieger ¹¹⁷, M. Rijssenbeek ¹⁴⁹, M. Rimoldi ³⁷, L. Rinaldi ^{24b,24a},
 P. Rincke ^{56,166}, G. Ripellino ¹⁶⁶, I. Riu ¹³, J.C. Rivera Vergara ¹⁷⁰, F. Rizatdinova ¹²⁴,
 E. Rizvi ⁹⁶, B.R. Roberts ^{18a}, S.S. Roberts ¹³⁹, D. Robinson ³³, M. Robles Manzano ¹⁰²,
 A. Robson ⁶⁰, A. Rocchi ^{77a,77b}, C. Roda ^{75a,75b}, S. Rodriguez Bosca ³⁷, Y. Rodriguez Garcia ^{23a},
 A.M. Rodríguez Vera ¹¹⁸, S. Roe ³⁷, J.T. Roemer ³⁷, O. Røhne ¹²⁸, C.P.A. Roland ¹³⁰, J. Roloff ³⁰,
 A. Romaniouk ⁸⁰, E. Romano ^{74a,74b}, M. Romano ^{24b}, A.C. Romero Hernandez ¹⁶⁷,
 N. Rompotis ⁹⁴, L. Roos ¹³⁰, S. Rosati ^{76a}, B.J. Rosser ⁴¹, E. Rossi ¹²⁹, E. Rossi ^{73a,73b},
 L.P. Rossi ⁶², L. Rossini ⁵⁵, R. Rosten ¹²², M. Rotaru ^{28b}, B. Rottler ⁵⁵, D. Rousseau ⁶⁷,
 D. Rousso ⁴⁹, S. Roy-Garand ¹⁵⁹, A. Rozanov ¹⁰⁴, Z.M.A. Rozario ⁶⁰, Y. Rozen ¹⁵⁴,
 A. Rubio Jimenez ¹⁶⁸, V.H. Ruelas Rivera ¹⁹, T.A. Ruggeri ¹, A. Ruggiero ¹²⁹,
 A. Ruiz-Martinez ¹⁶⁸, A. Rummler ³⁷, Z. Rurikova ⁵⁵, N.A. Rusakovich ⁴⁰, H.L. Russell ¹⁷⁰,
 G. Russo ^{76a,76b}, J.P. Rutherford ⁷, S. Rutherford Colmenares ³³, M. Rybar ¹³⁶, E.B. Rye ¹²⁸,
 A. Ryzhov ⁴⁶, J.A. Sabater Iglesias ⁵⁷, H.F.W. Sadrozinski ¹³⁹, F. Safai Tehrani ^{76a}, S. Saha ¹,
 M. Sahinsoy ⁸³, A. Saibel ¹⁶⁸, B.T. Saifuddin ¹²³, M. Saimpert ¹³⁸, M. Saito ¹⁵⁷, T. Saito ¹⁵⁷,
 A. Sala ^{72a,72b}, D. Salamani ³⁷, A. Salnikov ¹⁴⁷, J. Salt ¹⁶⁸, A. Salvador Salas ¹⁵⁵,
 D. Salvatore ^{45b,45a}, F. Salvatore ¹⁵⁰, A. Salzburger ³⁷, D. Sammel ⁵⁵, E. Sampson ⁹³,
 D. Sampsonidis ^{156,d}, D. Sampsonidou ¹²⁶, J. Sánchez ¹⁶⁸, V. Sanchez Sebastian ¹⁶⁸,
 H. Sandaker ¹²⁸, C.O. Sander ⁴⁹, J.A. Sandesara ¹⁰⁵, M. Sandhoff ¹⁷⁶, C. Sandoval ^{23b},
 L. Sanfilippo ^{64a}, D.P.C. Sankey ¹³⁷, T. Sano ⁸⁹, A. Sansoni ⁵⁴, L. Santi ³⁷, C. Santoni ⁴²,
 H. Santos ^{133a,133b}, A. Santra ¹⁷⁴, E. Sanzani ^{24b,24a}, K.A. Saoucha ¹⁶⁵, J.G. Saraiva ^{133a,133d},
 J. Sardain ⁷, O. Sasaki ⁸⁵, K. Sato ¹⁶¹, C. Sauer ³⁷, E. Sauvan ⁴, P. Savard ^{159,af}, R. Sawada ¹⁵⁷,
 C. Sawyer ¹³⁷, L. Sawyer ⁹⁹, C. Sbarra ^{24b}, A. Sbrizzi ^{24b,24a}, T. Scanlon ⁹⁸,
 J. Schaarschmidt ¹⁴², U. Schäfer ¹⁰², A.C. Schaffer ^{67,46}, D. Schaile ¹¹¹, R.D. Schamberger ¹⁴⁹,
 C. Scharf ¹⁹, M.M. Schefer ²⁰, V.A. Schegelsky ³⁹, D. Scheirich ¹³⁶, M. Schernau ^{140e},
 C. Scheulen ⁵⁷, C. Schiavi ^{58b,58a}, M. Schioppa ^{45b,45a}, B. Schlag ¹⁴⁷, S. Schlenker ³⁷,
 J. Schmeing ¹⁷⁶, M.A. Schmidt ¹⁷⁶, K. Schmieden ¹⁰², C. Schmitt ¹⁰², N. Schmitt ¹⁰²,
 S. Schmitt ⁴⁹, L. Schoeffel ¹³⁸, A. Schoening ^{64b}, P.G. Scholer ³⁵, E. Schopf ¹⁴⁵, M. Schott ²⁵,
 S. Schramm ⁵⁷, T. Schroer ⁵⁷, H-C. Schultz-Coulon ^{64a}, M. Schumacher ⁵⁵, B.A. Schumm ¹³⁹,
 Ph. Schune ¹³⁸, H.R. Schwartz ¹³⁹, A. Schwartzman ¹⁴⁷, T.A. Schwarz ¹⁰⁸, Ph. Schwemling ¹³⁸,
 R. Schwienhorst ¹⁰⁹, F.G. Sciacca ²⁰, A. Sciandra ³⁰, G. Sciolla ²⁷, F. Scuri ^{75a},
 C.D. Sebastiani ³⁷, K. Sedlaczek ¹¹⁸, S.C. Seidel ¹¹⁵, A. Seiden ¹³⁹, B.D. Seidlitz ⁴³,
 C. Seitz ⁴⁹, J.M. Seixas ^{84b}, G. Sekhniaidze ^{73a}, L. Selem ⁶¹, N. Semprini-Cesari ^{24b,24a},
 A. Semushin ^{178,39}, D. Sengupta ⁵⁷, V. Senthilkumar ¹⁶⁸, L. Serin ⁶⁷, M. Sessa ^{77a,77b},
 H. Severini ¹²³, F. Sforza ^{58b,58a}, A. Sfyrla ⁵⁷, Q. Sha ¹⁴, E. Shabalina ⁵⁶, H. Shaddix ¹¹⁸,

A.H. Shah ³³, R. Shaheen ¹⁴⁸, J.D. Shahinian ¹³¹, D. Shaked Renous ¹⁷⁴, M. Shamim ³⁷,
 L.Y. Shan ¹⁴, M. Shapiro ^{18a}, A. Sharma ³⁷, A.S. Sharma ¹⁶⁹, P. Sharma ³⁰, P.B. Shatalov ³⁹,
 K. Shaw ¹⁵⁰, S.M. Shaw ¹⁰³, Q. Shen ^{63c}, D.J. Sheppard ¹⁴⁶, P. Sherwood ⁹⁸, L. Shi ⁹⁸,
 X. Shi ¹⁴, S. Shimizu ⁸⁵, C.O. Shimmin ¹⁷⁷, I.P.J. Shipsey ^{129,*}, S. Shirabe ⁹⁰,
 M. Shiyakova ^{40,y}, M.J. Shochet ⁴¹, D.R. Shope ¹²⁸, B. Shrestha ¹²³, S. Shrestha ^{122,aj},
 I. Shreyber ³⁹, M.J. Shroff ¹⁷⁰, P. Sicho ¹³⁴, A.M. Sickles ¹⁶⁷, E. Sideras Haddad ^{34g,164},
 A.C. Sidley ¹¹⁷, A. Sidoti ^{24b}, F. Siegert ⁵¹, Dj. Sijacki ¹⁶, F. Sili ⁹², J.M. Silva ⁵³,
 I. Silva Ferreira ^{84b}, M.V. Silva Oliveira ³⁰, S.B. Silverstein ^{48a}, S. Simion ⁶⁷, R. Simoniello ³⁷,
 E.L. Simpson ¹⁰³, H. Simpson ¹⁵⁰, L.R. Simpson ¹⁰⁸, S. Simsek ⁸³, S. Sindhu ⁵⁶, P. Sinervo ¹⁵⁹,
 S.N. Singh ²⁷, S. Singh ³⁰, S. Sinha ⁴⁹, S. Sinha ¹⁰³, M. Sioli ^{24b,24a}, K. Sioulas ⁹, I. Siral ³⁷,
 E. Sitnikova ⁴⁹, J. Sjölin ^{48a,48b}, A. Skaf ⁵⁶, E. Skorda ²¹, P. Skubic ¹²³, M. Slawinska ⁸⁸,
 I. Slazyk ¹⁷, V. Smakhtin ¹⁷⁴, B.H. Smart ¹³⁷, S.Yu. Smirnov ^{140b}, Y. Smirnov ³⁹,
 L.N. Smirnova ^{39,a}, O. Smirnova ¹⁰⁰, A.C. Smith ⁴³, D.R. Smith ¹⁶³, E.A. Smith ⁴¹, J.L. Smith ¹⁰³,
 M.B. Smith ³⁵, R. Smith ¹⁴⁷, H. Smitmanns ¹⁰², M. Smizanska ⁹³, K. Smolek ¹³⁵, A.A. Snesarev ⁴⁰,
 H.L. Snoek ¹¹⁷, S. Snyder ³⁰, R. Sobie ^{170,aa}, A. Soffer ¹⁵⁵, C.A. Solans Sanchez ³⁷,
 E.Yu. Soldatov ³⁹, U. Soldevila ¹⁶⁸, A.A. Solodkov ^{34g}, S. Solomon ²⁷, A. Soloshenko ⁴⁰,
 K. Solovieva ⁵⁵, O.V. Solovyanov ⁴², P. Sommer ⁵¹, A. Sonay ¹³, W.Y. Song ^{160b},
 A. Sopczak ¹³⁵, A.L. Soppio ⁵³, F. Sopkova ^{29b}, J.D. Sorenson ¹¹⁵, I.R. Sotarriva Alvarez ¹⁴¹,
 V. Sothilingam ^{64a}, O.J. Soto Sandoval ^{140c,140b}, S. Sottocornola ⁶⁹, R. Soualah ¹⁶⁵,
 Z. Soumami ^{36e}, D. South ⁴⁹, N. Soybelman ¹⁷⁴, S. Spagnolo ^{71a,71b}, M. Spalla ¹¹²,
 D. Sperlich ⁵⁵, B. Spisso ^{73a,73b}, D.P. Spiteri ⁶⁰, M. Spousta ¹³⁶, E.J. Staats ³⁵, R. Stamen ^{64a},
 E. Stanecka ⁸⁸, W. Stanek-Maslouska ⁴⁹, M.V. Stange ⁵¹, B. Stanislaus ^{18a}, M.M. Stanitzki ⁴⁹,
 B. Stapf ⁴⁹, E.A. Starchenko ³⁹, G.H. Stark ¹³⁹, J. Stark ⁹¹, P. Staroba ¹³⁴, P. Starovoitov ¹⁶⁵,
 R. Staszewski ⁸⁸, G. Stavropoulos ⁴⁷, A. Steff ³⁷, P. Steinberg ³⁰, B. Stelzer ^{146,160a},
 H.J. Stelzer ¹³², O. Stelzer-Chilton ^{160a}, H. Stenzel ⁵⁹, T.J. Stevenson ¹⁵⁰, G.A. Stewart ³⁷,
 J.R. Stewart ¹²⁴, M.C. Stockton ³⁷, G. Stoicea ^{28b}, M. Stolarski ^{133a}, S. Stonjek ¹¹²,
 A. Straessner ⁵¹, J. Strandberg ¹⁴⁸, S. Strandberg ^{48a,48b}, M. Stratmann ¹⁷⁶, M. Strauss ¹²³,
 T. Strebler ¹⁰⁴, P. Strizenec ^{29b}, R. Ströhmer ¹⁷¹, D.M. Strom ¹²⁶, R. Stroynowski ⁴⁶,
 A. Strubig ^{48a,48b}, S.A. Stucci ³⁰, B. Stugu ¹⁷, J. Stupak ¹²³, N.A. Styles ⁴⁹, D. Su ¹⁴⁷,
 S. Su ^{63a}, W. Su ^{63d}, X. Su ^{63a}, D. Suchy ^{29a}, K. Sugizaki ¹³¹, V.V. Sulin ³⁹, M.J. Sullivan ⁹⁴,
 D.M.S. Sultan ¹²⁹, L. Sultanaliyeva ³⁹, S. Sultansoy ^{3b}, S. Sun ¹⁷⁵, W. Sun ¹⁴,
 O. Sunneborn Gudnadottir ¹⁶⁶, N. Sur ¹⁰⁴, M.R. Sutton ¹⁵⁰, H. Suzuki ¹⁶¹, M. Svatos ¹³⁴,
 M. Swiatlowski ^{160a}, T. Swirski ¹⁷¹, I. Sykora ^{29a}, M. Sykora ¹³⁶, T. Sykora ¹³⁶, D. Ta ¹⁰²,
 K. Tackmann ^{49,x}, A. Taffard ¹⁶³, R. Tafirout ^{160a}, J.S. Tafoya Vargas ⁵⁷, Y. Takubo ⁸⁵,
 M. Talby ¹⁰⁴, A.A. Talyshev ³⁹, K.C. Tam ^{65b}, N.M. Tamir ¹⁵⁵, A. Tanaka ¹⁵⁷, J. Tanaka ¹⁵⁷,
 R. Tanaka ⁶⁷, M. Tanasini ¹⁴⁹, Z. Tao ¹⁶⁹, S. Tapia Araya ^{140f}, S. Tapprogge ¹⁰²,
 A. Tarek Abouelfadl Mohamed ¹⁰⁹, S. Tarem ¹⁵⁴, K. Tariq ¹⁴, G. Tarna ^{28b}, G.F. Tartarelli ^{72a},
 M.J. Tartarin ⁹¹, P. Tas ¹³⁶, M. Tasevsky ¹³⁴, E. Tassi ^{45b,45a}, A.C. Tate ¹⁶⁷, G. Tateno ¹⁵⁷,
 Y. Tayalati ^{36e,z}, G.N. Taylor ¹⁰⁷, W. Taylor ^{160b}, A.S. Tegetmeier ⁹¹, P. Teixeira-Dias ⁹⁷,
 J.J. Teoh ¹⁵⁹, K. Terashi ¹⁵⁷, J. Terron ¹⁰¹, S. Terzo ¹³, M. Testa ⁵⁴, R.J. Teuscher ^{159,aa},
 A. Thaler ⁸⁰, O. Theiner ⁵⁷, T. Theveneaux-Pelzer ¹⁰⁴, O. Thielmann ¹⁷⁶, D.W. Thomas ⁹⁷,
 J.P. Thomas ²¹, E.A. Thompson ^{18a}, P.D. Thompson ²¹, E. Thomson ¹³¹, R.E. Thornberry ⁴⁶,
 C. Tian ^{63a}, Y. Tian ⁵⁷, V. Tikhomirov ^{39,a}, Yu.A. Tikhonov ³⁹, S. Timoshenko ³⁹,
 D. Timoshyn ¹³⁶, E.X.L. Ting ¹, P. Tipton ¹⁷⁷, A. Tishelman-Charny ³⁰, S.H. Tlou ^{34g},
 K. Todome ¹⁴¹, S. Todorova-Nova ¹³⁶, S. Todt ⁵¹, L. Toffolin ^{70a,70c}, M. Togawa ⁸⁵, J. Tojo ⁹⁰,
 S. Tokár ^{29a}, O. Toldaiev ⁶⁹, G. Tolkachev ¹⁰⁴, M. Tomoto ^{85,113}, L. Tompkins ^{147,n},
 E. Torrence ¹²⁶, H. Torres ⁹¹, E. Torró Pastor ¹⁶⁸, M. Toscani ³¹, C. Toscirri ⁴¹, M. Tost ¹¹,

D.R. Tovey ¹⁴³, T. Trefzger ¹⁷¹, A. Tricoli ³⁰, I.M. Trigger ^{160a}, S. Trincaz-Duvoid ¹³⁰,
 D.A. Trischuk ²⁷, A. Tropina ⁴⁰, L. Truong ^{34c}, M. Trzebinski ⁸⁸, A. Trzupke ⁸⁸, F. Tsai ¹⁴⁹,
 M. Tsai ¹⁰⁸, A. Tsiamis ¹⁵⁶, P.V. Tsiarehka ⁴⁰, S. Tsigaridas ^{160a}, A. Tsirigotis ^{156,t},
 V. Tsiskaridze ¹⁵⁹, E.G. Tskhadadze ^{153a}, M. Tsopoulou ¹⁵⁶, Y. Tsujikawa ⁸⁹, I.I. Tsukerman ³⁹,
 V. Tsulaia ^{18a}, S. Tsuno ⁸⁵, K. Tsuri ¹²¹, D. Tsybychev ¹⁴⁹, Y. Tu ^{65b}, A. Tudorache ^{28b},
 V. Tudorache ^{28b}, S. Turchikhin ^{58b,58a}, I. Turk Cakir ^{3a}, R. Turra ^{72a}, T. Turtuvshin ⁴⁰,
 P.M. Tuts ⁴³, S. Tzamarias ^{156,d}, E. Tzovara ¹⁰², F. Ukegawa ¹⁶¹, P.A. Ulloa Poblete ^{140c,140b},
 E.N. Umaka ³⁰, G. Unal ³⁷, A. Undrus ³⁰, G. Unel ¹⁶³, J. Urban ^{29b}, P. Urrejola ^{140a}, G. Usai ⁸,
 R. Ushioda ¹⁵⁸, M. Usman ¹¹⁰, F. Ustuner ⁵³, Z. Uysal ⁸³, V. Vacek ¹³⁵, B. Vachon ¹⁰⁶,
 T. Vafeiadis ³⁷, A. Vaitkus ⁹⁸, C. Valderanis ¹¹¹, E. Valdes Santurio ^{48a,48b}, M. Valente ^{160a},
 S. Valentinetti ^{24b,24a}, A. Valero ¹⁶⁸, E. Valiente Moreno ¹⁶⁸, A. Vallier ⁹¹, J.A. Valls Ferrer ¹⁶⁸,
 D.R. Van Arneeman ¹¹⁷, T.R. Van Daalen ¹⁴², A. Van Der Graaf ⁵⁰, H.Z. Van Der Schyf ^{34g},
 P. Van Gemmeren ⁶, M. Van Rijnbach ³⁷, S. Van Stroud ⁹⁸, I. Van Vulpen ¹¹⁷, P. Vana ¹³⁶,
 M. Vanadia ^{77a,77b}, U.M. Vande Voorde ¹⁴⁸, W. Vandelli ³⁷, E.R. Vandewall ¹²⁴, D. Vannicola ¹⁵⁵,
 L. Vannoli ⁵⁴, R. Vari ^{76a}, E.W. Varnes ⁷, C. Varni ^{18b}, D. Varouchas ⁶⁷, L. Varriale ¹⁶⁸,
 K.E. Varvell ¹⁵¹, M.E. Vasile ^{28b}, L. Vaslin ⁸⁵, A. Vasyukov ⁴⁰, L.M. Vaughan ¹²⁴, R. Vavricka ¹³⁶,
 T. Vazquez Schroeder ¹³, J. Veatch ³², V. Vecchio ¹⁰³, M.J. Veen ¹⁰⁵, I. Veliscek ³⁰,
 L.M. Veloce ¹⁵⁹, F. Veloso ^{133a,133c}, S. Veneziano ^{76a}, A. Ventura ^{71a,71b}, S. Ventura Gonzalez ¹³⁸,
 A. Verbytskyi ¹¹², M. Verducci ^{75a,75b}, C. Vergis ⁹⁶, M. Verissimo De Araujo ^{84b},
 W. Verkerke ¹¹⁷, J.C. Vermeulen ¹¹⁷, C. Vernieri ¹⁴⁷, M. Vessella ¹⁶³, M.C. Vetterli ^{146.af},
 A. Vgenopoulos ¹⁰², N. Viaux Maira ^{140f}, T. Vickey ¹⁴³, O.E. Vickey Boeriu ¹⁴³,
 G.H.A. Viehhauser ¹²⁹, L. Vigani ^{64b}, M. Vigil ¹¹², M. Villa ^{24b,24a}, M. Villaplana Perez ¹⁶⁸,
 E.M. Villhauer ⁵³, E. Vilucchi ⁵⁴, M.G. Vincter ³⁵, A. Visibile ¹¹⁷, C. Vittori ³⁷, I. Vivarelli ^{24b,24a},
 E. Voevodina ¹¹², F. Vogel ¹¹¹, J.C. Voigt ⁵¹, P. Vokac ¹³⁵, Yu. Volkotrub ^{87b}, E. Von Toerne ²⁵,
 B. Vormwald ³⁷, K. Vorobev ³⁹, M. Vos ¹⁶⁸, K. Voss ¹⁴⁵, M. Vozak ³⁷, L. Vozdecky ¹²³,
 N. Vranjes ¹⁶, M. Vranjes Milosavljevic ¹⁶, M. Vreeswijk ¹¹⁷, N.K. Vu ^{63d}, R. Vuillermet ³⁷,
 O. Vujinovic ¹⁰², I. Vukotic ⁴¹, I.K. Vyas ³⁵, S. Wada ¹⁶¹, C. Wagner ¹⁴⁷, J.M. Wagner ^{18a},
 W. Wagner ¹⁷⁶, S. Wahdan ¹⁷⁶, H. Wahlberg ⁹², C.H. Waits ¹²³, J. Walder ¹³⁷, R. Walker ¹¹¹,
 W. Walkowiak ¹⁴⁵, A. Wall ¹³¹, E.J. Wallin ¹⁰⁰, T. Wamorkar ^{18a}, A.Z. Wang ¹³⁹, C. Wang ¹⁰²,
 C. Wang ¹¹, H. Wang ^{18a}, J. Wang ^{65c}, P. Wang ¹⁰³, P. Wang ⁹⁸, R. Wang ⁶², R. Wang ⁶,
 S.M. Wang ¹⁵², S. Wang ¹⁴, T. Wang ^{63a}, W.T. Wang ⁸¹, W. Wang ¹⁴, X. Wang ¹⁶⁷,
 X. Wang ^{63c}, Y. Wang ^{114a}, Y. Wang ^{63a}, Z. Wang ¹⁰⁸, Z. Wang ^{63d,52,63c}, Z. Wang ¹⁰⁸,
 C. Wanotayaroj ⁸⁵, A. Warburton ¹⁰⁶, R.J. Ward ²¹, A.L. Warnerbring ¹⁴⁵, N. Warrack ⁶⁰,
 S. Waterhouse ⁹⁷, A.T. Watson ²¹, H. Watson ⁵³, M.F. Watson ²¹, E. Watton ⁶⁰, G. Watts ¹⁴²,
 B.M. Waugh ⁹⁸, J.M. Webb ⁵⁵, C. Weber ³⁰, H.A. Weber ¹⁹, M.S. Weber ²⁰, S.M. Weber ^{64a},
 C. Wei ^{63a}, Y. Wei ⁵⁵, A.R. Weidberg ¹²⁹, E.J. Weik ¹²⁰, J. Weingarten ⁵⁰, C. Weiser ⁵⁵,
 C.J. Wells ⁴⁹, T. Wenaus ³⁰, B. Wendland ⁵⁰, T. Wengler ³⁷, N.S. Wenke ¹¹², N. Wermes ²⁵,
 M. Wessels ^{64a}, A.M. Wharton ⁹³, A.S. White ⁶², A. White ⁸, M.J. White ¹, D. Whiteson ¹⁶³,
 L. Wickremasinghe ¹²⁷, W. Wiedenmann ¹⁷⁵, M. Wielers ¹³⁷, C. Wiglesworth ⁴⁴, D.J. Wilbern ¹²³,
 H.G. Wilkens ³⁷, J.J.H. Wilkinson ³³, D.M. Williams ⁴³, H.H. Williams ¹³¹, S. Williams ³³,
 S. Willocq ¹⁰⁵, B.J. Wilson ¹⁰³, D.J. Wilson ¹⁰³, P.J. Windischhofer ⁴¹, F.I. Winkel ³¹,
 F. Winklmeier ¹²⁶, B.T. Winter ⁵⁵, M. Wittgen ¹⁴⁷, M. Wobisch ⁹⁹, T. Wojtkowski ⁶¹, Z. Wolffs ¹¹⁷,
 J. Wollrath ³⁷, M.W. Wolter ⁸⁸, H. Wolters ^{133a,133c}, M.C. Wong ¹³⁹, E.L. Woodward ⁴³,
 S.D. Worm ⁴⁹, B.K. Wosiek ⁸⁸, K.W. Woźniak ⁸⁸, S. Wozniewski ⁵⁶, K. Wraight ⁶⁰, C. Wu ²¹,
 M. Wu ^{114b}, M. Wu ¹¹⁶, S.L. Wu ¹⁷⁵, X. Wu ⁵⁷, X. Wu ^{63a}, Y. Wu ^{63a}, Z. Wu ⁴,
 J. Wuerzinger ^{112.ad}, T.R. Wyatt ¹⁰³, B.M. Wynne ⁵³, S. Xella ⁴⁴, L. Xia ^{114a}, M. Xia ¹⁵,
 M. Xie ^{63a}, A. Xiong ¹²⁶, J. Xiong ^{18a}, D. Xu ¹⁴, H. Xu ^{63a}, L. Xu ^{63a}, R. Xu ¹³¹, T. Xu ¹⁰⁸,

Y. Xu ¹⁴², Z. Xu ⁵³, Z. Xu ^{114a}, B. Yabsley ¹⁵¹, S. Yacoob ^{34a}, Y. Yamaguchi ⁸⁵,
E. Yamashita ¹⁵⁷, H. Yamauchi ¹⁶¹, T. Yamazaki ^{18a}, Y. Yamazaki ⁸⁶, S. Yan ⁶⁰, Z. Yan ¹⁰⁵,
H.J. Yang ^{63c,63d}, H.T. Yang ^{63a}, S. Yang ^{63a}, T. Yang ^{65c}, X. Yang ³⁷, X. Yang ¹⁴, Y. Yang ⁴⁶,
Y. Yang ^{63a}, W.-M. Yao ^{18a}, H. Ye ⁵⁶, J. Ye ¹⁴, S. Ye ³⁰, X. Ye ^{63a}, Y. Yeh ⁹⁸, I. Yeletsikh ⁴⁰,
B. Yeo ^{18b}, M.R. Yexley ⁹⁸, T.P. Yildirim ¹²⁹, P. Yin ⁴³, K. Yorita ¹⁷³, S. Younas ^{28b},
C.J.S. Young ³⁷, C. Young ¹⁴⁷, Y. Yu ^{63a}, J. Yuan ^{14,114c}, M. Yuan ¹⁰⁸, R. Yuan ^{63d,63c},
L. Yue ⁹⁸, M. Zaazoua ^{63a}, B. Zabinski ⁸⁸, I. Zahir ^{36a}, Z.K. Zak ⁸⁸, T. Zakareishvili ¹⁶⁸,
S. Zambito ⁵⁷, J.A. Zamora Saa ^{140d,140b}, J. Zang ¹⁵⁷, D. Zanzi ⁵⁵, R. Zanzottera ^{72a,72b},
O. Zaplatilek ¹³⁵, C. Zeitnitz ¹⁷⁶, H. Zeng ¹⁴, J.C. Zeng ¹⁶⁷, D.T. Zenger Jr ²⁷, O. Zenin ³⁹,
T. Ženiš ^{29a}, S. Zenz ⁹⁶, S. Zerradi ^{36a}, D. Zerwas ⁶⁷, M. Zhai ^{14,114c}, D.F. Zhang ¹⁴³,
J. Zhang ^{63b}, J. Zhang ⁶, K. Zhang ^{14,114c}, L. Zhang ^{63a}, L. Zhang ^{114a}, P. Zhang ^{14,114c},
R. Zhang ¹⁷⁵, S. Zhang ⁹¹, T. Zhang ¹⁵⁷, X. Zhang ^{63c}, Y. Zhang ¹⁴², Y. Zhang ⁹⁸,
Y. Zhang ^{63a}, Y. Zhang ^{114a}, Z. Zhang ^{18a}, Z. Zhang ^{63b}, Z. Zhang ⁶⁷, H. Zhao ¹⁴²,
T. Zhao ^{63b}, Y. Zhao ³⁵, Z. Zhao ^{63a}, Z. Zhao ^{63a}, A. Zhemchugov ⁴⁰, J. Zheng ^{114a},
K. Zheng ¹⁶⁷, X. Zheng ^{63a}, Z. Zheng ¹⁴⁷, D. Zhong ¹⁶⁷, B. Zhou ¹⁰⁸, H. Zhou ⁷, N. Zhou ^{63c},
Y. Zhou ¹⁵, Y. Zhou ^{114a}, Y. Zhou ⁷, C.G. Zhu ^{63b}, J. Zhu ¹⁰⁸, X. Zhu ^{63d}, Y. Zhu ^{63c}, Y. Zhu ^{63a},
X. Zhuang ¹⁴, K. Zhukov ⁶⁹, N.I. Zimine ⁴⁰, J. Zinsser ^{64b}, M. Ziolkowski ¹⁴⁵, L. Živković ¹⁶,
A. Zoccoli ^{24b,24a}, K. Zoch ⁶², T.G. Zorbas ¹⁴³, O. Zormpa ⁴⁷, W. Zou ⁴³, L. Zwalinski ³⁷.

¹Department of Physics, University of Adelaide, Adelaide; Australia.

²Department of Physics, University of Alberta, Edmonton AB; Canada.

^{3(a)}Department of Physics, Ankara University, Ankara; ^(b)Division of Physics, TOBB University of Economics and Technology, Ankara; Türkiye.

⁴LAPP, Université Savoie Mont Blanc, CNRS/IN2P3, Annecy; France.

⁵APC, Université Paris Cité, CNRS/IN2P3, Paris; France.

⁶High Energy Physics Division, Argonne National Laboratory, Argonne IL; United States of America.

⁷Department of Physics, University of Arizona, Tucson AZ; United States of America.

⁸Department of Physics, University of Texas at Arlington, Arlington TX; United States of America.

⁹Physics Department, National and Kapodistrian University of Athens, Athens; Greece.

¹⁰Physics Department, National Technical University of Athens, Zografou; Greece.

¹¹Department of Physics, University of Texas at Austin, Austin TX; United States of America.

¹²Institute of Physics, Azerbaijan Academy of Sciences, Baku; Azerbaijan.

¹³Institut de Física d'Altes Energies (IFAE), Barcelona Institute of Science and Technology, Barcelona; Spain.

¹⁴Institute of High Energy Physics, Chinese Academy of Sciences, Beijing; China.

¹⁵Physics Department, Tsinghua University, Beijing; China.

¹⁶Institute of Physics, University of Belgrade, Belgrade; Serbia.

¹⁷Department for Physics and Technology, University of Bergen, Bergen; Norway.

^{18(a)}Physics Division, Lawrence Berkeley National Laboratory, Berkeley CA; ^(b)University of California, Berkeley CA; United States of America.

¹⁹Institut für Physik, Humboldt Universität zu Berlin, Berlin; Germany.

²⁰Albert Einstein Center for Fundamental Physics and Laboratory for High Energy Physics, University of Bern, Bern; Switzerland.

²¹School of Physics and Astronomy, University of Birmingham, Birmingham; United Kingdom.

^{22(a)}Department of Physics, Bogazici University, Istanbul; ^(b)Department of Physics Engineering, Gaziantep University, Gaziantep; ^(c)Department of Physics, Istanbul University, Istanbul; Türkiye.

^{23(a)}Facultad de Ciencias y Centro de Investigaciones, Universidad Antonio Nariño,

- Bogotá;^(b)Departamento de Física, Universidad Nacional de Colombia, Bogotá; Colombia.
- ^{24(a)}Dipartimento di Fisica e Astronomia A. Righi, Università di Bologna, Bologna;^(b)INFN Sezione di Bologna; Italy.
- ²⁵Physikalisches Institut, Universität Bonn, Bonn; Germany.
- ²⁶Department of Physics, Boston University, Boston MA; United States of America.
- ²⁷Department of Physics, Brandeis University, Waltham MA; United States of America.
- ^{28(a)}Transilvania University of Brasov, Brasov;^(b)Horia Hulubei National Institute of Physics and Nuclear Engineering, Bucharest;^(c)Department of Physics, Alexandru Ioan Cuza University of Iasi, Iasi;^(d)National Institute for Research and Development of Isotopic and Molecular Technologies, Physics Department, Cluj-Napoca;^(e)National University of Science and Technology Politehnica, Bucharest;^(f)West University in Timisoara, Timisoara;^(g)Faculty of Physics, University of Bucharest, Bucharest; Romania.
- ^{29(a)}Faculty of Mathematics, Physics and Informatics, Comenius University, Bratislava;^(b)Department of Subnuclear Physics, Institute of Experimental Physics of the Slovak Academy of Sciences, Kosice; Slovak Republic.
- ³⁰Physics Department, Brookhaven National Laboratory, Upton NY; United States of America.
- ³¹Universidad de Buenos Aires, Facultad de Ciencias Exactas y Naturales, Departamento de Física, y CONICET, Instituto de Física de Buenos Aires (IFIBA), Buenos Aires; Argentina.
- ³²California State University, CA; United States of America.
- ³³Cavendish Laboratory, University of Cambridge, Cambridge; United Kingdom.
- ^{34(a)}Department of Physics, University of Cape Town, Cape Town;^(b)iThemba Labs, Western Cape;^(c)Department of Mechanical Engineering Science, University of Johannesburg, Johannesburg;^(d)National Institute of Physics, University of the Philippines Diliman (Philippines);^(e)University of South Africa, Department of Physics, Pretoria;^(f)University of Zululand, KwaDlangezwa;^(g)School of Physics, University of the Witwatersrand, Johannesburg; South Africa.
- ³⁵Department of Physics, Carleton University, Ottawa ON; Canada.
- ^{36(a)}Faculté des Sciences Ain Chock, Université Hassan II de Casablanca;^(b)Faculté des Sciences, Université Ibn-Tofail, Kénitra;^(c)Faculté des Sciences Semlalia, Université Cadi Ayyad, LPHEA-Marrakech;^(d)LPMR, Faculté des Sciences, Université Mohamed Premier, Oujda;^(e)Faculté des sciences, Université Mohammed V, Rabat;^(f)Institute of Applied Physics, Mohammed VI Polytechnic University, Ben Guerir; Morocco.
- ³⁷CERN, Geneva; Switzerland.
- ³⁸Affiliated with an institute formerly covered by a cooperation agreement with CERN.
- ³⁹Affiliated with an institute covered by a cooperation agreement with CERN.
- ⁴⁰Affiliated with an international laboratory covered by a cooperation agreement with CERN.
- ⁴¹Enrico Fermi Institute, University of Chicago, Chicago IL; United States of America.
- ⁴²LPC, Université Clermont Auvergne, CNRS/IN2P3, Clermont-Ferrand; France.
- ⁴³Nevis Laboratory, Columbia University, Irvington NY; United States of America.
- ⁴⁴Niels Bohr Institute, University of Copenhagen, Copenhagen; Denmark.
- ^{45(a)}Dipartimento di Fisica, Università della Calabria, Rende;^(b)INFN Gruppo Collegato di Cosenza, Laboratori Nazionali di Frascati; Italy.
- ⁴⁶Physics Department, Southern Methodist University, Dallas TX; United States of America.
- ⁴⁷National Centre for Scientific Research "Demokritos", Agia Paraskevi; Greece.
- ^{48(a)}Department of Physics, Stockholm University;^(b)Oskar Klein Centre, Stockholm; Sweden.
- ⁴⁹Deutsches Elektronen-Synchrotron DESY, Hamburg and Zeuthen; Germany.
- ⁵⁰Fakultät Physik, Technische Universität Dortmund, Dortmund; Germany.
- ⁵¹Institut für Kern- und Teilchenphysik, Technische Universität Dresden, Dresden; Germany.
- ⁵²Department of Physics, Duke University, Durham NC; United States of America.

- ⁵³SUPA - School of Physics and Astronomy, University of Edinburgh, Edinburgh; United Kingdom.
- ⁵⁴INFN e Laboratori Nazionali di Frascati, Frascati; Italy.
- ⁵⁵Physikalisches Institut, Albert-Ludwigs-Universität Freiburg, Freiburg; Germany.
- ⁵⁶II. Physikalisches Institut, Georg-August-Universität Göttingen, Göttingen; Germany.
- ⁵⁷Département de Physique Nucléaire et Corpusculaire, Université de Genève, Genève; Switzerland.
- ⁵⁸(^a) Dipartimento di Fisica, Università di Genova, Genova; (^b) INFN Sezione di Genova; Italy.
- ⁵⁹II. Physikalisches Institut, Justus-Liebig-Universität Giessen, Giessen; Germany.
- ⁶⁰SUPA - School of Physics and Astronomy, University of Glasgow, Glasgow; United Kingdom.
- ⁶¹LPSC, Université Grenoble Alpes, CNRS/IN2P3, Grenoble INP, Grenoble; France.
- ⁶²Laboratory for Particle Physics and Cosmology, Harvard University, Cambridge MA; United States of America.
- ⁶³(^a) Department of Modern Physics and State Key Laboratory of Particle Detection and Electronics, University of Science and Technology of China, Hefei; (^b) Institute of Frontier and Interdisciplinary Science and Key Laboratory of Particle Physics and Particle Irradiation (MOE), Shandong University, Qingdao; (^c) School of Physics and Astronomy, Shanghai Jiao Tong University, Key Laboratory for Particle Astrophysics and Cosmology (MOE), SKLPPC, Shanghai; (^d) Tsung-Dao Lee Institute, Shanghai; (^e) School of Physics, Zhengzhou University; China.
- ⁶⁴(^a) Kirchhoff-Institut für Physik, Ruprecht-Karls-Universität Heidelberg, Heidelberg; (^b) Physikalisches Institut, Ruprecht-Karls-Universität Heidelberg, Heidelberg; Germany.
- ⁶⁵(^a) Department of Physics, Chinese University of Hong Kong, Shatin, N.T., Hong Kong; (^b) Department of Physics, University of Hong Kong, Hong Kong; (^c) Department of Physics and Institute for Advanced Study, Hong Kong University of Science and Technology, Clear Water Bay, Kowloon, Hong Kong; China.
- ⁶⁶Department of Physics, National Tsing Hua University, Hsinchu; Taiwan.
- ⁶⁷IJCLab, Université Paris-Saclay, CNRS/IN2P3, 91405, Orsay; France.
- ⁶⁸Centro Nacional de Microelectrónica (IMB-CNM-CSIC), Barcelona; Spain.
- ⁶⁹Department of Physics, Indiana University, Bloomington IN; United States of America.
- ⁷⁰(^a) INFN Gruppo Collegato di Udine, Sezione di Trieste, Udine; (^b) ICTP, Trieste; (^c) Dipartimento Politecnico di Ingegneria e Architettura, Università di Udine, Udine; Italy.
- ⁷¹(^a) INFN Sezione di Lecce; (^b) Dipartimento di Matematica e Fisica, Università del Salento, Lecce; Italy.
- ⁷²(^a) INFN Sezione di Milano; (^b) Dipartimento di Fisica, Università di Milano, Milano; Italy.
- ⁷³(^a) INFN Sezione di Napoli; (^b) Dipartimento di Fisica, Università di Napoli, Napoli; Italy.
- ⁷⁴(^a) INFN Sezione di Pavia; (^b) Dipartimento di Fisica, Università di Pavia, Pavia; Italy.
- ⁷⁵(^a) INFN Sezione di Pisa; (^b) Dipartimento di Fisica E. Fermi, Università di Pisa, Pisa; Italy.
- ⁷⁶(^a) INFN Sezione di Roma; (^b) Dipartimento di Fisica, Sapienza Università di Roma, Roma; Italy.
- ⁷⁷(^a) INFN Sezione di Roma Tor Vergata; (^b) Dipartimento di Fisica, Università di Roma Tor Vergata, Roma; Italy.
- ⁷⁸(^a) INFN Sezione di Roma Tre; (^b) Dipartimento di Matematica e Fisica, Università Roma Tre, Roma; Italy.
- ⁷⁹(^a) INFN-TIFPA; (^b) Università degli Studi di Trento, Trento; Italy.
- ⁸⁰Universität Innsbruck, Department of Astro and Particle Physics, Innsbruck; Austria.
- ⁸¹University of Iowa, Iowa City IA; United States of America.
- ⁸²Department of Physics and Astronomy, Iowa State University, Ames IA; United States of America.
- ⁸³Istinye University, Sariyer, Istanbul; Türkiye.
- ⁸⁴(^a) Departamento de Engenharia Elétrica, Universidade Federal de Juiz de Fora (UFJF), Juiz de Fora; (^b) Universidade Federal do Rio De Janeiro COPPE/EE/IF, Rio de Janeiro; (^c) Instituto de Física, Universidade de São Paulo, São Paulo; (^d) Rio de Janeiro State University, Rio de Janeiro; (^e) Federal University of Bahia, Bahia; Brazil.

- ⁸⁵KEK, High Energy Accelerator Research Organization, Tsukuba; Japan.
- ⁸⁶Graduate School of Science, Kobe University, Kobe; Japan.
- ⁸⁷(^a) AGH University of Krakow, Faculty of Physics and Applied Computer Science, Krakow; (^b) Marian Smoluchowski Institute of Physics, Jagiellonian University, Krakow; Poland.
- ⁸⁸Institute of Nuclear Physics Polish Academy of Sciences, Krakow; Poland.
- ⁸⁹Faculty of Science, Kyoto University, Kyoto; Japan.
- ⁹⁰Research Center for Advanced Particle Physics and Department of Physics, Kyushu University, Fukuoka ; Japan.
- ⁹¹L2IT, Université de Toulouse, CNRS/IN2P3, UPS, Toulouse; France.
- ⁹²Instituto de Física La Plata, Universidad Nacional de La Plata and CONICET, La Plata; Argentina.
- ⁹³Physics Department, Lancaster University, Lancaster; United Kingdom.
- ⁹⁴Oliver Lodge Laboratory, University of Liverpool, Liverpool; United Kingdom.
- ⁹⁵Department of Experimental Particle Physics, Jožef Stefan Institute and Department of Physics, University of Ljubljana, Ljubljana; Slovenia.
- ⁹⁶School of Physics and Astronomy, Queen Mary University of London, London; United Kingdom.
- ⁹⁷Department of Physics, Royal Holloway University of London, Egham; United Kingdom.
- ⁹⁸Department of Physics and Astronomy, University College London, London; United Kingdom.
- ⁹⁹Louisiana Tech University, Ruston LA; United States of America.
- ¹⁰⁰Fysiska institutionen, Lunds universitet, Lund; Sweden.
- ¹⁰¹Departamento de Física Teórica C-15 and CIAFF, Universidad Autónoma de Madrid, Madrid; Spain.
- ¹⁰²Institut für Physik, Universität Mainz, Mainz; Germany.
- ¹⁰³School of Physics and Astronomy, University of Manchester, Manchester; United Kingdom.
- ¹⁰⁴CPPM, Aix-Marseille Université, CNRS/IN2P3, Marseille; France.
- ¹⁰⁵Department of Physics, University of Massachusetts, Amherst MA; United States of America.
- ¹⁰⁶Department of Physics, McGill University, Montreal QC; Canada.
- ¹⁰⁷School of Physics, University of Melbourne, Victoria; Australia.
- ¹⁰⁸Department of Physics, University of Michigan, Ann Arbor MI; United States of America.
- ¹⁰⁹Department of Physics and Astronomy, Michigan State University, East Lansing MI; United States of America.
- ¹¹⁰Group of Particle Physics, University of Montreal, Montreal QC; Canada.
- ¹¹¹Fakultät für Physik, Ludwig-Maximilians-Universität München, München; Germany.
- ¹¹²Max-Planck-Institut für Physik (Werner-Heisenberg-Institut), München; Germany.
- ¹¹³Graduate School of Science and Kobayashi-Maskawa Institute, Nagoya University, Nagoya; Japan.
- ¹¹⁴(^a) Department of Physics, Nanjing University, Nanjing; (^b) School of Science, Shenzhen Campus of Sun Yat-sen University; (^c) University of Chinese Academy of Science (UCAS), Beijing; China.
- ¹¹⁵Department of Physics and Astronomy, University of New Mexico, Albuquerque NM; United States of America.
- ¹¹⁶Institute for Mathematics, Astrophysics and Particle Physics, Radboud University/Nikhef, Nijmegen; Netherlands.
- ¹¹⁷Nikhef National Institute for Subatomic Physics and University of Amsterdam, Amsterdam; Netherlands.
- ¹¹⁸Department of Physics, Northern Illinois University, DeKalb IL; United States of America.
- ¹¹⁹(^a) New York University Abu Dhabi, Abu Dhabi; (^b) United Arab Emirates University, Al Ain; United Arab Emirates.
- ¹²⁰Department of Physics, New York University, New York NY; United States of America.
- ¹²¹Ochanomizu University, Otsuka, Bunkyo-ku, Tokyo; Japan.
- ¹²²Ohio State University, Columbus OH; United States of America.

- ¹²³Homer L. Dodge Department of Physics and Astronomy, University of Oklahoma, Norman OK; United States of America.
- ¹²⁴Department of Physics, Oklahoma State University, Stillwater OK; United States of America.
- ¹²⁵Palacký University, Joint Laboratory of Optics, Olomouc; Czech Republic.
- ¹²⁶Institute for Fundamental Science, University of Oregon, Eugene, OR; United States of America.
- ¹²⁷Graduate School of Science, Osaka University, Osaka; Japan.
- ¹²⁸Department of Physics, University of Oslo, Oslo; Norway.
- ¹²⁹Department of Physics, Oxford University, Oxford; United Kingdom.
- ¹³⁰LPNHE, Sorbonne Université, Université Paris Cité, CNRS/IN2P3, Paris; France.
- ¹³¹Department of Physics, University of Pennsylvania, Philadelphia PA; United States of America.
- ¹³²Department of Physics and Astronomy, University of Pittsburgh, Pittsburgh PA; United States of America.
- ¹³³(^a)Laboratório de Instrumentação e Física Experimental de Partículas - LIP, Lisboa; (^b)Departamento de Física, Faculdade de Ciências, Universidade de Lisboa, Lisboa; (^c)Departamento de Física, Universidade de Coimbra, Coimbra; (^d)Centro de Física Nuclear da Universidade de Lisboa, Lisboa; (^e)Departamento de Física, Universidade do Minho, Braga; (^f)Departamento de Física Teórica y del Cosmos, Universidad de Granada, Granada (Spain); (^g)Departamento de Física, Instituto Superior Técnico, Universidade de Lisboa, Lisboa; Portugal.
- ¹³⁴Institute of Physics of the Czech Academy of Sciences, Prague; Czech Republic.
- ¹³⁵Czech Technical University in Prague, Prague; Czech Republic.
- ¹³⁶Charles University, Faculty of Mathematics and Physics, Prague; Czech Republic.
- ¹³⁷Particle Physics Department, Rutherford Appleton Laboratory, Didcot; United Kingdom.
- ¹³⁸IRFU, CEA, Université Paris-Saclay, Gif-sur-Yvette; France.
- ¹³⁹Santa Cruz Institute for Particle Physics, University of California Santa Cruz, Santa Cruz CA; United States of America.
- ¹⁴⁰(^a)Departamento de Física, Pontificia Universidad Católica de Chile, Santiago; (^b)Millennium Institute for Subatomic physics at high energy frontier (SAPHIR), Santiago; (^c)Instituto de Investigación Multidisciplinario en Ciencia y Tecnología, y Departamento de Física, Universidad de La Serena; (^d)Universidad Andres Bello, Department of Physics, Santiago; (^e)Instituto de Alta Investigación, Universidad de Tarapacá, Arica; (^f)Departamento de Física, Universidad Técnica Federico Santa María, Valparaíso; Chile.
- ¹⁴¹Department of Physics, Institute of Science, Tokyo; Japan.
- ¹⁴²Department of Physics, University of Washington, Seattle WA; United States of America.
- ¹⁴³Department of Physics and Astronomy, University of Sheffield, Sheffield; United Kingdom.
- ¹⁴⁴Department of Physics, Shinshu University, Nagano; Japan.
- ¹⁴⁵Department Physik, Universität Siegen, Siegen; Germany.
- ¹⁴⁶Department of Physics, Simon Fraser University, Burnaby BC; Canada.
- ¹⁴⁷SLAC National Accelerator Laboratory, Stanford CA; United States of America.
- ¹⁴⁸Department of Physics, Royal Institute of Technology, Stockholm; Sweden.
- ¹⁴⁹Departments of Physics and Astronomy, Stony Brook University, Stony Brook NY; United States of America.
- ¹⁵⁰Department of Physics and Astronomy, University of Sussex, Brighton; United Kingdom.
- ¹⁵¹School of Physics, University of Sydney, Sydney; Australia.
- ¹⁵²Institute of Physics, Academia Sinica, Taipei; Taiwan.
- ¹⁵³(^a)E. Andronikashvili Institute of Physics, Iv. Javakhishvili Tbilisi State University, Tbilisi; (^b)High Energy Physics Institute, Tbilisi State University, Tbilisi; (^c)University of Georgia, Tbilisi; Georgia.
- ¹⁵⁴Department of Physics, Technion, Israel Institute of Technology, Haifa; Israel.

- ¹⁵⁵Raymond and Beverly Sackler School of Physics and Astronomy, Tel Aviv University, Tel Aviv; Israel.
- ¹⁵⁶Department of Physics, Aristotle University of Thessaloniki, Thessaloniki; Greece.
- ¹⁵⁷International Center for Elementary Particle Physics and Department of Physics, University of Tokyo, Tokyo; Japan.
- ¹⁵⁸Graduate School of Science and Technology, Tokyo Metropolitan University, Tokyo; Japan.
- ¹⁵⁹Department of Physics, University of Toronto, Toronto ON; Canada.
- ¹⁶⁰^(a)TRIUMF, Vancouver BC; ^(b)Department of Physics and Astronomy, York University, Toronto ON; Canada.
- ¹⁶¹Division of Physics and Tomonaga Center for the History of the Universe, Faculty of Pure and Applied Sciences, University of Tsukuba, Tsukuba; Japan.
- ¹⁶²Department of Physics and Astronomy, Tufts University, Medford MA; United States of America.
- ¹⁶³Department of Physics and Astronomy, University of California Irvine, Irvine CA; United States of America.
- ¹⁶⁴University of West Attica, Athens; Greece.
- ¹⁶⁵University of Sharjah, Sharjah; United Arab Emirates.
- ¹⁶⁶Department of Physics and Astronomy, University of Uppsala, Uppsala; Sweden.
- ¹⁶⁷Department of Physics, University of Illinois, Urbana IL; United States of America.
- ¹⁶⁸Instituto de Física Corpuscular (IFIC), Centro Mixto Universidad de Valencia - CSIC, Valencia; Spain.
- ¹⁶⁹Department of Physics, University of British Columbia, Vancouver BC; Canada.
- ¹⁷⁰Department of Physics and Astronomy, University of Victoria, Victoria BC; Canada.
- ¹⁷¹Fakultät für Physik und Astronomie, Julius-Maximilians-Universität Würzburg, Würzburg; Germany.
- ¹⁷²Department of Physics, University of Warwick, Coventry; United Kingdom.
- ¹⁷³Waseda University, Tokyo; Japan.
- ¹⁷⁴Department of Particle Physics and Astrophysics, Weizmann Institute of Science, Rehovot; Israel.
- ¹⁷⁵Department of Physics, University of Wisconsin, Madison WI; United States of America.
- ¹⁷⁶Fakultät für Mathematik und Naturwissenschaften, Fachgruppe Physik, Bergische Universität Wuppertal, Wuppertal; Germany.
- ¹⁷⁷Department of Physics, Yale University, New Haven CT; United States of America.
- ¹⁷⁸Yerevan Physics Institute, Yerevan; Armenia.
- ^a Also Affiliated with an institute covered by a cooperation agreement with CERN.
- ^b Also at An-Najah National University, Nablus; Palestine.
- ^c Also at Borough of Manhattan Community College, City University of New York, New York NY; United States of America.
- ^d Also at Center for Interdisciplinary Research and Innovation (CIRI-AUTH), Thessaloniki; Greece.
- ^e Also at CERN, Geneva; Switzerland.
- ^f Also at CMD-AC UNEC Research Center, Azerbaijan State University of Economics (UNEC); Azerbaijan.
- ^g Also at Département de Physique Nucléaire et Corpusculaire, Université de Genève, Genève; Switzerland.
- ^h Also at Departament de Física de la Universitat Autònoma de Barcelona, Barcelona; Spain.
- ⁱ Also at Department of Financial and Management Engineering, University of the Aegean, Chios; Greece.
- ^j Also at Department of Mathematical Sciences, University of South Africa, Johannesburg; South Africa.
- ^k Also at Department of Physics, Bolu Abant İzzet Baysal University, Bolu; Türkiye.
- ^l Also at Department of Physics, California State University, Sacramento; United States of America.
- ^m Also at Department of Physics, King's College London, London; United Kingdom.
- ⁿ Also at Department of Physics, Stanford University, Stanford CA; United States of America.
- ^o Also at Department of Physics, Stellenbosch University; South Africa.

- p* Also at Department of Physics, University of Fribourg, Fribourg; Switzerland.
- q* Also at Department of Physics, University of Thessaly; Greece.
- r* Also at Department of Physics, Westmont College, Santa Barbara; United States of America.
- s* Also at Faculty of Physics, Sofia University, 'St. Kliment Ohridski', Sofia; Bulgaria.
- t* Also at Hellenic Open University, Patras; Greece.
- u* Also at Henan University; China.
- v* Also at Imam Mohammad Ibn Saud Islamic University; Saudi Arabia.
- w* Also at Institutio Catalana de Recerca i Estudis Avancats, ICREA, Barcelona; Spain.
- x* Also at Institut für Experimentalphysik, Universität Hamburg, Hamburg; Germany.
- y* Also at Institute for Nuclear Research and Nuclear Energy (INRNE) of the Bulgarian Academy of Sciences, Sofia; Bulgaria.
- z* Also at Institute of Applied Physics, Mohammed VI Polytechnic University, Ben Guerir; Morocco.
- aa* Also at Institute of Particle Physics (IPP); Canada.
- ab* Also at Institute of Physics, Azerbaijan Academy of Sciences, Baku; Azerbaijan.
- ac* Also at National Institute of Physics, University of the Philippines Diliman (Philippines); Philippines.
- ad* Also at Technical University of Munich, Munich; Germany.
- ae* Also at The Collaborative Innovation Center of Quantum Matter (CICQM), Beijing; China.
- af* Also at TRIUMF, Vancouver BC; Canada.
- ag* Also at Università di Napoli Parthenope, Napoli; Italy.
- ah* Also at University of Colorado Boulder, Department of Physics, Colorado; United States of America.
- ai* Also at University of the Western Cape; South Africa.
- aj* Also at Washington College, Chestertown, MD; United States of America.
- ak* Also at Yeditepe University, Physics Department, Istanbul; Türkiye.
- * Deceased